MEMS Thin Film Teflon Electret Condenser Microphones

Thesis by

Wen H. Hsieh

In Partial Fulfillment of the Requirements
for the Degree of Doctor of Philosophy

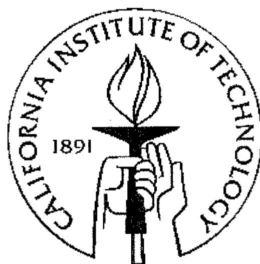

California Institute of Technology

Pasadena, California, USA

2001

© 2001

Wen H. Hsieh

All Rights Reserved

To my parents

Acknowledgements

First, I would like to express my sincere appreciation to Professor Yu-Chong Tai for his academic and personal guidance and support. His enthusiasm and faith in this project has carried me through many hard times and has helped me out of many dead ends.

I would also like to thank the staff and students of the Caltech Micromachining Group for their assistance both inside and outside our lab. In particular I would like to thank the 'BrF_3 and dicing saw guys' Dr. X.Q. Wang and Ken Walsh for always being there for me. I'd also like to thank Dr. Amish Desai for teaching me how to 'fly' while leading a balanced life as a graduate student. I could not have learned so much throughout this Ph.D. program without the support of Dr. Shuyun Wu, Dr. Tom Tsao, Dr. Fukang Jiang, Dr. Xing Yang, Charles Grosjean, Ellis Meng, Tze-Jung Yao, Jun Xie, Yong Xu and Han Zhigang for lending me their technical expertise as well as their quality time. My appreciation also extends to Trevor Roper, Hung Bui and Tanya Hefner who have done an excellent job in keeping the Caltech Micromachining Lab running smoothly.

Outside of the lab I would like to thank Dr. Sigfrid Soli of the House Ear Institute for being a mentor and for believing in my MEMS microphone; as well as Dr. Katsushi Furutani who helped me break-ground at the beginning when I struggled with the Teflon electret material.

For the help with the electron implantation using a Back-Lighted Thyratron I thank Dr. T. Yang Hsu, and my appreciation also extends to Herb Adams for machining the numerous cumbersome test set-up apparatuses.

I am deeply grateful to my best friends Niki Ren and Albert Lee, without who I could not have accomplished so much. Your encouragement, companionship and devotion have been invaluable to me.

Finally, I would like to express my deepest thanks to my brother for always being there for me, and to my parents for all their sacrifices and support. Their love and patience have made this work possible.

MEMS Thin Film Teflon Electret Condenser Microphones

Thesis by

Wen H. Hsieh

In Partial Fulfillment of the Requirements

For the Degree of

Doctor of Philosophy

Abstract

The goal of this thesis is to develop miniature, inexpensive, high-quality, self-biasing electret condenser microphones that are fabricated using Micro Electro Mechanical Systems (MEMS) technology. These MEMS electret microphones are to be used in any application where a conventional electret microphone can be used (such as in cell phones, and hearing aids) and in new acoustic sensing applications where current microphone technology cannot be applied (such as in smart cards of the future or in new applications where it is advantageous to integrate microelectronics with the microphone).

To accomplish this, a MEMS-compatible Teflon electret technology has been developed. The electret material used is thin film spin-on Teflon AF. A custom-built pulsed electron gun, called the Back-Lighted Thyratron (BLT), is used for charge implantation. Thermal annealing is used to stabilize (age) the implanted charge. An electric field compensation method is used to measure the charge density of the electrets. The electrets obtained have stable charge densities on the order of 10^{-5} to 10^{-4} C/m^2.

Two main types of MEMS thin film Teflon electret condenser microphones have been successfully fabricated and tested. Both microphones use silicon substrates and are fabricated using bulk-micromachining techniques. Each microphone is manufactured as a two piece structure, comprising a microphone membrane unit having an extremely thin diaphragm and a perforated microphone backplate unit. When one is placed on top of the other, the two units form a highly reliable, inexpensive microphone that can produce a

signal without the need for external biasing. This reduces system volume and complexity. One type of microphone uses a silicon nitride/Teflon AF composite diaphragm, while the other type uses a Parylene C/Teflon AF composite diaphragm. Both microphones use the same perforated silicon nitride/Parylene C composite backplate.

Both types of millimeter-scale electret microphones have very low stray capacitance, are self-biasing, mass producible, arrayable, integratable with on-chip electronics, structurally simple and extremely stable over time in the ordinary environment. The dynamic range is from less than 30 dB to above 110 dB SPL (re. 20 μPa) and the open-circuit sensitivities obtained range from 3.5 - 44 mV/Pa over the frequency range 100 Hz - 13 kHz. The total harmonic distortion of both devices is less than 2% at 110 dB SPL, 1 kHz.

Table of Contents

Chapter 1: Introduction

1.1 Motivation 1

1.2 Micro Electro Mechanical Systems (MEMS) 3

1.3 Thesis Outline 5

1.4 References 7

Chapter 2: Electret Condenser Microphone Theory

2.1 Principle of Operation 1

2.1.1 Externally Biased 2

2.1.2 Electret: Self-Biasing 3

2.2 Electret Microphone Characteristics 4

2.3 Open-Circuit Sensitivity 6

2.3.1 Mechanical Sensitivity 7

2.3.2 Electrical Sensitivity 10

2.3.3 Loaded Sensitivity and Electrical Response 11

2.3.4 Total Microphone and Preamplifier Sensitivity 12

2.4 Frequency Response 13

2.4.1 Low-Frequency Cut-Off 14

2.4.2 High-Frequency Cut-Off 15

2.5 Dynamic Range 18

2.5.1 Lower-Limit: Noise Floor 19

2.5.2 Upper-Limit 20

2.6 Stability 22

2.6.1 Temperature 22

2.6.2 Atmospheric Pressure 23

2.6.3 Humidity 24

2.6.4 Vibration 24

2.6.5 Electromagnetic Fields 25

2.7 Electret Charge Induced Static Diaphragm Deflection 25
2.7.1 Rigid Backplate 25
2.7.2 Flexible Backplate 26
2.8 Summary 27
2.9 References 28

Chapter 3: A Review of Capacitive Microphones

3.1 Conventional Capacitive Microphones 1
3.2 MEMS Capacitive Microphones 5
3.3 Summary 13
3.4 References 15

Chapter 4: Thin Film Teflon AF Electrets

4.1 Theory and History of Electrets 1
4.2 Electret Formation 4
4.2.1 Back-Lighted Thyratron 5
4.3 Charge Measurement 9
4.3.1 PZT-shaker 9
4.3.2 Monroe Isoprobe Electrostatic Voltmeter 12
4.4 Electret Materials 14
4.4.1 Teflon AF 15
4.5 Working Process 18
4.6 Teflon AF Physical Characteristics 19
4.7 Teflon AF Electret Characteristics 20
4.7.1 Thermal Stability 22
4.7.2 UV Stability 25
4.7.3 Humidity Stability 25
4.7.4 Chemical Stability 25
4.8 Summary 26
4.9 References 27

Chapter 5: MEMS Electret Microphones with Nitride Diaphragms

5.1 Preface 1

5.2 Silicon Nitride Diaphragms 1

5.3 Silicon Nitride/Teflon AF Composite Diaphragm Characteristics 3

5.4 Silicon Backplate Microphone 5

 5.4.1 Fabrication and Packaging 5

 5.4.2 Testing and Performance 7

 5.4.3 Analysis 8

5.5 Glass Backplate Microphone 9

 5.5.1 Fabrication and Packaging 9

 5.5.2 Testing and Performance 12

 5.5.3 Analysis 16

5.6 Parylene C/Silicon Nitride Composite Backplate Microphone 17

 5.6.1 Fabrication and Packaging 17

 5.6.2 Testing and Performance 21

 5.6.3 Analysis 27

5.7 Summary 31

5.8 References 32

Chapter 6: MEMS Electret Microphones with Parylene Diaphragms

6.1 Preface 1

6.2 Parylene Diaphragms 1

6.3 Parylene C/Teflon AF Composite Diaphragm Characteristics 4

6.4 Parylene C/Silicon Nitride Composite Backplate Microphone 6

 6.4.1 Fabrication and Packaging 6

 6.4.2 Testing and Performance 9

 6.4.3 Analysis 14

6.5 Summary 16

6.6 References 17

Chapter 7: Conclusion 1

List of Figures

Chapter 1

Figure 1-1: Conventional electret microphones vs. MEMS electret microphone 2

Chapter 2

Figure 2-1: Externally biased and self-biasing (electret) condenser microphones 1
Figure 2-2: Schematic cross-section of an electret microphone w/ housing 4
Figure 2-3: Sound pressure level of familiar sounds 6
Figure 2-4: Open-circuit sensitivity 7
Figure 2-5: Deflection of a square membrane 9
Figure 2-6: Model of microphone electret system in equilibrium 10
Figure 2-7: Schematic of microphone and preamplifier circuit 11
Figure 2-8: Typical frequency response of an electret microphone 13
Figure 2-9: Pressure equalization hole positions 14
Figure 2-10: Low frequency response vs. location of pressure equalization hole. 15
Figure 2-11: Different degrees of microphone response damping 16
Figure 2-12: Upper dynamic range of different size electret microphones 21

Chapter 3

Figure 3-1: Wente's original condenser microphone 2
Figure 3-2: A cut-away of an old electret microphone design 3
Figure 3-3: Cross-section of a miniature hearing aid electret microphone 4
Figure 3-4: Silicon electret microphone of Hohm and Gerhard-Multhaupt (1984). 6
Figure 3-5: Silicon condenser microphone of Hohm and Hess (1986). 6
Figure 3-6: Silicon electret microphone of Sprenkels (1988) 7
Figure 3-7: First silicon condenser microphone of Bergqvist and Rudolf (1990) 8
Figure 3-8: Second silicon condenser microphone of Bergqvist and Rudolf (1991) 8
Figure 3-9: FET condenser microphone of Kuhnel (1991) 9

Figure 3-10: Silicon condenser microphone with feedback of van der Donk (1992) 10
Figure 3-11: Surface micromachined Si condenser microphone of Scheeper (1992) 10
Figure 3-12: Electroplated silicon condenser microphone of Bergqvist (1994) 11
Figure 3-13: Silicon microphone w/ integrated preamplifier of Bernstein (1996) 11
Figure 3-14: Integrated MEMS microphone for hearing aid applications (1998). 12
Figure 3-15: Picture of all-surface-micromachined microphone of Pardo (1999) 13

Chapter 4

Figure 4-1: Different types of electret charge 1
Figure 4-2: Energy diagram for electron (T_e) and hole (T_h) traps in polymers 2
Figure 4-3: The Back-Lighted Thyratron 6
Figure 4-4: Helium electrical breakdown curve for the BLT 6
Figure 4-5: Picture and schematic of the BLT charge implantation chamber 7
Figure 4-6: Picture and drawing of the BLT charge implantation system 8
Figure 4-7: Schematic of the PZT-shaker 10
Figure 4-8: Schematic of the electric field compensation circuit 10
Figure 4-9: Oscilloscope screen views 11
Figure 4-10: Pictures of the PZT-shaker setup 12
Figure 4-11: Simplified block diagram of the Monroe voltmeter and probe 12
Figure 4-12: Pictures of the Monroe voltmeter and probe setup 13
Figure 4-13: Monomers of Teflon AF 16
Figure 4-14: Spin curve of Teflon AF 1601S-6 solution 17
Figure 4-15: Surface of Teflon AF 1601S film on gold annealed at 115°C & 170°C 20
Figure 4-16: Charge saturation with number of BLT shots using 10 keV electrons 21
Figure 4-17: Charge density of Teflon AF electret at 25°C 23
Figure 4-18: Charge density of Teflon AF electret at elevated temperatures 23
Figure 4-19: Significant charge loss in Teflon AF electret at 190°C 23
Figure 4-20: Charge density of Teflon AF electret under UV light exposure 25

Chapter 5

Figure 5-1: Laser Doppler Vibrometer setup for resonant frequency measurements 4

Figure 5-2: Frequency response of (a) PZT and (b) a composite diaphragm on PZT 4
Figure 5-3: Process flow of a MEMS electret microphone with silicon backplate............. 6
Figure 5-4: Pictures of silicon nitride diaphragm and silicon backplate............................ 7
Figure 5-5: The assembled silicon nitride diaphragm and silicon backplate package........ 7
Figure 5-6: An oscilloscope display of a human voice detected without an amplifier 8
Figure 5-7: Process flow of a MEMS electret microphone with glass backplate 10
Figure 5-8: Pictures of silicon nitride diaphragm and glass backplate 11
Figure 5-9: The assembled silicon nitride diaphragm and glass backplate package......... 11
Figure 5-10: Microphone measurement test setup 12
Figure 5-11: Schematic of microphone-preamplifier circuit... 13
Figure 5-12: Microphone output for a 2 Pa RMS, 650 Hz input signal (Gain = 50 dB) .. 14
Figure 5-13: Input sound pressure level for frequency response measurements 15
Figure 5-14: Frequency response of MEMS electret microphone with glass blackplate.. 15
Figure 5-15: Process flow of 8 × 8 mm^2 silicon nitride/Teflon AF diaphragm 18
Figure 5-16: Process flow of 8 × 8 mm^2 perforated Parylene C/silicon nitride backplate 19
Figure 5-17: Pictures of nitride diaphragm and perforated Parylene C/nitride backplate 19
Figure 5-18: Cross-section of MEMS electret microphone with nitride diaphragm......... 20
Figure 5-19: Picture of MEMS electret microphone brass housing............................... 20
Figure 5-20: Cross-section of MEMS electret microphone housing 21
Figure 5-21: Resonance of nitride/Teflon diaphragm and Parylene/nitride backplate 22
Figure 5-22: Input sound pressure level for frequency response measurement............... 23
Figure 5-23: Frequency response of MEMS electret microphone w/ nitride diaphragm.. 24
Figure 5-24: Disturbance of a plane sound wave by a microphone body 25
Figure 5-25: Ratio between press. at diaphragm and press. of undisturbed sound field... 25
Figure 5-26: Compensation for the upward sloping microphone frequency response 29
Figure 5-27: Pictures of wires used to connect the MEMS microphone to its housing.... 30

Chapter 6

Figure 6-1: Chemical structures of Parylene N, C and D... 2
Figure 6-2: A schematic of the Parylene deposition system 3
Figure 6-3: Process flow of 8 × 8 mm^2 perforated Parylene C/silicon nitride backplate.... 6

Figure 6-4: Process flow of 8×8 mm^2 Parylene C/Teflon AF diaphragm......................... 7
Figure 6-5: Cross-section of MEMS electret microphone with Parylene C diaphragm 8
Figure 6-6: Cross-section of MEMS electret microphone housing 8
Figure 6-7: Resonance of Parylene/Teflon diaphragm and Parylene/nitride backplate...... 9
Figure 6-8: Input sound pressure level for frequency response measurement.................. 10
Figure 6-9: Frequency response of MEMS electret microphone w/ Parylene diaphragm 11
Figure 6-10: Parylene C diaphragm cracking problems.. 15

Chapter 7 (no figures)

List of Tables

Chapter 1 (no tables)

Chapter 2 (no tables)

Chapter 3

Table 3-1: Summary of historical MEMS silicon capacitive microphones 14

Chapter 4

Table 4-1: Distribution of traps for negative charges in 25 μm Teflon-FEP-A................. 2

Table 4-2: Electret forming techniques.. 4

Table 4-3: Discharge and glass transition temperature of various polyolefine electrets .. 15

Table 4-4: Solvents for Teflon AF 16

Table 4-5: Typical property data for Teflon AF 1601S 17

Chapter 5

Table 5-1: Environmental influences on silicon nitride/Teflon AF diaphragms 5

Table 5-2: Characteristics of MEMS electret microphone w/ silicon nitride diaphragm . 27

Chapter 6

Table 6-1: Properties of Parylene N, C and D.. 2

Table 6-2: Environmental influences on Parylene C/Teflon AF diaphragms..................... 5

Table 6-3: Characteristics of MEMS electret microphone w/ Parylene C diaphragm...... 13

Table 6-4: Nitride diaphragm vs. Parylene diaphragm in MEMS electret microphones.. 14

Chapter 7 (no tables)

Chapter 1
Introduction

1.1 Motivation

Electret condenser microphones have been around for almost half a century. They are used in a wide variety of devices ranging from telephones to hearing aids. Over the past 40 years some advances have been made in microphone design. This has resulted in slight improvements in microphone sensitivity, bandwidth, ruggedness, and signal-to-noise ratio, while moderately reducing the size and power requirements.

Today, almost all portable devices which incorporate acoustic sensors, such as hearing aids and cell phones, use electret microphones because of favorable characteristics such as: self-biasing (requires no external power supply), high sensitivity, wide-band frequency response, vibration resistance, low noise and stability in the environment. However, the modular nature and primitive manufacturing techniques of today's electret microphones has been a limiting factor in making them smaller, cheaper, more reliable and better performing. This is because modern electret microphones are still made from discrete mechanical and electrical components that require numerous assembly steps (Figures 1-1). Consequently, small **and** high performing ones are difficult and expensive to manufacture. In many cases hand-assembly is still unavoidable. This piece-wise approach to microphone production is unfavorable in terms of device optimization for small form-factors. A silicon electret microphone fabricated from MEMS techniques eliminates these disadvantages, embraces all the advantages of their conventional brethren, while conferring additional benefits such as:

- a high degree of miniaturization with no or minimal loss in performance
- repeatable and precise dimensional control
- volume manufacturing with a high degree of reproducibility
- ability to array multiple microphones on the same substrate
- ability to integrate with on-chip microelectronics
- freedom to choose from a wide range of materials and processing techniques

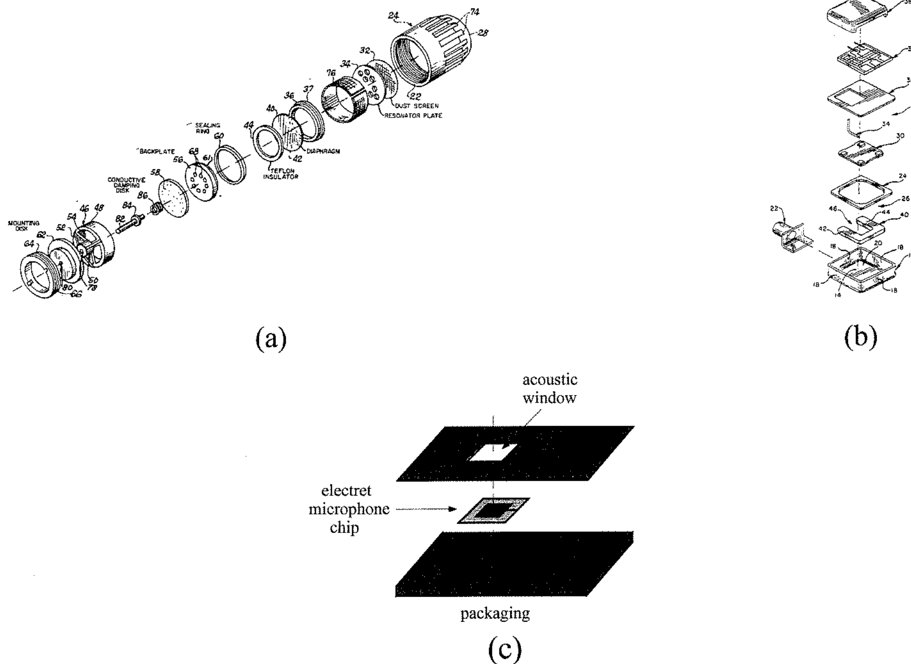

Figure 1-1. Conventional electret microphones vs. MEMS electret microphone. (a) Electro-Voice electret microphone [1], (b) Knowles hearing aid electret microphone [2], and the (c) embodiment of a MEMS electret microphone that is small in size and has minimal assembly requirements other than packaging.

There are currently no commercially available MEMS electret microphones on the market. Knowles Electronics LLC [3], Siemens Semiconductors of Siemens AG [4] and Lucent Technologies Inc. [5] have the technology to manufacture MEMS microphones that can be integrated with microelectronics, but all these devices are non-electret (require an external bias/power supply). This increases overall system size, increases power consumption, degrades microphone noise performance and is generally less favorable for use in portable electronics applications. Almost 99% of all acoustic-based portable electronic devices use conventional (non-MEMS) electret microphones that are incapable of being fully integrated with microelectronics and are difficult to miniaturize cheaply and effectively. In the near future, traditional electret microphones will have a hard time fulfilling the new stringent miniaturization and integration requirements. The

MEMS electret microphone technology described in this thesis was developed as a first step to take full advantage of this new acoustic sensing opportunity.

1.2 Micro Electro Mechanical Systems (MEMS)

Traditionally, silicon and other semiconductor materials have been used to fabricate electrical devices such as transistors [6] and diodes for use in integrated circuits [7]. In these examples, the semiconductor material is utilized for its *electrical* properties only. Since the 1980s, extensive research has been conducted on utilizing the *mechanical* properties of these same semiconductor materials [8]. This effort has resulted in the birth of a new and rapidly growing technology platform called Micro Electro Mechanical Systems (MEMS).

MEMS allows millimeter- to micron-sized sensors, actuators, mechanical elements and microelectronics to be built on the same semiconductor substrate [9]. While the electronics are fabricated using integrated circuit (IC) process sequences (e.g., CMOS, Bipolar, or BICMOS), the micromechanical components are fabricated using compatible "micromachining" processes that selectively etch away parts of the silicon wafer or add new structural layers to form the mechanical and electromechanical devices. Bulk micromachining [10] describes the process that selectively etches away large pieces of the bulk substrate leaving behind the desired 3-D micromechanical elements. Surface micromachining [11] describes the sequential deposition and selective removal of thin films that can serve as the structural and/or sacrificial layer. These two MEMS process technologies allow for the fabrication of micromechanical structures such as beams [12], cavities [13], channels [14], membranes [15], nozzles [16], posts and tips using materials such as silicon, silicon dioxide, silicon nitride, polysilicon, various metals and other silicon derivatives. Together with a host of new MEMS technologies such as LIGA [17], plastic injection molding [18], microstereolithography [19], laser micromachining [20], micro electrical discharge machining [21], silicon carbide processes [22] and selective Parylene deposition/etching [23], MEMS promises to revolutionize nearly every product category by bringing together (silicon-based) microelectronics with miniature sensor and actuator technology.

MEMS is truly an enabling technology allowing the development of smart products by augmenting the computational ability of microelectronics with the perception and control capabilities of microsensors and microactuators. For the first time in scientific history, this enables the creation of sophisticated multifunctional microchips that can take input directly from their surrounding environment through a MEMS microsensor (e.g., as sound, heat, moisture, pressure, etc.), process the information through a microelectronic circuit, and relay a response back to the physical environment through a MEMS microactuator (e.g., through force, magnetic field, etc.). The ideal embodiment is for all of this to take place on the same microchip substrate.

Because MEMS devices are built with the same underlying technology and utilize the same infrastructure as that used in the microelectronics industry, they can be effectively miniaturized and mass-produced reliably and cost-efficiently. In the past decade, the United States Defense Advanced Research Project Agency (DARPA) has poured millions of dollars into MEMS research. Since the 1990s, the commercialization of MEMS devices has also developed at a torrid pace. Today, almost all the accelerometers used in car airbag deployment systems are MEMS accelerometers [24]. Many of the most precise pressure sensors used in portable devices are MEMS pressure sensors [25]. Most recently, the biotech industry has embraced MEMS micro-fluidic technology to develop microchip bioassays, gene screening and chemical analysis systems [26]. Booming communication infrastructure companies (such as Lucent Technologies Inc. and Nortel Networks Corp.) are now turning to MEMS technology to develop micro-optical switches [27] that will re-route the packets of light blazing down fiber optic cables around the globe. MEMS devices are beginning to revolutionize the way we interact with our macroscopic and microscopic environments.

As the boom in wireless and voice-driven communication gets under way, miniature acoustic chip systems, such as microphones monolithically integrated with microelectronic circuitry, will eventually serve as the ears of new handheld wireless communication devices, biometric-based computer systems, wearable computers, smart home appliances as well as the guts of the next generation of digital hearing aids. At the heart of these new integrated acoustic sensor systems will hopefully be a MEMS electret condenser microphone.

1.3 Thesis Outline

The aim of this work is to develop miniature, inexpensive, high-quality, self-biasing electret condenser microphones that can be fabricated using Micro Electro Mechanical systems (MEMS) technology. These MEMS electret microphones are to be used in any application where a conventional electret microphone can be used (such as in cell phones, and hearing aids) and in new acoustic sensing applications where current microphone technology cannot be applied (such as in smart cards of the future or in new applications where it is advantageous to integrate microelectronics with the microphone).

Although a complete MEMS electret microphone affords many advantages, there are many components of the technology that need to be developed or refined before a fully functional device can be fabricated. With respect to the MEMS electret microphone history, theory, material selection, design, modeling, fabrication, packaging, testing and performance specs, this thesis is organized as follows:

- Chapter 2 introduces the principle of operation of condenser microphones and explains the theory behind important electret microphone characteristics such as open-circuit sensitivity, frequency response, dynamic range, stability and electret charge induced static diaphragm deflections.
- Chapter 3 reviews the history of conventional and MEMS capacitive microphones.
- Chapter 4 provides the theory and history behind electrets and examines various types of electret materials, formation techniques and charge measurement instruments. It also provides an analysis of the thin film Teflon electret technology that is used in the MEMS electret microphone.
- Chapter 5 details the design, fabrication, testing and analysis of MEMS electret microphones that utilize silicon nitride diaphragms. The performance of three different microphone designs are covered and the characteristics of silicon nitride/Teflon AF composite diaphragms are provided.
- Chapter 6 details the design, fabrication, testing and analysis of MEMS electret microphones that utilize Parylene C diaphragms. The performance of one particular

microphone design is covered and the characteristics of Parylene C/Teflon AF composite diaphragms are provided.

- Chapter 7 summarizes the entire thesis.

1.4 References

[1] T.C. Lininger and Electro-Voice Inc., "Electret Microphone," US Patent 3,944,756, March 1976

[2] K.G. Holesha and Knowles Electronics Inc., "Hearing Aid Microphone with Modified High-Frequency Response," US Patent 5,319,717, June 1994

[3] D. Schafer, S. Shoaf and P. Loeppert, "Micromachined Condenser Microphone for Hearing Aid Use," Technical Digest, IEEE Solid-State Sensor and Actuator Workshop, pp. 27-30, Hilton Head Island, South Carolina, USA, June 1998

[4] J. Lipper, "Siemens Licenses Silicon Micromachined Microphone Chip," European Microsystems Technology Online, January 5, 1998

[5] F. Pardo, R. Boie, G. Elko, R. Sarpeshkar and D.J. Bishop, "All-Surface-Micromachined Si Microphone," Technical Digest 10th International Conference on Solid State Sensors and Actuators (Transducers '99), pp. 1068- 1069, Sendai, Japan, June 1999

[6] Fairchild Semiconductor Corp, http://www.Fairchildsemi.com/company/history.html

[7] Texas Instruments Inc., http://www.ti.com/corp/docs/kilbyctr/jackbuilt.shtml

[8] K.E. Petersen, "Silicon as a Mechanical Material," Proceedings of the IEEE, Vol. 70 (5), pp. 420-457, May 1982

[9] "Special Issue: Integrated Sensors, Microactuators and Microsystems (MEMS)," Proceedings of the IEEE, August 1998

[10] G.T.A. Kovacs, N.I. Maluf and K.E. Petersen, "Bulk Micromachining of Silicon," Proceedings of the IEEE, Vol. 86, No. 8, August 1998

[11] J.M. Bustillo, R.T. Howe and R.S. Muller, "Surface Micromachining for Microelectromechanical Systems," Proceedings of the IEEE, Vol. 86, No. 8, August 1998

[12] W.H. Hsieh, M. Lucas, C.R. Marsh, S. Wu, C.I. Grosjean and Y.C. Tai, "A Novel Silicon Holder for Three-Point Bending of Micro Silicon Beams," 1996 ASME Mechanics and Materials Conference

[13] M. Madou, "Fundamentals of Microfabrication," CRC Press, Boca Raton, 1997

[14] E.B. Arkilic, M.A. Schmidt and K.S. Breuer, "Gaseous Slip-Flow in Long Microchannels," Journal of Microelectromechanical Systems, Vol 6 (2), pp. 167-178, 1997

[15] W.H. Hsieh, T.Y. Hsu and Y.C. Tai, "A Micromachined Thin Film Teflon Electret Microphone," Technical Digest 9th International Conference on Solid State Sensors and Actuators (Transducers '97), Vol. 2, pp. 425-428, Chicago, USA, June 1997

[16] S. Wu, J. Mai, Y.C. Tai and C.M. Ho, "Micro Heat Exchanger Using MEMS Impinging Jets," Proc. 12th Annual International Workshop on Micro Electro Mechanical Systems, pp. 171-176, Orlando, USA, January 1999

[17] A. Rogner, W. Ehrfeld, D. Munchmeyer, P. Bley, C. Burbaum and J. Mohr, "LIGA-Based Flexible Microstructures for Fiber-Chip Coupling," Journal of Micromechanics and Microengineering, Vol. 1 (3), pp. 167-170, 1991

[18] R.C. Anderson, G.J. Bogdan and R.J. Lipshutz, "Miniaturized Genetic-Analysis System," Technical Digest, IEEE Solid-State Sensors and Actuators Workshop, pp. 258-261, Hilton Head Island, South Carolina, USA, June 1996

[19] K. Ikuta and K. Hirowatari, "Real Three-Dimensional Micro Fabrication Using Stereo Lithography," Proceedings of IEEE Workshop on Micro Electro Mechanical Systems, MEMS '93, pp. 42-47, Fort Lauderdale, USA, 1993

[20] T.R. Anthony, "Diodes Formed by Laser Drilling and Diffusion," Journal of Applied Physics, Vol. 53, No. 12, pp. 9154-9164, December 1982

[21] T. Masaki, K. Kawata and T. Masuzawa, "Micro Electro-Discharge Machining and Its Applications," Proceedings of IEEE Workshop on Micro Electro Mechanical Systems, MEMS '90, pp. 21-26, Napa Valley, USA, 1990

[22] A.J. Fleischman, S. Roy, C.A. Zorman and M. Mehregany, "Polycrystalline Silicon Carbide for Surface Micromachining," Proceedings of IEEE Workshop on Micro Electro Mechanical Systems, MEMS '96, pp. 234-238, San Diego, USA, 1996

[23] X.Q. Wang, "Integrated Parylene Micro Electro Mechanical Systems (MEMS)," Ph.D. Thesis, Caltech, 2000

[24] L. Spangler and C.J. Kemp, "ISAAC - Integrated Silicon Automotive Accelerometer," Technical Digest 8th International Conference on Solid State

Sensors and Actuators (Transducers '95), pp. 585-588, Stockholm, Sweden, June 1995

[25] S. Sugiyama, T. Suzuki, K. Kawahata, K. Shimaoka, M. Takigawa and I. Igarashi, "Micro-Diaphragm Pressure Sensor," Proceedings of IEEE International Electron Devices Meeting, pp. 184-187, Los Angeles, USA, December 1986

[26] A. Manz, N. Graber, H.M. Widmer, "Miniaturized Total Chemical Analysis Systems; A Novel Concept for Chemical Sensing," Sensors and Actutaors, B1, pp. 244-248, 1990

[27] P. Heywood, "The Optical Future: Optical Switching Fabric," Light Reading Online, www.lightreading.com/document.asp?doc_id=355&page_number=9, March 29, 2000

Chapter 2

Electret Condenser Microphone Theory

2.1 Principle of Operation

In its simplest form, a condenser microphone consists of two parallel conductive plates separated by an air gap. Together, these plates form the electrodes of an air capacitor (condenser) as shown in Figure 2-1. The lower plate is rigid, whereas the top plate is a very thin and flexible diaphragm that can be deflected by impinging sound waves. The diaphragm can be a thin metal membrane or a metallized dielectric membrane. The backplate usually consists of a planar metal electrode resting on a solid electrically insulating substrate.

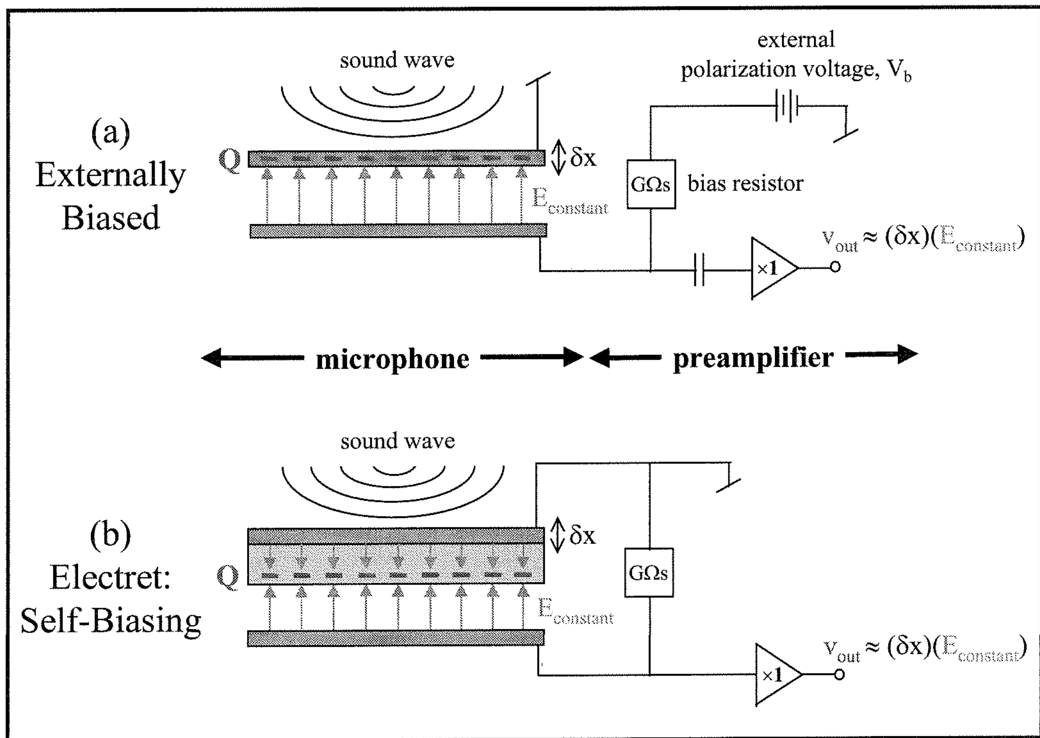

Figure 2-1. Externally biased and self-biasing (electret) condenser microphones.

The plates are polarized either by an external voltage source, V_b, or an internal voltage source (electret). An external resistor of a few GΩ is placed across the parallel

plates to ensure an essentially constant charge, Q, on the microphone, even when its capacitance changes due to an impinging sound pressure on the diaphragm. Since the fixed charge, Q, sets up a fixed electric field, $E_{constant}$, between the diaphragm and backplate, when an impinging sound pressure causes the diaphragm to displace a small distance, δx, relative to the stationary backplate, a small output AC voltage, $v_{out} = (\delta x)(E_{constant})$, results across the air gap. Here we assume that the diaphragm is moving like a rigid piston.

This small AC voltage can be detected by an external, high input impedance, low input capacitance, unity-gain preamplifier (Figure 2-1). Since the capacitive microphone has a very large output impedance, the preamplifier also acts as an impedance converter for coupling to the input of other accessory equipment (such as a gain stage).

In the case of a condenser microphone, the output voltage of the system is proportional to the displacement of the moveable diaphragm. In other words, under normal operating conditions, there is a linear relationship between output voltage and diaphragm displacement.

2.1.1 Externally Biased

Figure 2-1a illustrates the schematic representation of an externally biased condenser microphone. The value of the bias resistor is typically 1 to 10 GΩ [1] and the AC output voltage produced is separated from the polarization voltage by a blocking capacitor (usually contained in the preamplifier). The polarization voltage is on the order of 10V to 200V and comes from an external power supply [2]. Because hundreds of volts may be applied across an air gap that is only a few tens of microns wide, the field strengths in the air gap may approach or even exceed the break down field strength for air. Consequently, the diaphragm and backplate must have particle free, very flat and high quality surfaces so as to prevent or minimize noise due to arching in the air gap.

Externally biased microphones are favorable under operating conditions where small size and low power requirements are not important criteria. Since they are easier to make, they are also usually cheaper than equivalent self-biasing (electret) microphones. For acoustic measurements that are done indoors and/or require several microphones, externally biased microphones provide the economical solution.

However, adverse noise performance may be encountered while using externally biased condenser microphones if the external bias voltage, V_b, is itself noisy. This is because the rail noise may propagate to the microphone output. This often occurs when externally biased MEMS condenser microphones are used in portable devices, such as hearing aids, and a charge pump is used to raise the single-digit battery voltage to a noisier double-digit one to bias the microphone [3].

2.1.2 Electret: Self-Biasing

Self-biasing condenser microphones contain an electret (Figure 2-1b). The electret consists of a stabilized, highly insulating, chemically inert and charge-holding dielectric material (often a polymer) that can be applied to the diaphragm or backplate. The electret contains trapped mono-polar electrical charges, Q, which then produce a fixed electric field, $E_{constant}$, across the air gap. Usable electrets are typically polymers that can trap charges for tens to hundreds of years under the range of operating conditions of the microphone. The sign of the trapped charge is dependent on the type of electret material used. Some materials are better at trapping negative charges, while others are better at trapping positive charges. Like externally biased microphones, the AC output voltage, v_{out}, is proportional to the electric field in the air gap.

The fixed charge is usually located near the electret-air interface. This fixed charge attracts image charges of the opposite sign. These image charges reside on both the diaphragm and backplate, and their relative distribution depends on the ratio between the thickness of the electret and that of the air gap. The result is that two electric fields are produced in the microphone, one across the air gap and one across the electret. As in externally biased microphones, these electric fields must remain constant during the operation of the device. Thus, a very high loading resistance (usually several GΩ) is required across the microphone so that output voltages produced do not lead to any significant interchange of image charge between the two microphone electrodes. Furthermore, since the electret acts as a series capacitor for the active air gap capacitance, electret microphones have lower capacitances than identically-sized externally biased condenser microphones.

Electret microphones are generally more complex to manufacture than their externally biased counterparts, so they tend to cost more. However, for acoustic sensing applications where small form factor (such as in hand-held devices), low noise (since no external bias is required) and low power (such as battery operated instruments) are important criteria, electret microphones are the ideal solution.

For its ingenious design, functional simplicity and challenge of manufacturing using MEMS processes, electret condenser microphones will be the main topic of study for the remainder of this thesis. From this point onwards, they will simply be referred to as 'electret microphones.'

2.2 Electret Microphone Characteristics

The schematic representation of the electret microphone structure in Figure 2-1b will not yield a working device, nor will it allow us to fully understand the details of its operation. Many other structural features are present in an actual electret microphone (both conventional and MEMS). The schematic in Figure 2-2 illustrates typical components.

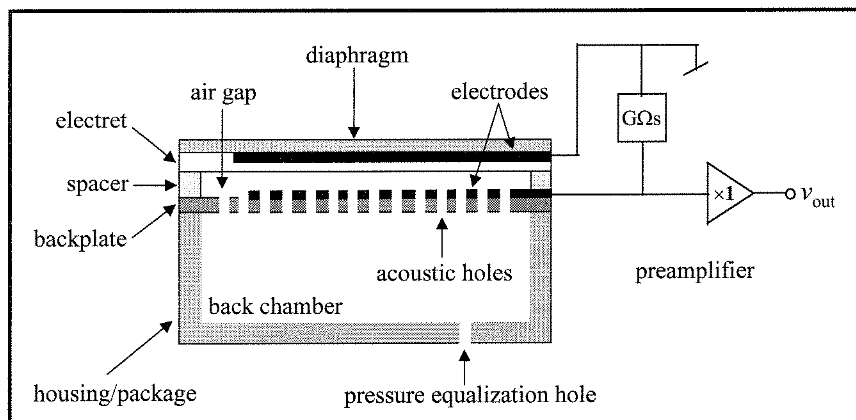

Figure 2-2. Schematic cross-section of an electret microphone w/ housing.

The microphone diaphragm may be a thin metal membrane or a metalized dielectric membrane. For the sake of calculations in this chapter, we will assume that the diaphragm electrode area is the same as the deformable diaphragm area. Since the sensitivity of the microphone is inversely proportional to the stiffness of the diaphragm

system, the tension of the diaphragm must be carefully controlled. When the electret is a structural part of the diaphragm, as in Figure 2-2, the mechanical properties of the electret material will also contribute to the behavior of the diaphragm. For this reason, some electret microphone designs place the electret on the backplate so that diaphragm properties can be controlled independently of electret properties. In the MEMS electret microphone designs detailed in this thesis, the electret has been placed on the diaphragm for ease of backplate fabrication.

The backplate electrode and electrically insulating backplate structure is constructed with an array of through-holes to allow air in the air gap to flow to and from the back chamber when the diaphragm is displaced. The diameter of each acoustic hole is generally larger than the air gap thickness. In the absence of these acoustic holes, the compression and expansion of air in the air gap during microphone operation would reduce diaphragm movement - an effect called 'squeezed-film damping' [4]. This effect becomes more pronounced at higher frequencies because air in the air gap cannot travel across the air gap fast enough, to exit or enter the back chamber through the acoustic holes. This decreases the effective compliance of the diaphragm and provides another path for energy to leave the system. The number and distribution of acoustic holes must be carefully controlled because too many holes (low squeezed-film damping) reduces the amount of electrode area that can pick up image charge, while too few holes (large squeezed-film damping) increases the effective stiffness of the diaphragm. Both effects reduce microphone sensitivity. For the sake of calculations in this chapter, we will assume that the backplate electrode covers the entire usable backplate area.

The diaphragm and backplate are typically separated by an electrically insulating spacer. The thickness of this spacer determines the capacitance of the microphone as well as the degree of squeezed-film damping. Because a microphone is designed to measure differential pressure across its diaphragm, the air gap needs to be isolated from ambient pressure differentials by a small housing/package. The housing forms the back chamber whose volume is much larger (usually at least 100 times) than the volume of the air gap. This provides a large reservoir of air to and from which air in the air gap can flow with minimal resistance. The back chamber is further exposed to atmospheric pressure by a small hole that serves to equalize the static (DC) differential pressure across

the diaphragm. In this way, the microphone performs as an AC acoustic pressure sensor, rather than a DC one.

Now that we have discussed some general structural features of electret microphones, we can look in more detail at the characteristics of these devices. Characteristics such as open-circuit sensitivity, frequency response, dynamic range and long term stability describe the performance of a microphone. This information is invaluable in determining whether a given microphone has been correctly built for the measurement task for which it was chosen.

2.3 Open-Circuit Sensitivity

Electret microphones are energy transducers. They convert sound energy into an electrical form. They detect changes in sound pressure at the diaphragm and present a voltage variation at the output terminals. The input sound pressure level (amplitude) is typically expressed in units of dB SPL. The expression is as follow: Sound Pressure Level (dB SPL) = 20 Log $_{10}$ { rms pressure in Pa / 20×10^{-6} Pa }. The dB scale is logarithmic and uses the human threshold of hearing (20×10^{-6} Pa) as the reference level. Figure 2-3 illustrates familiar sounds and their corresponding sound pressure levels in Pa and dB SPL.

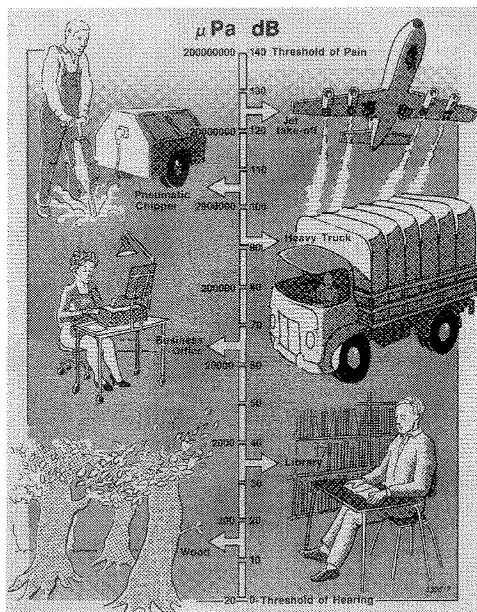

Figure 2-3. Sound pressure level of familiar sounds [5].

The open-circuit sensitivity, S_{oc}, of an electret microphone describes the output voltage that can be expected for every unit of sound pressure acting on the diaphragm when the microphone is **not** attached to a preamplifier (Figure 2-4). The conventional units are V/Pa at the stated frequency. Open-circuit sensitivity is the quantity to which many other microphone characteristics are referenced (e.g., frequency response). Typical commercial (non-MEMS) electret microphone values are 1 to 50 mV/Pa. The single digit values are for conventional electret microphones (less than $1 each) that are used in consumer electronic devices such as cordless phones and toys [6], while the high double-digit values are for reference microphones [7] that are often built by hand and can cost hundreds of dollars each. In between this range are hearing aid [8] and performing art microphones ($8-15 each) that are small, yet have open-circuit sensitivities in the teens of mV/Pa.

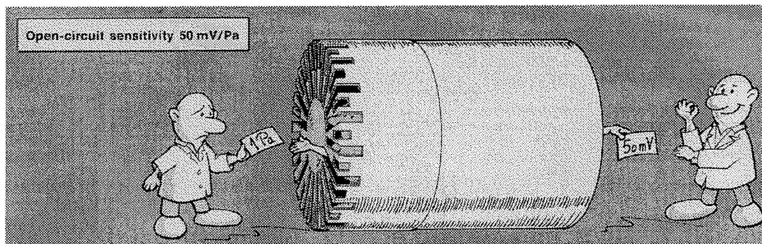

Figure 2-4. Open-circuit sensitivity [5].

The open-circuit sensitivity can be thought of as the product of two separate microphone parameters: the mechanical sensitivity, S_m, and the electrical sensitivity, S_e. Thus,

$$S_{oc} = (S_m)(S_e) \quad [\mathrm{V/Pa}] \tag{2-1}$$

The mechanical sensitivity of the microphone is the movement of the diaphragm in response to an incident sound pressure, dx/dP, and is given in m/Pa. The electrical sensitivity is the output voltage that can be expected for every unit displacement of the diaphragm, dV/dx, and is given by the electric field in the air gap with the units V/m. Below is a detailed analysis of these two components.

2.3.1 Mechanical Sensitivity

Diaphragms are typically made of rectangular or circular membranes. Since circular diaphragms are difficult to fabricate in bulk-micromachining processes (that which is

used in this thesis) the diaphragm theory here will only refer to square membranes of homogeneous materials. We will also assume that all electret microphone diaphragms experience residual tensile stress - a requirement for high frequency response (see section 2.4.2).

P. Scheeper [9] found that a square microphone diaphragm can be described with the membrane model (where the effect of bending can be neglected) if:

$$\left(\frac{\sigma}{E}\right)\left(\frac{a}{t}\right)^2 >> 5 \tag{2-2}$$

where:

σ: residual tensile stress in the membrane [N/m^2]

E: Young's modulus of the membrane material [N/m^2]

a: length of one side of square membrane [m]

t: thickness of membrane [m]

Since the MEMS microphone diaphragms described in this thesis are very thin (a few microns thick) compared with the length of the diaphragm (a few millimeters long), (a/t) is on the order of 10^3. Furthermore, since the Young's modulus of most diaphragm materials used are on the order of 10^{11} N/m^2, the residual tensile stress needs only be larger than 5×10^5 N/m^2 for the membrane model to be valid. Because most MEMS microphone diaphragms have tensile stresses on the order of 10^6 to 10^7 N/m^2, the membrane model can be correctly applied since equation (2-2) is satisfied.

Figure 2-5 shows the maximum deflection, h, at the center of a square membrane due to an applied static homogeneous pressure, P. Using an energy minimization method that incorporates the strain energy due to both deformation and internal tensile stress, we get the equation [10]:

$$P = \frac{C_1 \sigma t h}{a^2} + \frac{C_2 E t h^3}{a^4} \tag{2-3}$$

where σ, E, a and t are defined above and:

P: applied pressure [Pa]

h: maximum defection of the membrane [m]

C_1: 3.04

C_2: 1.83

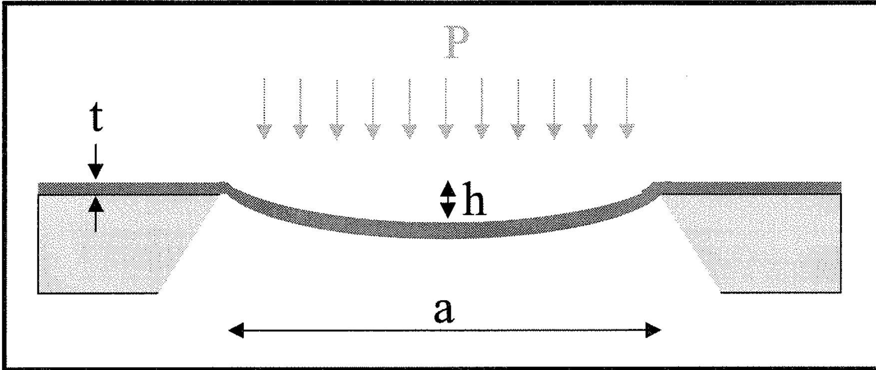

Figure 2-5. Deflection of a square membrane.

It can be seen from equation (2-3) that the relationship between the applied pressure and deflection of the membrane is non-linear for large deflections. Calculations by other authors [9], however, show that equation (2-3) can be linearized with reasonable accuracy (<10% error) if we assume that the compression of air in the air gap can be ignored, that $t/a << 1$ and that the deflections are very small (less than the several micron thick air gap). The load deflection equation (2-3) can then be rewritten as:

$$P \approx \frac{3.04 t \sigma h}{a^2} \tag{2-4}$$

Thus, the mechanical sensitivity of the microphone is:

$$S_m = \left(\frac{a^2}{3.04 t \sigma} \right) \left(\frac{1}{2} \right) \quad \text{[m/Pa]} \tag{2-5}$$

The factor of 1/2 is used because we assume the microphone diaphragm acts as a rigid piston that only moves half the maximum displacement of the actual diaphragm.

Since most MEMS electret microphone diaphragms are composite membrane structures rather than one homogeneous material, the value for the residual tensile stress, σ, is empirically measured. The thickness, t, would be taken as the effective thickness of the main stress-contributing material that would result in the same total mass of the composite diaphragm structure (electret + metal electrode + diaphragm material).

2.3.2 Electrical Sensitivity

If we assume the diaphragm is a conductor with piston-like movement, the output voltage of an electret microphone is proportional to the homogeneous electric field in the air gap, $E_{constant}$. If we model the microphone electret system in equilibrium as shown in Figure 2-6, the electric field in the air gap becomes [11]:

$$S_e = E_{constant} = \frac{\left(\frac{\sigma_e s_e}{\varepsilon_0 \varepsilon_e}\right)}{\left(\frac{s_e}{\varepsilon_e} + s_a\right)} \quad [\text{V/m}] \tag{2-6}$$

where:

σ_e: electret surface charge density [C/m^2]

s_e: electret thickness [m]

ε_e: relative dielectric constant of electret [unitless]

ε_0: permittivity of free space [8.85×10^{-12} F/m]

s_a: air gap thickness [m]

S_e: electrical sensitivity of the microphone [V/m]

Since the microphone electrical sensitivity, S_e, is the output voltage that can be expected for every unit displacement of the diaphragm, equation (2-6) is also equal to S_e. The term $(\sigma_e s_e/\varepsilon_0\varepsilon_e)$ in (2-6) is the equivalent voltage of an electret with surface charge density σ_e. If the electret is omitted and an external bias of this value is used, the electric field strength in the air gap will be larger since the term (s_e/ε_e) in equation (2-6) is also omitted.

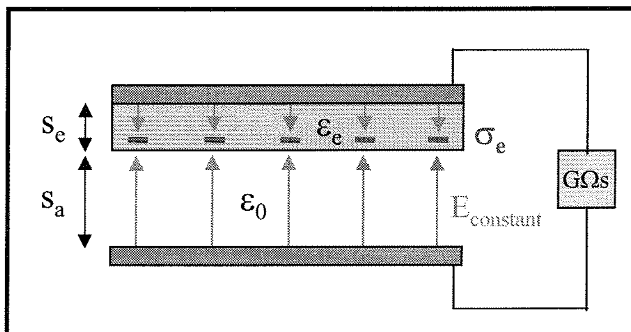

Figure 2-6. Model of microphone electret system in equilibrium.

2.3.3 Loaded Sensitivity and Electrical Response

When the electret microphone is **not** connected to a preamplifier, the open-circuit sensitivity, S_{oc}, can be expressed as:

$$S_{oc} = (S_m)(S_e) = \left(\frac{a^2}{3.04t\sigma 2}\right)\left(\frac{\dfrac{\sigma_e s_e}{\varepsilon_0 \varepsilon_e}}{\dfrac{s_e}{\varepsilon_e} + s_a}\right) \quad \text{[V/Pa]} \tag{2-7}$$

where the variables are the same as the ones given in equations (2-5) and (2-6) above.

However, when the microphone is packaged and connected to a preamplifier that has a gain G (usually $\cong$ 1), loading/input resistor, R_i, input capacitance, C_i, and stray capacitance due to the housing/packaging, C_s, the open circuit sensitivity of the microphone, S_{oc}, must be multiplied by the gain of the preamplifier, G, and the gain of this electrical loading network, $H_e(\omega)$, to obtain the combined microphone and preamplifier sensitivity, S_t.

C_s and C_i are typically obtained from experimental measurements and preamplifier data sheets, respectively, while the electret microphone capacitance, C_m, can be calculated during the initial design of the microphone from the equation:

$$C_m = \frac{\left(\dfrac{\varepsilon_0 \varepsilon_e A}{s_e}\right)\left(\dfrac{\varepsilon_0 A}{s_a}\right)}{\left(\dfrac{\varepsilon_0 \varepsilon_e A}{s_e}\right) + \left(\dfrac{\varepsilon_0 A}{s_a}\right)} \quad \text{[F]} \tag{2-8}$$

where s_e, ε_e, ε_0, s_a are the same variables as in equation (2-6) and A is the electrode area of the microphone (assumes diaphragm and backplate electrodes are the same size).

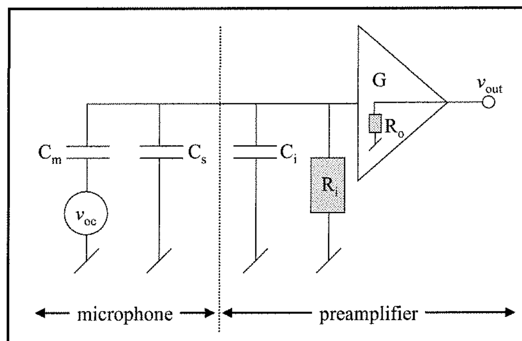

Figure 2-7. Schematic of microphone and preamplifier circuit.

Figure 2-7 is a schematic of the microphone and preamplifier circuit. The microphone is modeled as a small-signal voltage source, v_{oc}, in series with the microphone capacitance, C_m. R_o is the output impedance of the preamplifier and v_{out} is its output voltage. The response of the above circuit is given by the transfer function:

$$H_e(\omega) = \frac{v_{out}}{v_{oc}} = \frac{j\omega R_i C_m}{1 + j\omega R_i (C_s + C_m + C_i)} \tag{2-9}$$

where ω is the frequency in rad/s. The electrical loading due to equation (2-9) acts as a high-pass filter that has a lower corner frequency:

$$f_{e-lower} = \frac{1}{2\pi R_i (C_s + C_m + C_i)} \quad \text{[Hz]} \tag{2-10}$$

For the R_i, C_s, C_m and C_i values of most MEMS electret microphone-preamplifier systems, $f_{e\text{-}lower}$ is usually below 20 Hz, a suitable frequency floor for audio-frequency range measurements (20 Hz to 20 kHz). For frequencies above $f_{e\text{-}lower}$, and below the electronic upper cut-off frequency of the preamplifier (usually over 100 kHz), equation (2-9) becomes the frequency independent function:

$$H_e = \frac{C_m}{C_s + C_m + C_i} \tag{2-11}$$

Ideally, H_e should be as close to 1 as possible to minimize the electrical loading due to the preamplifier and housing. This can be achieved by making the microphone capacitance, C_m, as high as possible while minimizing the preamplifier input capacitance, C_i, and stray capacitance, C_s. For MEMS electret microphones, however, this is usually a challenge since the small size of the device results in very low values for C_m (on the order of tens of pF). C_s is usually a few pF and C_i can even be lower than 1 pF for well-designed preamplifiers.

2.3.4 Total Microphone and Preamplifier Sensitivity

When equation (2-5), (2-6) and (2-11) are co-multiplied with the gain of the preamplifier, G, the total sensitivity, S_t, of the combined electret microphone-preamplifier system in the flat-band portion of its response becomes:

$$S_t = S_{oc}H_eG = S_eS_mH_eG = \left\{ \left(\frac{a^2}{3.04t\sigma 2} \right) \left(\frac{\frac{\sigma_e s_e}{\varepsilon_0 \varepsilon_e}}{\frac{s_e}{\varepsilon_e} + s_a} \right) \left(\frac{C_m}{C_s + C_m + C_i} \right) G \right\} \text{ [V/Pa]} \quad (2\text{-}12)$$

Since any electret microphone can be used with different types of preamplifiers (each with different C_i, R_i and G), the performance criteria that is most often quoted when measuring individual microphone performance is still open-circuit sensitivity, S_{oc}, since this parameter is unique to the microphone itself.

2.4 Frequency Response

The frequency response of a near-ideal electret microphone (without preamplifier) is shown in Figure 2-8. Above the low frequency cut-off, f_L, and below the high frequency cut-off, f_H, the open-circuit sensitivity should be nearly flat (± a few dB). For measurements in the normal audio range, f_L should be less than 20 Hz and f_H should be higher than 10 kHz. The best 1/2-inch reference electret microphones by Bruel & Kjaer have flat responses (± 2 dB) from 6 Hz to 20 kHz [12]. The smallest hearing aid electret microphone (3.63 × 3.63 × 1.76 mm^3) by Knowles Electronics has a relatively flat response (± 5 dB) between 150 Hz and 5 kHz [13]. The low and high frequency cut-offs are determined by the mechanical design of the microphone. These two frequency response limits are more closely examined in the following subsections.

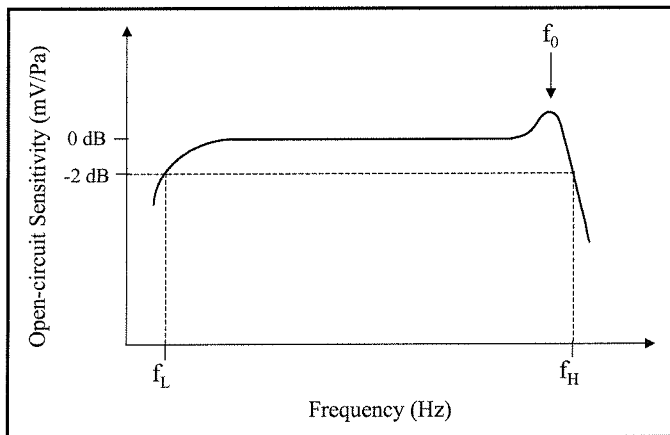

Figure 2-8. Typical frequency response of an electret microphone.

2.4.1 Low-Frequency Cut-Off

At low frequencies, the frequency response of an electret microphone (without a preamplifier) is influenced by the size and position of the static pressure equalization hole - whose purpose is to prevent the diaphragm from responding to ambient DC pressure level changes. At most frequencies in the audio range, this hole is small enough for its acoustic resistance to prevent sound waves impinging on the diaphragm from concurrently entering the back chamber and air gap. However, at lower frequencies, a small portion of the sound wave acting on the diaphragm is able to enter the back chamber and air gap through the pressure equalization hole. As a result, this low frequency sound pressure starts to oppose the motion of the diaphragm from the inside of the microphone causing the frequency response curve to tail off for lower and lower frequencies. The low frequency cut-off, f_L, is typically defined as the frequency at which the response curve has dropped 2-3 dB below the 0 dB open-circuit sensitivity reference level (Figure 2-8). At very low frequencies, the decay slope reaches a maximum of 20 dB/decade [1].

When the electret microphone is connected to a preamplifier, the high-pass filter lower corner frequency, $f_{e\text{-}lower}$ (see section 2.3.3), will also come into effect. This electrical lower cut-off frequency can be lower or higher than the mechanically controlled lower cut-off frequency, f_L. In general microphone design, it is more favorable to pick a preamplifier system such that $f_{e\text{-}lower}$ is less than f_L.

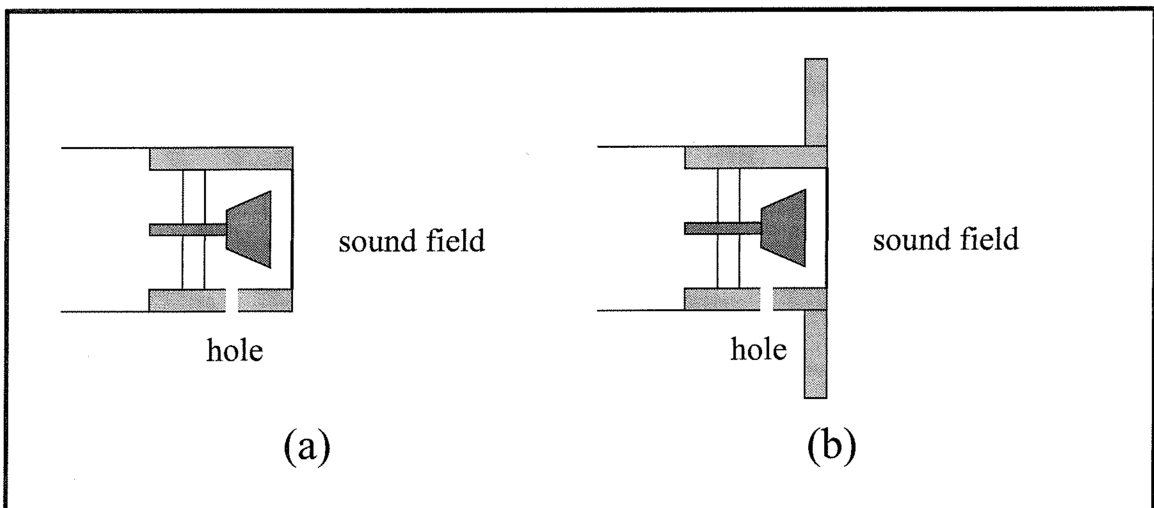

Figure 2-9. Pressure equalization hole positions. (a) Hole exposed. (b) Hole unexposed.

In most conventional electret microphone structures, the pressure equalization hole is exposed to the sound field (Figure 2-9a). Under these circumstances the hole will equalize the sound pressure in front and behind the diaphragm at low frequencies and the microphone response will drop off. However, in many MEMS electret microphone designs, where the entire microphone structure is encapsulated by an external package, the pressure equalization hole is sometimes not directly exposed to the sound field (Figure 2-9b). In this case, the frequency response does not fall with decreasing frequency, but rather increases (Figure 2-10). This is because the fraction of stiffness (ratio between air gap stiffness and total diaphragm system stiffness) which is due to the reactive pressure in the internal cavities of the microphone becomes smaller as this is equalized through the hole.

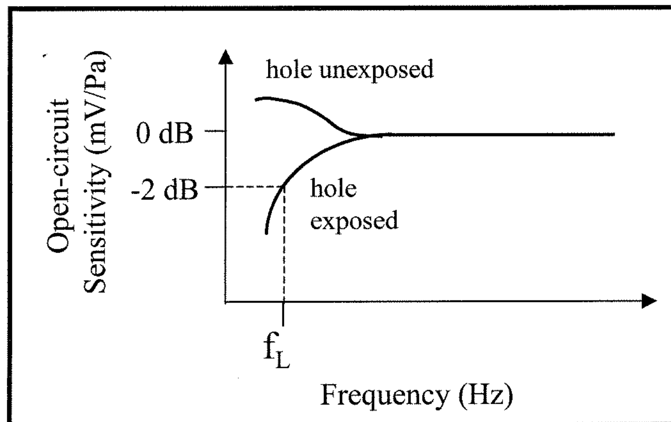

Figure 2-10. Low frequency response vs. location of pressure equalization hole.

In most MEMS electret microphone designs, it is difficult to predict the low frequency cut-off, f_L, before making the device because of complex packaging and assembly configuration issues. Consequently, the design, size and location of the pressure equalization hole is usually adjusted in an iterative manner based on measured experimental data.

2.4.2 High-Frequency Cut-Off

The high frequency cut-off of an electret microphone (without preamplifier) is mainly determined by the fundamental resonant frequency of the diaphragm. If we use the membrane model to describe the mechanical behavior of a square diaphragm (see

section 2.3.1), the fundamental resonant frequency, f_0, can be described with equation [14]:

$$f_0 = \sqrt{\frac{\sigma}{2a^2\rho}} \qquad \text{[Hz]} \qquad (2\text{-}13)$$

where:

σ: residual tensile stress in the membrane [N/m^2]

ρ: density of the membrane material [kg/m^3]

a: length of one side of square membrane [m]

The high frequency cut-off, f_H, is typically defined as the frequency after f_0, at which the response curve has dropped 2-3 dB below the 0 dB open-circuit sensitivity reference level (Figure 2-8).

In MEMS eletcret microphones, the diaphragm resonant frequency is dependent on diaphragm materials as well as the processing history of the device. Since the microphone diaphragm is usually a composite structure, consisting of the electret material, metal electrode and diaphragm material, f_0 is measured experimentally after the diaphragm has been made and before the microphone is assembled. This measurement can also provide the residual tensile stress of a composite microphone diaphragm.

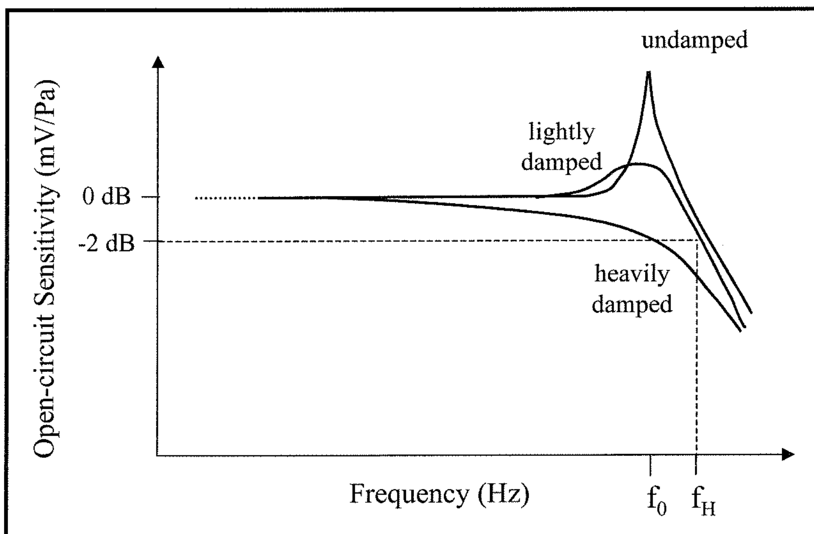

Figure 2-11. Different degrees of microphone response damping.

At the resonant frequency, the sensitivity of the microphone would peak sharply if the diaphragm is undamped. This is obviously undesirable, but is usually not a problem in actual MEMS electret microphones. Rather, when the diaphragm is placed on top of the microphone backplate, the response of the diaphragm becomes damped due to the compression of air in the small air gap (Figure 2-11). To prevent the microphone response from being too heavily damped (limits flat-band region of response), acoustic through-holes are placed in the microphone backplate so as to minimize the squeezed-film effect first defined in section 2.2. The through-holes allow air in the air gap to flow to and from the back chamber when the diaphragm is displaced. Because the size of the acoustic holes is generally much larger than the air gap thickness, the resistance of the air travelling through the acoustic holes can be neglected with respect to the resistance of the air travelling through the air gap.

Skvor [15] calculated the mechanical air-streaming resistance, R_a, for air travelling through the air gap to the through-holes. Assuming the diaphragm moves like a rigid piston, the backplate is rigid, the air flow is laminar, the air behaves as a Newtonian fluid, the air in the air gap is incompressible, the air gap thickness is small in comparison with the length of the diaphragm, the air only exits the air gap through the acoustic holes, and all dimensions of the diaphragm are small in comparison to the wavelength of sound, R_a, can be expressed as:

$$R_a = \frac{12\eta_a a^2}{n\pi s_a^3}\left(\frac{1}{4}\ln\frac{1}{F} - \frac{3}{8} + \frac{F}{2} - \frac{F^2}{8}\right) \quad \text{[Ns/m]} \qquad (2\text{-}14)$$

where:

η_a: viscosity of air [17.1×10^{-6} Pa s]

a: length of one side of square diaphragm [m]

n: number of acoustic holes per unit area [m^{-2}]

s_a: air gap thickness at zero applied pressure [m]

F: fraction of backplate area occupied by acoustic holes [unitless]

Since an electret microphone can be modeled as a 2nd order damped spring-mass system with mass M, stiffness constant K, and mechanical air-streaming resistance R_a, the

electret microphone can also be considered as two 1st order systems in series if it is damped strongly enough [16]. This criteria is fulfilled if:

$$\frac{0.5R_a}{\sqrt{MK}} \geq 1 \qquad (2\text{-}15)$$

where R_a is given by equation (2-14) and:

M: diaphragm mass [kg]

K: stiffness constant of the diaphragm - given by ($13.57\sigma t$) for a square diaphragm [N/m]

σ: residual tensile stress in the diaphragm [N/m^2]

t: effective thickness of the diaphragm [m]

If condition (2-15) is satisfied, the upper cut-off frequency of an electret microphone due to mechanical air-streaming resistance, R_a, becomes:

$$f_{streaming} = \left(\frac{K}{2\pi R_a}\right) \quad \text{[Hz]} \qquad (2\text{-}16)$$

For an electret microphone with fixed diaphragm mechanical properties and physical dimensions, this value can be raised by increasing the backplate acoustic hole density, n, increasing the fraction of backplate area occupied by acoustic holes, F, and by increasing the air gap thickness, s_a. Above $f_{streaming}$, the sensitivity of the microphone decreases by 6 dB/octave. Depending on the degree of diaphragm damping desired, good electret microphone designs try to place $f_{streaming}$ slightly above or below the diaphragm resonant frequency, f_0.

2.5 Dynamic Range

The difference between the lowest and highest measurable sound pressure level in an electret microphone and preamplifier system is called the dynamic range (given in dB SPL). The lower limit is controlled by the preamplifier electrical noise and microphone thermal noise. The upper limit is defined by the clipping of the preamplifier, the non-linearity of diaphragm movement when the microphone is exposed to very high sound pressure levels and/or the non-linear relationship between capacitance and diaphragm displacement. The dynamic range of some Bruel & Kjaer 1/2-inch reference electret

microphones is from 0 dB (the threshold of hearing) to over 140 dB SPL (the threshold of pain) [17]. That of most commercially available hearing aid electret microphones is from 30 dB to above 100 dB SPL [13]. The following subsections will explore the factors that contribute to the noise floor and upper distortion limit of electret microphone-preamplifier systems.

2.5.1 Lower-Limit: Noise Floor

Both electret microphones and preamplifiers produce noise. Under most circumstances, the incident sound pressure at the diaphragm produces signals that are above this noise. However, when the sound pressure drops to lower levels, a point may be reached where the measured sound signal cannot be distinguished from the inherent noise of the microphone-preamplifier system. The measured inherent noise level is dependent on the bandwidth. The broader the measurement bandwidth, the higher the noise level. Filtering can, therefore, allow lower signal levels to be measured. The noise produced by an electret microphone-preamplifier system is given in equivalent SPL (in Pa or dB form). This is obtained by taking the total noise voltage produced at the output of the preamplifier and dividing by the total sensitivity, S_t. In most electret microphone-preamplifier systems, the preamplifier noise dominates at low frequencies, whereas the microphone noise dominates from about 200 Hz to 10 kHz [1].

The noise produced by the electret microphone itself is due to the thermal movement of the diaphragm [18]. The noise pressure, p_n, produced is dominated by the diaphragm acoustic damping resistance, R_d, and is given by:

$$p_n = \sqrt{4kTR_d(\delta f)} \qquad \text{[Pa]} \qquad (2\text{-}17)$$

where:

k: Boltzmanns constant [1.38×10^{-23} Nm/K]

T: absolute temperature [K]

δf: frequency bandwidth [Hz]

R_d: diaphragm acoustic damping resistance that is also equal to (R_a/a^4) [Ns/m^5]

The dB SPL form of equation (2-17) is the 'linear' expression of rms noise pressure since the noise is integrated over the full bandwidth. Another way to specify noise pressure is

to pass the noise signal through an A-weighted filter (inverted U-shaped function centered around 2 kHz) that resembles the response of the human ear. The 'A-weighted' noise level is then expressed as dBA SPL and is significantly lower because of filtering.

In MEMS electret microphones, R_d is often quite large due to the close spacing between the diaphragm and backplate (on the order of several microns). Consequently, a MEMS electret microphone usually sets the higher noise floor when combined with commercial microphone preamplifiers. Microphones with lower noise floors can be designed by increasing the diaphragm size, since R_d varies inversely as the square of the membrane length, a. The noise spectrum at the output terminals of an electret microphone looks like its frequency response.

The preamplifier noise is comprised of two parts: a low frequency component and a broad-spectrum component. The low frequency noise is the thermal noise created by the high value resistor, R_i, in the input circuit, shunted by the capacitance of the microphone, C_m, which has the effect of low-pass filtering the noise signal. This noise voltage is therefore proportional to the preamplifier input resistance and absolute temperature, and inversely proportional to the frequency as well as to the microphone capacitance. The broad-spectrum noise, on the other hand, is caused by the active part of the preamplifier input stage, namely the FET channel noise. This component becomes responsible for the preamplifier noise from about 1 kHz and above [1].

When MEMS electret microphones are used with commercially available preamplifiers, the noise performance of the preamplifier is usually known and can be used to help determine the noise of the MEMS microphone itself. When the preamplifier is built from off-the-shelf components or monolithically from on-chip transistors, the designer must first measure the noise criteria of the preamplifier.

2.5.2 Upper-Limit

When a very high sound pressure level is incident on the microphone diaphragm, both the microphone and preamplifier may distort the output signal. However, when MEMS electret microphones are used in conjunction with commercial microphone preamplifiers, the preamplifier distortion may generally be ignored since this is usually much lower than the microphone distortion [1].

In most MEMS electret microphones, the non-linear membrane elasticity at high sound pressure levels is the **less** dominant harmonic distortion source [1]. This is because the diaphragm displacement is usually small enough to be linearized. Rather, the main microphone distortion is caused by the static stray capacitance, C_s, and preamplifier input capacitance, C_i, that is in parallel with the dynamic diaphragm capacitance, C_m (Figure 2-7). The static capacitance generates a second harmonic distortion that increases proportionally with the sound pressure level, as well as a third harmonic that varies as the sound pressure level squared. Harmonic distortion that arises from the microphone itself is usually measured as a percentage of the amplitude of the main signal at a given frequency and sound pressure level. This value can be easily obtained using modern spectrum analyzers. Furthermore, since the distortion limit is related to the displacement of the microphone diaphragm, microphones with larger-sized and/or lower tensile-stressed diaphragms will produce more distortion than microphones with smaller-sized and/or higher tensile-stressed diaphragms, at the same sound pressure level (Figure 2-12). It is because of the harmonic distortion criteria that miniature MEMS electret microphones cannot be made more sensitive simply by decreasing the diaphragm tension, while keeping the area of the diaphragm the same. At some point the harmonic distortion will simply become intolerable even at moderate sound pressure levels.

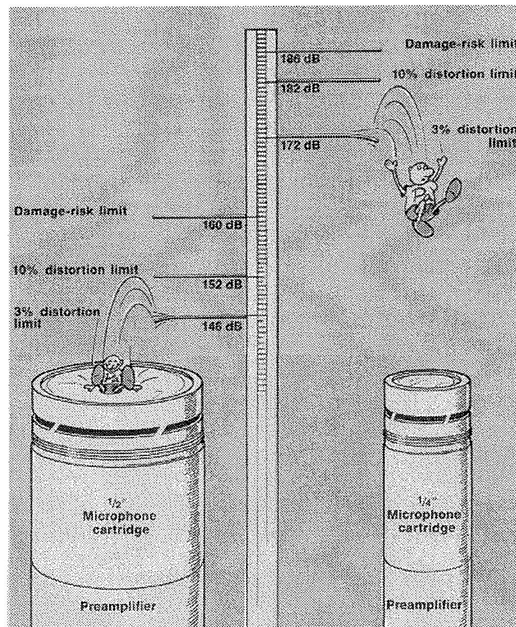

Figure 2-12. Upper dynamic range of different size electret microphones [5].

Bruel & Kjaer specifies the upper dynamic range of an electret microphone (without preamplifier) as the 3% distortion limit. The operation of the microphone can be used above this limit, but exceeding this value by too much may risk the chance of permanently damaging the microphone diaphragm - if it is forced to hit the microphone backplate. The typical 3% distortion limit of Bruel & Kjaer 1/2-inch reference electret microphones is over 140 dB SPL [17].

2.6 Stability

For MEMS electret microphones to be useful in the ordinary environment, their performance parameters such as open-circuit sensitivity, frequency response and dynamic range must stay as constant as possible over the range of operating temperatures, atmospheric pressures, humidity, vibrations and electromagnetic fields encountered in its use. Changes in these performance parameters may be categorized as 'reversible changes' or 'irreversible changes.' Coefficients for reversible changes, e.g., {-dB change in sensitivity}/°C, should be provided if the change is found to be significant. Irreversible changes should be avoided whenever possible.

The two main parameters that are susceptible to change as a result of exposure to the above environmental factors are the mechanical tension of the diaphragm and the electrical charge of the electret. A decrease in the mechanical tension of the diaphragm will result in an increase in microphone sensitivity and a decrease in the upper cut-off frequency and upper distortion limit of the device. A decrease in the electret charge will cause a decrease in microphone sensitivity. The following subsections will describe the reversible and/or irreversible influence that each environmental factor has on the diaphragm stress and electret charge. Where applicable, manufacturing processes that may prevent irreversible changes from occurring during microphone operation will be suggested.

2.6.1 Temperature

This is one of the environmental fluctuations that an electret microphone will most often encounter. Thus, it is crucial that temperature variations do not cause a measurable loss of diaphragm tension or a decrease in electret charge density. For MEMS electret microphones that use high temperature diaphragm materials such as LPCVD silicon

nitride (deposition temperature approx. 850°C) and whose electret layer does not reside on the diaphragm, microphone operating temperatures as high as 100°C are not likely to result in any significant reversible or irreversible changes in the tension of the diaphragm. However, for other MEMS electret microphones whose composite diaphragms contain low temperature electret or polymer materials that contribute to the tensile stress, experiments must be carried out to determine how this stress varies (reversibly) with exposure to different temperatures. The typical measure of the outcome due to these reversible changes is the 'mean-temperature coefficient,' given in {-dB change in sensitivity}/°C over a temperature range at a given frequency [1]. Good values for conventional 1/2-inch electret microphones are - 0.001 dB/°C from -10°C to 50°C at 250 Hz [17]. Pre-exposing the diaphragm to the expected upper operating temperature range for extended periods of time before microphone assembly may prevent irreversible stress relaxation in the diaphragm at normal operating temperatures.

In terms of the electret charge, pre-exposure to the expected upper operating temperature range (aging) has been the common method of conditioning microphone electrets, so that the charge stays constant at normal operating temperatures. Electret charges do not usually undergo reversible changes when exposed to temperature extremes. Charges that are lost do not return. Aging conditions from 100°C to 150°C for a few hours is typical of commercial electret microphones. The high temperature permanently removes electrical charges that reside in energetically shallow traps, leaving only deeply trapped charges that are more stable.

2.6.2 Atmospheric Pressure

Changes in ambient DC pressure levels reversibly alter the stiffness and density of the air in the air gap. This causes the electret microphone sensitivity to decrease with increasing ambient pressure. The effect on microphone sensitivity is given by the 'ambient-pressure coefficient,' which is expressed in {-dB change in sensitivity}/Pa at a given frequency [1]. This value can be obtained for any microphone using a barometric chamber. Atmospheric pressure changes do not directly affect the diaphragm tensile stress or charge in the electret.

2.6.3 Humidity

High levels of humidity can decrease the diaphragm resonance as well as decrease the charge in the electret. If the diaphragm is polymeric, it may temporarily absorb water and cause a decrease in the tension of the diaphragm. When this occurs, the electret microphone sensitivity will increase slightly - although reversibly. Electrets may be reversibly or irreversibly affected by high humidity. High concentrations of water vapor may permanently remove surface charge from the electret or it may temporarily reduce the electric field in the air gap. Both phenomena decrease the electrical sensitivity of the microphone. The 'humidity coefficient' measures the effect of humidity and is given in {dB change in sensitivity}/%RH at a given frequency [1]. A good value for conventional 1/2-inch electret microphones is < 0.1 dB change at 100% RH and 250 Hz [17].

In MEMS electret microphones, another adverse by-product of high humidity is condensation. Because the air gap between the diaphragm and backplate in a MEMS microphone is only a few microns thick, water vapor condensing in this location may hinder the movement of the diaphragm or impeded air flow in the air gap. As a result, the microphone sensitivity may decrease due to damping of the diaphragm. Electret microphones, however, cannot be short-circuited by water condensation - another advantage over their externally biased counterparts.

2.6.4 Vibration

Vibrations to the electret microphone structure can have a reversible or irreversible effect on sensitivity. The reversible change occurs when the diaphragm mass is set in motion by the vibration and a small output voltage is produced whose magnitude is related to the mass per unit area of the diaphragm. Heavier diaphragms have higher vibration sensitivity. The sensitivity to vibration is given in terms of the equivalent sound pressure level produced by a rms acceleration amplitude of 1 m/s^2 acting at right angles to the diaphragm. The units are {dB SPL}/ms^{-2} over a specified frequency range [1]. Good values for conventional 1/2-inch electret microphones are 60-70 dB SPL/ms^{-2} from 10 Hz to 2 kHz [17].

The irreversible change occurs when the shock or vibration causes a permanent change in relative displacement between the microphone structural components, such as

the spacing between the diaphragm and backplate. Such an event can cause the microphone parameters to increase or decrease - depending on the change in relative displacement. The two-chip MEMS electret microphones described in this thesis are particularly prone to such irreversible vibration effects because it is easy for the diaphragm and backplate chips to shift with respect to each other.

2.6.5 Electromagnetic Fields

Although electromagnetic (EM) fields do not directly influence the diaphragm tensile stress or charge in the electret, the electrodes of an electret microphone can act as antennas and pick up signals from surrounding EM radiation. This pickup appears as an unwanted signal at the preamplifier output. It is not uncommon for poorly shielded MEMS electret microphones to pick up the 60 Hz EM radiation from light sources in test rooms. To minimize this effect, the diaphragm electrode and conductive microphone housing is typically grounded and the sensing backplate electrode is well shielded by the grounded housing and diaphragm electrode. It also helps to make sure the preamplifier shares a common ground with the electret microphone.

2.7 Electret Charge Induced Static Diaphragm Deflection

The electret charge on the microphone diaphragm causes an electrostatic attraction between the diaphragm and backplate. This attractive force is inversely proportional to the square of the distance between the electrodes, and is therefore highly non-linear [19]. The interaction between the non-linear attractive force and the linear mechanical restoring force of the diaphragm (due to its tension) may result in an unstable condition, whereby the diaphragm deflects towards the backplate without bound until it makes physical contact with the backplate. The maximum electret surface charge density that can be used before this instability point is reached will affect the maximum sensitivity and frequency response of an electret microphone.

2.7.1 Rigid Backplate

If the diaphragm is modeled as a square membrane, if the backplate is assumed to be rigid and without acoustic through-holes, and if $t < (0.01a)$, the maximum electret surface

charge density, $\sigma_{e,max}$, that can be used before the diaphragm collapses to the backplate is given by [20]:

$$\sigma_{e,\max} \approx \sqrt{\frac{8192\sigma t\varepsilon_e^2\varepsilon_0\left(s_a + \frac{s_e}{\varepsilon_e}\right)^3}{2205a^2 s_e^2}} \quad [\mathrm{C/m^2}] \tag{2-18}$$

where:

σ: residual tensile stress in the membrane [N/m^2]

t: thickness of membrane [m]

a: length of one side of square membrane [m]

s_e: electret thickness [m]

ε_e: relative dielectric constant of electret [unitless]

ε_0: permittivity of free space [8.85×10^{-12} F/m]

s_a: air gap thickness [m]

Equation (2-18) assumes the electret configuration shown in Figure 2-2. The assumption is that the area of the microphone diaphragm and backplate are equal.

2.7.2 Flexible Backplate

In many MEMS electret microphones (including some in this thesis), the backplate is not rigid, but is itself a flexible diaphragm that can also be modeled as a membrane. Under such circumstances, both the diaphragm and backplate will be attracted towards each other. This system can be modeled by an analogous diaphragm-rigid backplate system if the analogous diaphragm is assigned an effective tensile stress, σ_{eff}, and effective thickness, t_{eff}, where [9]:

$$\frac{1}{\sigma_{eff}t_{eff}} = \frac{1}{\sigma t} + \frac{1}{\sigma_b t_b} \tag{2-19}$$

and:

σ: residual tensile stress in the diaphragm [N/m^2]

t: thickness of diaphragm [m]

σ_b: residual tensile stress in the backplate [N/m^2]

t_b: thickness of backplate [m]

The maximum allowable electret charge density, $\sigma_{e,max}$, can be calculated using equation (2-18) with ($\sigma_{eff}t_{eff}$) substituted for (σt).

2.8 Summary

In this chapter we have learned about the principle of operation of both externally biased and self-biasing (electret) condenser microphones. The many structural features in a typical electret microphone have been examined, and formulas have been provided to predict how these features affect performance parameters such as open-circuit sensitivity, frequency response, dynamic range, microphone stability and static diaphragm deflection due to electret charge. Where possible, performance parameters from actual electret microphones are given.

From what we have learned so far, it is obvious that these formulas are not stand-alone models of microphone behavior, but rather, each formula closely influences the relevance and impact of the other formulas. In almost all cases, an increase in one performance parameter will lead to a trade-off in another. During the microphone design phase, the theory provided in this chapter should only be used as a guide to microphone performance. It should not be construed as the *exact* predicted outcome since the interaction between material properties, physical dimensions and electrical parameters will undoubtedly deviate from theory. The value of many device variables will not be able to be predicted on paper and will have to be obtained from experimental data. Often, the electro-mechanical-acoustic interactions in an electret microphone system are simply too complex to predict with high levels of accuracy through hand calculations. Iterative design and testing cycles are, therefore, the key to microphone optimization. For the curious reader, a more mathematically rigorous analysis of condenser microphone theory can be found in [21] and [22]. For now, the presented microphone theory will suffice as a practical tool for MEMS electret microphone design, fabrication, packaging and testing.

2.9 References

[1] "Bruel & Kjaer Microphone Handbook," Vol. 1, July 1996

[2] "Condenser Microphone Cartridges - Types 4133 to 4181," Bruel & Kjaer Product Data Sheet # BP 0100-17

[3] D. Schafer, S. Shoaf and P. Loeppert, "Micromachined Condenser Microphone for Hearing Aid Use," Technical Digest, IEEE Solid-State Sensor and Actuator Workshop, pp. 27-30, Hilton Head Island, South Carolina, USA, June 1998

[4] Y.J. Yang and S.D. Senturia, "Numerical Simulation of Compressible Squeezed-Film Damping," Technical Digest, IEEE Solid-State Sensor and Actuator Workshop, pp. 76-79, Hilton Head Island, South Carolina, USA, June 1996

[5] "Measuring Sound," Bruel & Kjaer Educational Pamphlet, September 1984

[6] "Communication Components Catalog," Japan Electronic Manufacturers Inc., 1997

[7] "Acoustic and Vibration Transducers," Bruel & Kjaer Product Catalog, 1998

[8] "General Brochure," Knowles Electronics Product Catalog, 1997

[9] P. Scheeper, "A Silicon Condenser Microphone: Materials and Technology," Ph.D. Thesis, University of Twente, April 1993

[10] O. Tabata, K. Kawahata, S. Sugiyama and I. Igarashi, "Mechanical Property Measurements of Thin Films Using Load-Deflection of Composite Rectangular Membrane," Proceedings of the IEEE Micro-Electro-Mechanical Systems Workshop, Salt Lake City, USA, 1989

[11] A.J. Sprenkels, "A Silicon Subminiature Electret Microphone," Ph.D. Thesis, University of Twente, 1988

[12] "Prepolarized Free-Field 1/2" Microphone Type 4189," Bruel & Kjaer microphone calibration chart, serial number 1931340

[13] "TM Series," Knowles Electronics Advance Information Release, 1997

[14] R.D. Blevins, "Formulas for Natural Frequency and Mode Shapes," Van Nostrand Reinhold Company, New York, 1979

[15] Z. Skvor, "On the Acoustical Resistance due to Viscous Losses in the Air Gap of Electrostatic Transducers," Acoustica 19, pp. 295, 1967/68

[16] P. R. Scheeper, A. G. H. van der Donk, W. Olthuis, and P. Bergveld, "Fabrication of Silicon Condenser Microphones using Single Wafer Technology," Journal of Microelectromechanical Systems, Vol. 1 (3), 147 (1992)

[17] "Measurement Microphones," Bruel & Kjaer Educational Pamphlet, August 1984

[18] T.B. Gabrielson, "Mechanical-Thermal Noise in Micromachined Acoustic and Vibration Sensors," IEEE Transactions on Electron Devices, Vol. 40, No. 5, pp. 903-909, May 1993

[19] J.E. Warren, "Capacitance Microphone Static Membrane Deflections: Comments and Further Results," J. Acoust. Soc. Am., Vol. 58, No. 3, September 1975

[20] P.C. Hsu, C.H. Mastrangelo and K.D. Wise, "A High Sensitivity Polysilicon Diaphragm Condenser Microphone," Proceedings of the IEEE Micro-Electro-Mechanical Systems Workshop, Heidelberg, Germany, 1998

[21] G.S.K. Wong and T.F.W. Embleton, "AIP Handbook of Condenser Microphones: Theory, Calibration and Measurement," AIP Press, New York, 1995

[22] M. Gayford, "Microphone Engineering Handbook," Butterworth-Heinemann Ltd., 1994

Chapter 3

A Review of Capacitive Microphones

3.1 Conventional Capacitive Microphones

The last chapter introduced many important performance parameters of capacitive microphones, such as sensitivity, frequency response, noise floor, upper cut-off frequency and stability. In this chapter, we will review some important historical milestones in the development of conventional and MEMS capacitive microphones. Where applicable, key performance parameters and physical dimensions will be provided. For clarity, externally biased capacitive microphones in this chapter will simply be referred to as 'condenser microphones,' while self-biasing ones will be described as 'electret microphones.'

Dolbear performed the first public demonstration of a condenser microphone in 1878 [1]. In 1917, Wente published the first comprehensive analysis and construction of a condenser microphone [2]. The reported device used a circular steel diaphragm (Figure 3-1) that had an undamped resonant frequency of 17 kHz. The 70 μm thick diaphragm area was 15 cm^2 and the backplate area was 8.5 cm^2. The 22 μm air gap spacing resulted in a capacitance of 335 pF. With an external bias of 320 V, the measured sensitivity was 20 mV/Pa.

The first commercial condenser microphones were improvements on Wente's seminal design. In one of Western Electric's first condenser microphones [3], the resonant frequency was lowered from 17 kHz to 5 kHz, the air gap thickness was changed from 22 μm to 25.4 μm, criss-crossing grooves were cut into the backplate and holes were bored through the backplate into the back cavity to reduce air-damping. This microphone was called the WE 394 transmitter and it was one of the first condenser microphones to enjoy great success in radio transmissions and sound recording. The device was more efficient than Wente's previous design and used a 28 μm thick aluminum alloy diaphragm, instead of a 70 μm thick steel one. With a 200 V bias

voltage, the pressure response was uniform for frequencies as high as 7 kHz and fell off gradually at higher frequencies. The Western Electric Company later manufactured many other condenser microphones whose basic designs were based on the WE 394. During the 1930s and 1940s, many of these became the unofficial standard microphones.

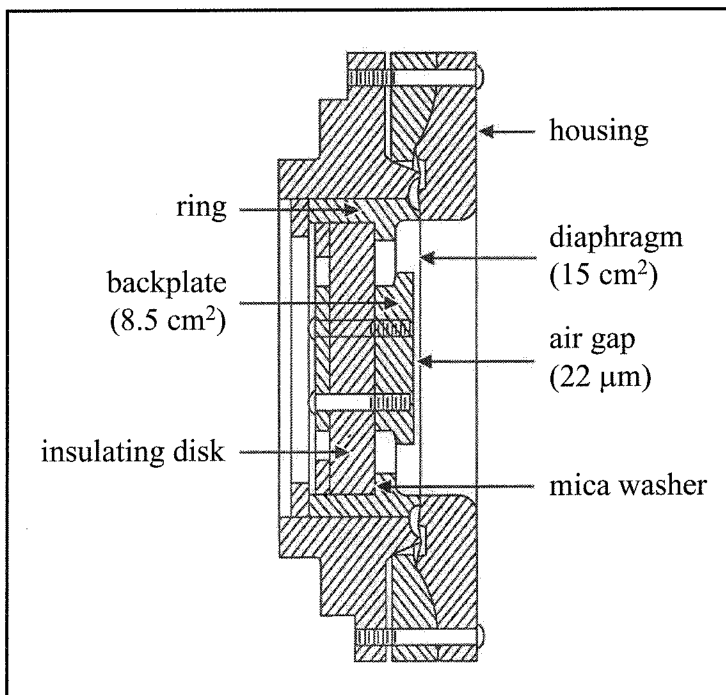

Figure 3-1. Wente's original condenser microphone [4].

Wente's microphone was intended for audio frequency applications (20 Hz to 20 kHz). The first ultrasonic condenser microphone was presented by Kuhl et al. in 1954 [5]. This microphone used a 10 μm thick and 14 mm diameter metalized plastic diaphragm. The measured microphone capacitance was 100 pF and grooves were cut into the backplate to reduce air-damping at the its high operating frequencies. The resonant frequency of the diaphragm was approximately 40 kHz, thus enabling the measurement of ultrasonic sound pressure levels (>20 kHz). The diaphragm tension could be manually adjusted to change the bandwidth of the device. Using a 150V external bias, sensitivities from 4 to 10 mV/Pa were obtained.

The rather large external bias voltage was one of the main drawbacks of these early condenser microphones designs. A solution arose from the systematic work on electrets by the Japanese physicist Eguchi [6]. It was discovered that electrets were dielectric

materials that could permanently trap electrical charges. They could therefore be incorporated into condenser microphone structures to supplant the external bias source (see section 2.1.2). In 1919, Eguchi began conducting electret experiments with waxes, to which he was able to impart charge using an electric field and heat. In the decades to follow, many more electret materials and charging techniques were discovered as a result of extensive scientific research [7].

In 1962, Sessler and West published the first successful application of stable polymer electrets to condenser microphones [8]. Their first device used a 6 μm thick metalized Mylar foil that acted as both the diaphragm and electret. The electret was charged to -200 V. The 38 mm diameter backplate was made of brass and contained 300 acoustic through-holes, each with a 1 mm diameter. The 14 μm thick air gap produced a capacitance of 700 pF. The measured sensitivity was 11 mV/Pa (± 3 dB) from 50 Hz to 15 kHz. Sessler and West presented other similar electret microphones in 1966 [9] and 1969 [10]. These had higher sensitivities and flatter frequency responses. Figure 3-2 shows an old electret microphone design.

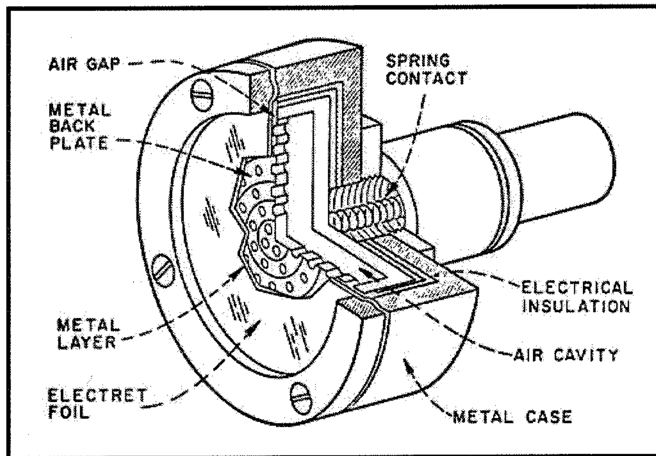

Figure 3-2. A cut-away of an old electret microphone design [11].

In 1968, Sony produced the first commercial electret microphone [12]. This was the start of widespread commercial acceptance. In 1970, Fraim and Murphy produced electret microphones that were more resistant to mechanical shock [13]. This was accomplished by placing diaphragm supports at many places. For plastic diaphragm diameters that ranged from 3.8 to 12.7 mm, the measured sensitivities were from 4 to 25

mV/Pa. Depending on the size of the diaphragm, the frequency responses were flat up to 30 kHz. In 1973, the same authors combined preamplifiers with electret microphones [14].

In the same year, Carlson and Killion presented a millimeter-scale electret microphone for use in hearing aids that placed the polymer electret on the metallic backplate, rather than on the diaphragm [15, 16]. By separating the electret and diaphragm functions, each could be optimized independently. The electret material could be chosen for its charge retention properties, and the polymer diaphragm for its mechanical properties. The sensitivity of these microphones was 10 mV/Pa over the frequency range 20 Hz to 20 kHz. Like Fraim and Murphy's design, multiple diaphragm supports were used to minimize vibration sensitivity and to prevent the non-tensioned diaphragm from collapsing to the backplate due to electrostatic attraction (Figure 3-3).

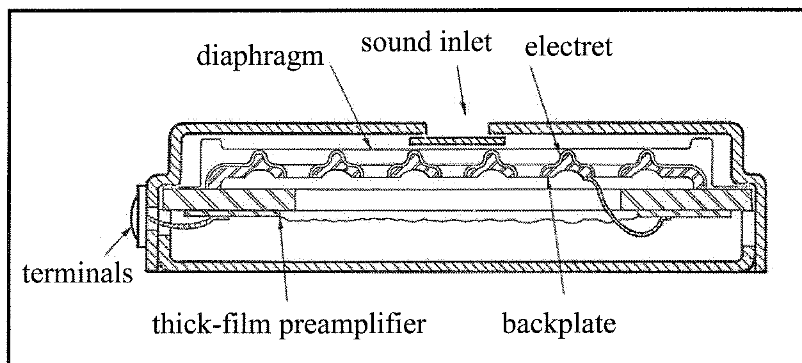

Figure 3-3. Cross-section of a miniature hearing aid electret microphone [16].

Since the first condenser and electret microphones were demonstrated by Wente and Sessler, respectively, many new designs of both types have been developed and commercialized. They are widely available in all sizes, performance specifications and price. At one (price) extreme are the expensive reference condenser microphones manufactured in low volume by companies such as Bruel & Kjaer [17]. These microphones can cost hundreds of dollars each, but have almost ideal performance parameters. At the other (size) extreme, millimeter-scale electret microphones can be bought for a few dollars from hearing aid component manufactures such as Knowles Electronics LLC [18]. These microphones trade high performance for a reduction in physical size.

Most commercial capacitive microphones used today are of the electret type. This is because of their favorable performance properties, simplicity, low cost and reliability. They are used as both research tools and in commercial applications. Over five hundred million of these microphones are produced each year. Their indispensability and pervasiveness in a wide range of acoustic sensing applications makes them ideal targets for further improvement in terms of miniaturization, performance and cost.

3.2 MEMS Capacitive Microphones

The modular nature and primitive manufacturing techniques of today's capacitive microphones has been a limiting factor in making them smaller, cheaper, more reliable and better performing. This is because modern capacitive microphones are still made from discrete mechanical and electrical components that require numerous assembly steps. Consequently, small **and** high performing ones are difficult and expensive to manufacture. This piece-wise approach to microphone production is unfavorable in terms of device optimization for small form-factors. A capacitive microphone fabricated from MEMS techniques (using silicon as a substrate) eliminates these disadvantages, while conferring benefits such as:

- a high degree of miniaturization
- repeatable and precise dimensional control
- volume manufacturing with a high degree of reproducibility
- ability to array multiple microphones on the same substrate
- ability to integrate with on-chip microelectronics
- freedom to choose from a wide range of materials and processing techniques

This section will review some of the important historical developments of MEMS silicon capacitive microphones. Where possible, schematics, physical dimensions and performance parameters from the actual references will be provided. As a convenience to the reader, a summary of all the reviewed MEMS capacitive microphones is presented at the end of this chapter in Table 3-1 (page 14).

In 1984, Hohm and Gerhard-Multhaupt presented the first MEMS electret microphone [19]. The features and dimensions are illustrated in Figure 3-4. The electret consisted of a 2 μm thick SiO_2 layer charged to -350 V by liquid-contact. A single circular acoustic hole was formed through the center of the silicon backplate by sand blasting. A 30 μm thick Mylar ring defined the air gap, resulting in a 9 pF capacitance. The measured open-circuit sensitivity was 8.8 mV/Pa and the resonant frequency was 8.5 kHz. This device was clearly a first-of-its kind, but the method of fabrication (e.g., sand blasting and charging by liquid-contact) was not repeatable or mass-producible.

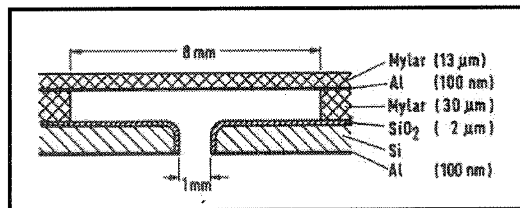

Figure 3-4. Silicon electret microphone of Hohm and Gerhard-Multhaupt (1984) [19].

In 1986, Hohm presented a MEMS condenser microphone [20, 21]. The microphone consisted of two chips, one carrying the 150 nm × 0.8 mm × 0.8 mm LPCVD silicon nitride diaphragm, and the other the silicon backplate and air gap spacer (Figure 3-5). Both chips were manufactured by bulk-micromachining and were glued together to form the microphone structure (1.7 mm × 2mm × 0.6 mm). The capacitance was 1.4 pF. To increase sensitivity, nitrogen ions were implanted into the nitride diaphragm to reduce the tensile stress. For a bias voltage of 28 V, the open-circuit sensitivity was as high as 4.3 mV/Pa for frequencies up to 2 kHz. This microphone was an improvement on the above electret microphone in terms of using reproducible MEMS fabrication techniques, but the lack of acoustic holes in the backplate severely limited the frequency bandwidth.

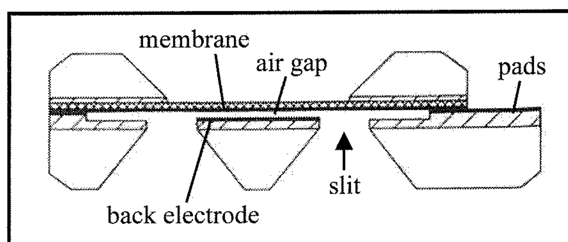

Figure 3-5. Silicon condenser microphone of Hohm and Hess (1986) [21].

Another MEMS electret microphone was presented by Sprenkels in 1988 [22]. The 2.45 mm × 2.45 mm square diaphragm was constructed from 6 μm thick Mylar foil (metalized by 50 nm of gold) and was manually glued to the silicon backplate (Figure 3-6). The SiO_2 electret was charged to -315 V. With a 20 μm thick air gap, the measured sensitivity was 14 mV/Pa. In 1989, Sprenkels et al. presented an improved version of his first device [23]. The Mylar diaphragm in this case was reduced to a thickness of 2.5 μm. With a 1.1 μm thick SiO_2 electret charged to -300 V, the measured open-circuit sensitivity was about 25 mV/Pa from 100 Hz to 15 kHz. Although the microphone substrate was made from MEMS fabrication techniques, the manually glued Mylar foil not only prevented thinner foils from being used, but most likely made the diaphragm stress difficult to control from wafer to wafer.

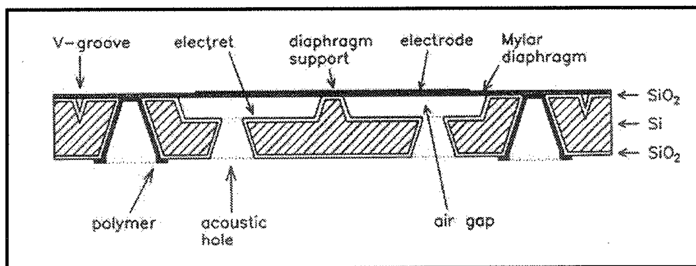

Figure 3-6. Silicon electret microphone of Sprenkels (1988) [22].

In 1989, Murphy et al. presented another silicon electret microphone [24]. Their two-chip device utilized a thin polyester diaphragm (2mm × 2mm × 1.5 μm) on one chip and SiO_2 (1.5 μm) or FEP/TFE Teflon electrets (8-12 μm) on the other. The electrets were charged to -200V. Both chips were manufactured by bulk-micromachining and when assembled, yielded a capacitance of 2 pF. The sensitivity ranged from 4 to 8 mV/Pa for frequencies in excess of 15 kHz. This was one of the first MEMS electret microphones to use fluoropolymer electrets.

In 1990, Bergqvist and Rudolf presented a MEMS condenser microphone with a lightly-doped silicon diaphragm [25]. The 2 mm × 2 mm square diaphragm (5-8 μm thick) was fabricated on one chip, while the glass-silicon-glass backplate sandwich structure was fabricated on another chip (Figure 3-7). 103 acoustic holes were provided through the glass backplate. With a 4 μm thick air gap, the capacitance of the

microphone was 3.5 pF. Using a 16 V bias voltage, open-circuit sensitivities from 1.4 to 13 mV/Pa were obtained for high frequencies cut-off values between 4 and 16 kHz. This was one of the smallest silicon-based microphones to show high sensitivity over decent bandwidth. The minor drawback was that the assembly involved many bonding steps between numerous substrates.

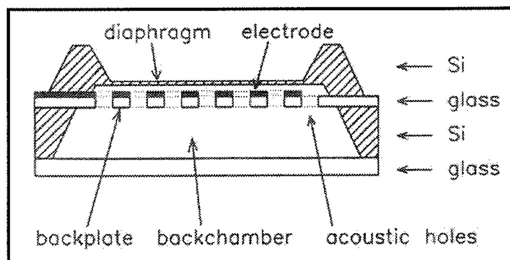

Figure 3-7. First silicon condenser microphone of Bergqvist and Rudolf (1990) [25].

In 1991, Bergqvist and Rudolf improved on their previous condenser microphone design with a device that utilized a highly-perforated (640 - 4000 holes/mm^2), 10 μm thick backplate in combination with an air gap thickness of only 2 μm [26]. The 4 mm^2 diaphragm area resulted in a capacitance of 5 pF. The silicon diaphragm and backplate were fabricated using an electrochemical etch stop process and were assembled together using silicon fusion bonding and medium temperature on titanium bonding (Figure 3-8). Due to the small air gap, a bias voltage of only 5 V was needed to achieve a sensitivity between 1 to 2 mV/Pa from 2 Hz to 20 kHz (± 3 dB). The measured noise level was between 37 and 44 dBA SPL. This highly perforated backplate design was the first to directly address the air-streaming resistance problem. The wideband frequency response is a testament to their success at tackling this issue.

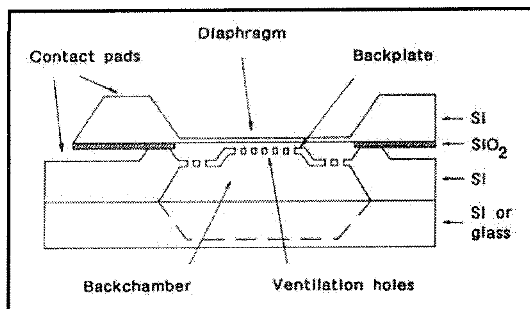

Figure 3-8. Second silicon condenser microphone of Bergqvist and Rudolf (1991) [26].

In 1991, Kuhnel presented a silicon condenser microphone of novel design. Figure 3-9 shows a schematic cross-section of the microphone with integrated field-effect transistor (FET) [27]. The gate of the transistor is the 1 mm × 1mm × 150 nm silicon nitride diaphragm of the microphone. An air gap exists between the diaphragm and the gate oxide of the FET. Movement of the diaphragm modulates the current through the transistor. The sensitivity varied from 0.1 to 1 mV/Pa from 100 Hz to 30 kHz. In 1992, an improved version of this FET microphone was presented by Kuhnel and Hess [28]. This new microphone had a sensitivity of 5 mV/Pa and a noise level of 62 dBA SPL. The advantage of such a device is low output impedance. The disadvantages are poor long-term stability due to drift of the FET gate potential and a high noise floor.

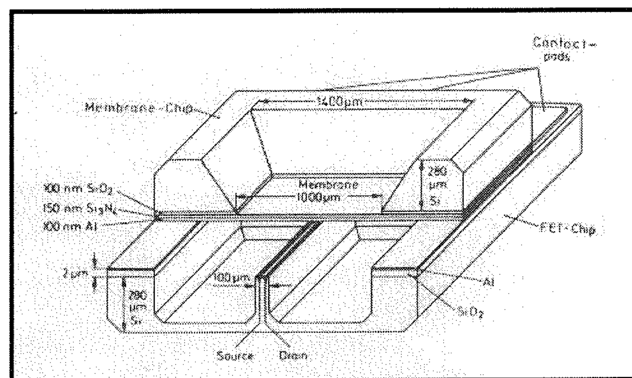

Figure 3-9. FET condenser microphone of Kuhnel (1991) [27].

In 1992, van der Donk presented a silicon condenser microphone that introduced an actuator electrode on the diaphragm for electromechanical feedback so that wider bandwidths could be achieved with smaller air gaps [29, 30]. The diaphragm of the condenser microphone (same type as the one developed by Sprenkels in Figure 3-6, but with a 2-3 µm air gap) contained two interdigitated electrodes (Figure 3-10). One electrode served as the sense electrode while the other was used to drive the diaphragm with an electrostatic force. This feedback configuration allowed the low cut-off frequencies of condenser microphones with narrow air gaps to be extended by about one order of magnitude. The drawback of this feedback configuration is the requirement of an external operational amplifier and the problem of parasitic capacitance and mechanical deformation of the diaphragm limiting the gain of the feedback amplifier. This in turn limits the reduction of diaphragm movement.

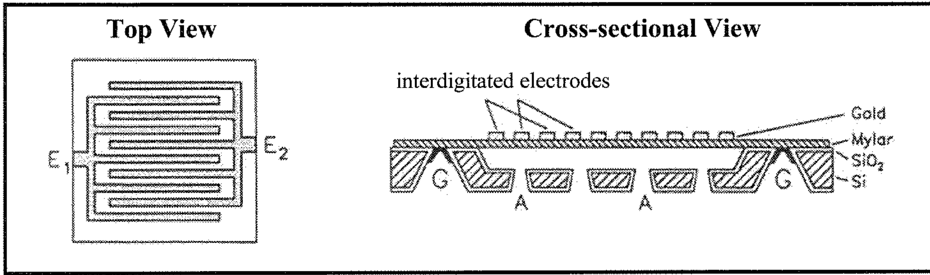

Figure 3-10. Silicon condenser microphone with feedback of van der Donk (1992) [30].

In 1992, Scheeper et al. presented one of the first condenser microphones to incorporate both surface and bulk micromachining [31]. Figure 3-11 shows a schematic cross-section of the microphone. The backplate is a 1 μm thick PECVD silicon nitride film with a high density of acoustic holes (120-525 holes/mm^2). The diaphragm is a 1 μm thick LPCVD silicon nitride film. A 1-3 μm thick aluminum sacrificial layer serves as both the air gap spacer and sacrificial layer. For 1.5 mm × 1.5 mm diaphragms and using relatively low bias voltages of 6-16 V, measured sensitivities of 1-2 mV/Pa were obtained for a relatively flat frequency response between 100 Hz and 14 kHz. In 1994, Scheeper et al. presented an improved version of this microphone [32]. This was done by increasing the stress and acoustic hole density in the backplate, by increasing the size of the diaphragm to 2mm × 2mm, and by decreasing the diaphragm thickness to 0.24 μm. For an external bias of 5 V, the improved condenser microphone (6.6 pF) had an open-circuit sensitivity of 10 mV/Pa. The measured noise level was a respectable 30 dBA SPL. This design was one of the first MEMS condenser microphones that could be made from a single wafer and that required no chip-to-chip bonding. The smart use of an aluminum sacrificial layer to precisely determine the air gap spacing, a high density of acoustic holes generously placed in the backplate, and an extremely thin diaphragm all contributed to an impressive sensitivity and bandwidth for such a small form factor.

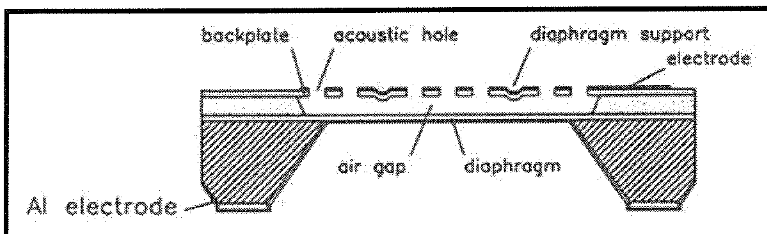

Figure 3-11. Surface micromachined Si condenser microphone of Scheeper (1992) [31].

In 1994, Bergqvist and Gobet presented one of the first applications of surface micromachined free-standing metal microstructures to MEMS condenser microphones [33]. Electroplating technology was used to implement a perforated 15 μm thick copper backplate electrode that was suspended over a 1.8 mm × 1.8 mm × 8 μm silicon diaphragm (Figure 3-12). A bias voltage of 28V produced a sensitivity of 1.4 mV/Pa. The measured microphone capacitance was 5.4 pF and the noise level was 23 dBA SPL. The clever metal backplate design allowed its rigidity to be controlled by the metal thickness, but compressive-stress buckling limited precise control over air gap height. The low sensitivity was mainly due to the relatively thick silicon diaphragm.

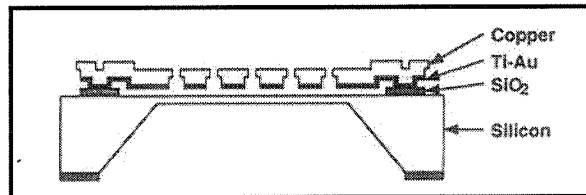

Figure 3-12. Electroplated silicon condenser microphone of Bergqvist (1994) [33].

In 1996, Bernstein and Borenstein presented an electroplated silicon condenser microphone with an on-chip JFET buffer amplifier [34]. The function of the on-chip amplifiers was to reduce stray capacitance and to eliminate off-chip circuitry. The perforated backplate was made of electroformed gold and the diaphragm was made of p+ doped silicon (Figure 3-13). Sensitivities as high as 40 mV/Pa were obtained for bandwidths of 70 Hz to 20 kHz. This impressive design is practically a performance benchmark for other MEMS capacitive microphones. This recognition was not lost on Noise Cancellation Technologies Inc., Siemens Semiconductors of Siemens AG and National Semiconductor Corp., who later licensed the device.

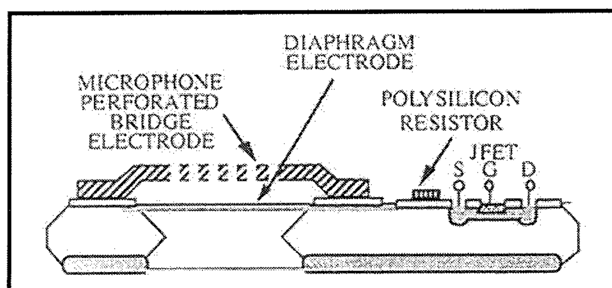

Figure 3-13. Silicon microphone w/ integrated preamplifier of Bernstein (1996) [34].

In 1998, D. Schafer et al. demonstrated the first commercial MEMS condenser microphone for specific use in hearing aids [35]. The plan view of the device is shown in Figure 3-14. The entire die size is only 2 mm × 2mm and the diaphragm diameter is 0.8 mm. The condenser microphone fabrication process combines low-voltage CMOS process with surface and bulk micromachining to produce a single-chip device that incorporates the diaphragm, backplate, buffer amplifier and backplate bias. Sensitivities of about 10 mV/Pa have been obtained for bandwidths of 150 Hz to 15 kHz. The measured noise level was between 28 to 32 dBA SPL. The device uses an on-chip ring oscillator and charge pump to increase the 1.3 V hearing aid battery voltage to a 12 V bias. Despite its comprehensive integrated design, adoption by hearing aid manufacturers has been slow due to its relatively high noise floor and power overhead, when compared to conventional hearing aid electret microphones.

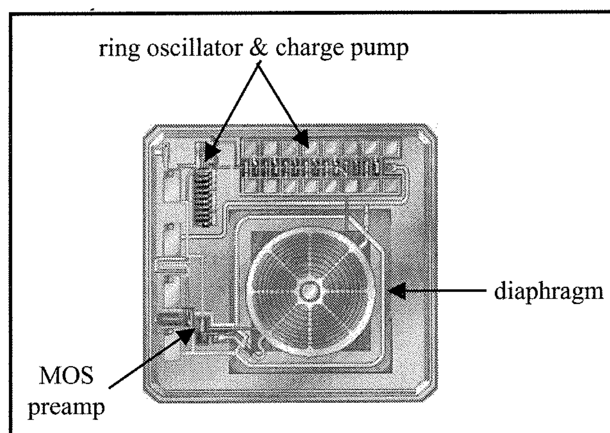

Figure 3-14. Integrated MEMS microphone for hearing aid applications (1998) [35].

The final MEMS capacitive microphone that will be reviewed in this chapter is an all-surface-micromachined condenser microphone presented in 1999 by Pardo et al. [36]. The advantage of only using a surface micromachining fabrication process is the ease of integration with microelectronics fabrication processes. Figure 3-15 shows an SEM picture of the device. The microphone body consists of a fold-up dual-polysilicon tent structure that must be manually assembled using micromanipulators. The cumbersome assembly step practically eliminates this design from mass production. The central plate has a Poly 2 hexagonal grid on top of a Poly 1 membrane, forming a 0.9 pF capacitor.

The microphone electrodes are connected to bonding pads by serpentine wires. Very few additional details have been published about this device, other than the claim that the maximum sensitivity is 100 mV/Pa at 20 kHz. Unfortunately, the device has an extremely high noise floor of 72 dB SPL in the 200 Hz to 20 kHz frequency range, even though the sophisticated external electronics used to drive the microphone implements synchronous modulation/demodulation at 1 MHz to reduce 1/f noise.

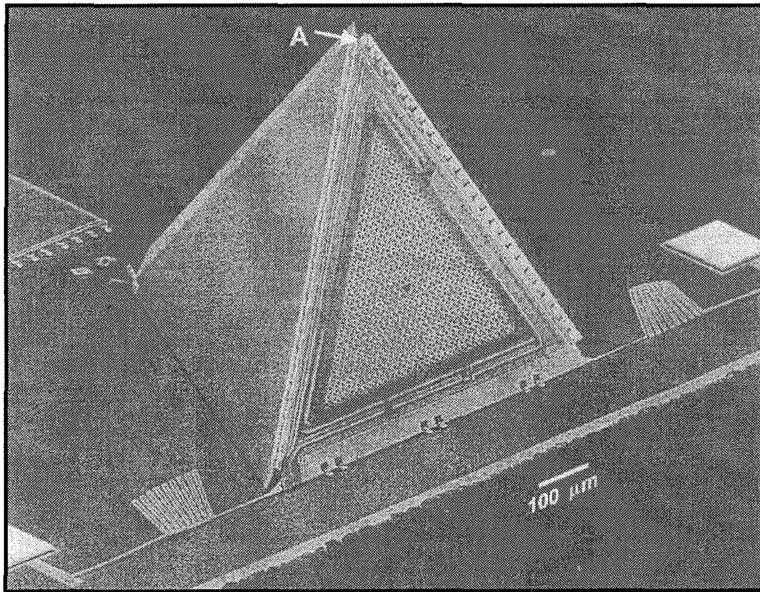

Figure 3-15. Picture of all-surface-micromachined microphone of Pardo (1999) [36].

3.3 Summary

We have just reviewed and critiqued over half a century of work on conventional capacitive microphones and nearly two decades of work on MEMS capacitive microphones (Table 3-1). While development and research in conventional devices has tapered off, strong academic and commercial interest still exists in the MEMS arena, where a fully integrated (with electronics) miniature MEMS electret microphone has been elusive. The holy grail in this field is to develop a reliable, low cost and high performance version of such a device, such that it will not only replace all the existing conventional electret microphones on the market, but will also unleash new applications that were never possible before. This thesis is a part of that quest.

Table 3-1. Summary of historical MEMS silicon capacitive microphones.

1st Author Year [Ref.] Mic. Type	Diaphragm Area [mm^2] Thickness [μm]	Number of Backplate Holes	Air Gap Thickness [μm]	Capacitance [pF]	Sensitivity [mV/Pa]	Noise Level [dBA SPL]	High Frequency Cut-off [kHz]
Hohm 1984 [19] SiO_2 Electret	64 13	1	30	9	8.8_{oc}	-	8.5
Hohm 1986 [20, 21] Condenser	0.64 0.15	2	2	1.4	$0.2 - 4.3_{oc}$	-	20 - 2
Sprenkels 1989 [23] SiO_2 Electret	6 2.5	9	20	2	25_{oc}	-	15
Murphy 1989 [24] SiO_2/Teflon Electret	4 1.5	1.5	25, 30, 95	2	4 - 8	-	15
Bergqvist 1990 [25] Condenser	4 5 - 8	103	4	3.5	$1.4 - 13_{oc}$	-	4 - 16
Bergqvist 1991 [26] Condenser	4 2-10	2560 - 16000	2	5	$1\text{-}2_{oc}$	37 - 44	20
Kuhnel 1991 [27] FET-Condenser	1 0.15	2	2	-	$0.1 - 1.0_{oc}$	-	30
Kuhnel 1992 [28] FET-Condenser	0.64 0.15	2 - 17	2	1 - 1.3	$0.44 - 10_{oc}$	62	5 - 20
van der Donk 1992 [29, 30] Condenser	6 2	16, 16, 81	2, 3, 2	-	-	-	0.2, 0.4, 8
Scheeper 1992 [31] Condenser	2.25 1	270 - 1181	1 - 3	-	1 - 2	-	14
Scheeper 1994 [32] Condenser	4 0.24	484 - 968	3.1	6.6	10_{oc}	30	14
Bergqvist 1994 [33] Condenser	3.24 8	-	5	5.4	1.4	23	14
Bernstein 1996 [34] Condenser	1 - 3.24 -	~ 1500	-	-	$16 - 40_{oc}$	25	15
Schafer 1998 [35] Condenser	0.5 0.75	-	4	0.2	10	28 - 32	15 - 17
Pardo 1999 [36] Condenser	~ 0.125 -	-	-	0.9	100	72	20

$_{oc}$: open-circuit sensitivity

3.4 References

[1] J.K. Hilliard, "Electroacoustics to 1940," J. Acoust. Soc. Am., 61, pp. 267-273, 1977

[2] E.C. Wente, "A Condenser Transmitter as a Uniformly Sensitive Instrument for Absolute Measurement of Sound Intensity," Phys. Rev. 10, pp. 39-63, 1917

[3] W.C. Jones, "Condenser and Carbon Microphones," Bell System Tech J., 10, pp. 46-62, 1931

[4] G.S.K. Wong and T.F.W. Embleton, "AIP Handbook of Condenser Microphones: Theory, Calibration and Measurement," AIP Press, New York, 1995

[5] W. Kuhl, G.R. Schodder and K.K. Schroder, "Condenser Transmitters and Microphones with Solid Dielectric for Airborne Ultrasonics," Acoustica, 4, pp. 519-532, 1954

[6] M. Eguchi, Proc. Phys. Math. Soc. Jpn, 1, pp. 326, 1919

[7] G.M. Sessler, "Topics in Applied Physics, Vol. 33: Electrets," Springer-Verlag, New York, 1987

[8] G.M. Sessler and J.E. West, "Self-biased Condenser Microphone with High Capacitance," J. Acoust. Soc. Am., 34, pp. 1787-1788, 1962

[9] G.M. Sessler and J.E. West, "Foil-electret Microphones," J. Acoust. Soc. Am., 40, pp. 1433-1440, 1966

[10] G.M. Sessler and J.E. West, "First-order Gradient Microphone Based on the Foil-electret principle: Discrimination Against Air-borne and Solid-borne Noises," J. Acoust. Soc. Am., 46, pp. 1081-1086, 1969

[11] G.M. Sessler and J.E. West, J. Acoust. Soc. Am., 53, pp. 1589, 1973

[12] Electronics, 41, No. 26, pp.133, December 1968

[13] F.W. Fraim and P.V. Murphy, "Miniature Electret Microphones," J. Audio Eng. Soc., 18, pp. 511-517, 1970

[14] F.W. Fraim, P.V. Murphy and R.J. Ferran, "Electrets in Miniature Microphones," J. Acoust. Soc. Am. 53, pp. 1601-1608, 1973

[15] E.V. Carlson, "A Subminiature Condenser Microphone, Using Electret Technology," The Hearing Dealer, April 1973

[16] M.C. Killion and E.V. Carlson, "A Subminiature Electret-Condenser Microphone of New Design," J. Audio Eng. Soc., Vol. 22, No. 4, pp. 237-243, 1974

[17] "Acoustic and Vibration Transducers," Bruel & Kjaer Product Catalog, 1998

[18] "General Brochure," Knowles Electronics Product Catalog, 1997

[19] D. Hohm and R. Gerghard-Multhaupt, "Silicon-dioxide Electret Transducer," J. Acoust. Soc. Amer., 75 (4), pp. 1297-1298, April 1984

[20] D. Hohm, "Kapazitive Silizium-Sensoren fur Horschallanwendungen," Fortschritt-Berichte VDI, VDI-Verlag, Dusseldorf, 1986

[21] D. Hohm and G. Hess, "A Subminiature Condenser Microphone with Silicon Nitride Membrane and Silicon Backplate," J. Acoust. Soc. Am., 85 (1), pp. 476-480, January 1989

[22] A.J. Sprenkels, "A Silicon Subminiature Electret Microphone," Ph.D. Thesis, University of Twente, 1988

[23] A.J. Sprenkels, R.A. Groothengel, A.J. Verloop and P. Bergveld, "Development of an Electret Microphone in Silicon," Sensors and Actuators, 17, pp. 509-512, 1989

[24] P. Murphy, K. Hubschi, N. De Rooij and C. Racine, "Subminiature Silicon Integrated Electret Capacitor Microphone," IEEE Transaction on Electrical Insulation, Vol. 24, No. 3, pp. 495-498, June 1989

[25] J. Bergqvist and F. Rudolf, "A New Condenser Microphone in Silicon," Sensors and Actuators, A21-A23, pp. 123-125, 1990

[26] J. Bergqvist, F. Rudolf, J. Maisano, P. Parodi and M. Rossi, "A Silicon Condenser Microphone with a Highly Perforated Backplate," Technical Digest 6th International Conference on Solid State Sensors and Actuators (Transducers '91), pp. 266-269, San Francisco, USA, June 1991

[27] W. Kuhnel, "Silicon Condenser Microphone with Integrated Field-effect Transistor," Sensors and Actuators A, 25-27, pp. 521-525, 1991

[28] W. Kuhnel and G. Hess, "Micromachined Subminiature Condenser Microphones in Silicon," Sensors and Actuators A, 32, pp. 560-564, 1992

[29] A.G.H. van der Donk, P.R. Scheeper, W. Olthuis and P. Bergveld, "Amplitude-modulated Electro-mechanical Feedback System for Silicon Condenser Microphones," J. Micromech. Microeng. 2, pp. 211-214, 1992

[30] A.G.H. van der Donk, "A Silicon Condenser Microphone: Modeling and Electronic Circuitry," Ph.D. Thesis, University of Twente, 1992

[31] P.R. Scheeper, A.G.H. van der Donk, W. Olthuis and P. Bergveld, "Fabrication of Silicon Condenser Microphones Using Single Wafer Technology," Journal of Microelectromechanical Systems, Vol. 1, No. 3, pp. 147-154, September 1992

[32] P.R. Scheeper, W. Olthuis and P. Bergveld, "Improvement of the Performance of Microphones with a Silicon Nitride Diaphragm and Backplate," Sensors and Actuators A, 40, pp. 179-186, 1994

[33] J. Bergqvist and J. Gobet, "Capacitive Microphone with Surface Micromachined Backplate Using Electroplating Technology," Journal of Microelectromechanical Systems, Vol. 3, No. 2, pp. 69-75, June 1994

[34] J.J. Bernstein and J.T. Borenstein, "A Micromachined Silicon Condenser Microphone with On-Chip Amplifier," Technical Digest, IEEE Solid-State Sensor and Actuator Workshop, pp. 239-243, Hilton Head Island, South Carolina, USA, June 1996

[35] D. Schafer, S. Shoaf and P. Loeppert, "Micromachined Condenser Microphone for Hearing Aid Use," Technical Digest, IEEE Solid-State Sensor and Actuator Workshop, pp. 27-30, Hilton Head Island, South Carolina, USA, June 1998

[36] F. Pardo, R. Boie, G. Elko, R. Sarpeshkar and D.J. Bishop, "All-Surface-Micromachined Si Microphone," Technical Digest 10th International Conference on Solid State Sensors and Actuators (Transducers '99), pp. 1068- 1069, Sendai, Japan, June 1999

Chapter 4

Thin Film Teflon AF Electrets

4.1 Theory and History of Electrets

An electret is a dielectric that produces an external electric field arising from quasi-permanent electrical charges trapped within the material [1]. The term "quasi-permanent" means that lifetime constants associated with these charges are much longer than the lifetime of the application in which these electrets will be used (typically over a few decades at standard temperature and pressure). The trapped charges can be permanently ordered dipole charges, stable uncompensated surface or space homocharges, heterocharges, or a combination of these. The sign of the uncompensated charges can be positive, negative or both. Figure 4-1 illustrates the various types of electret charges. When one side of the electret is metalized, as in many electret applications, image charges may also reside on the metal electrode.

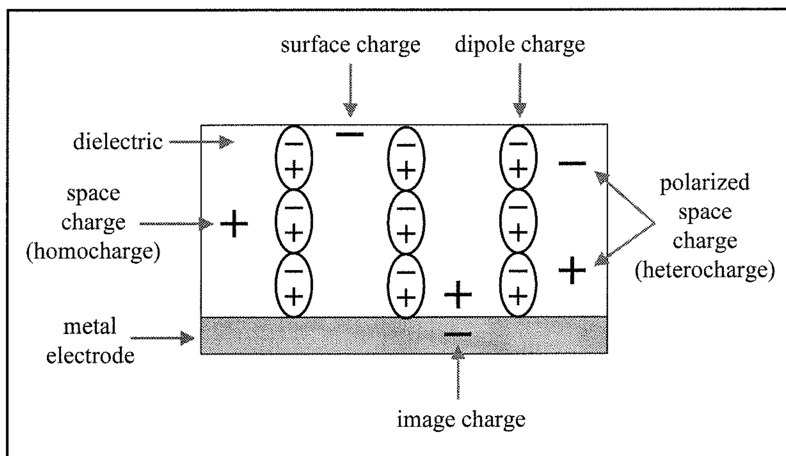

Figure 4-1. Different types of electret charge.

The types of charges that are of concern to us in this thesis are negative surface and space charges trapped in highly insulating polymer dielectrics. These charges are electrons that have become immobilized in the trap states that lie in the bandgap, below the conduction band of the polymer material (Figure 4-2).

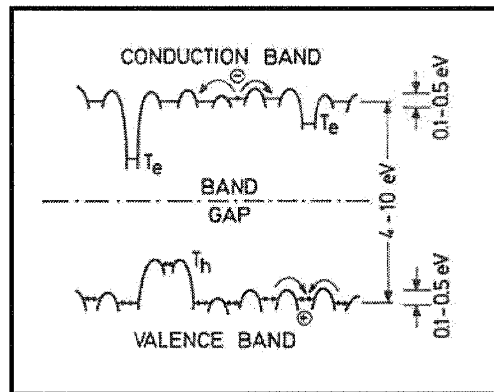

Figure 4-2. Energy diagram for electron (T_e) and hole (T_h) traps in polymers [1].

Localized trap levels in polymers exist for a number of reasons. Volume traps can be caused by the presence of impurities (catalyst molecules, monomers, oxygen vacancies), structural defects in the monomer units (furcations, double bonds), chain conformation irregularities in the vicinity of bending and chain ends, or imperfection of the crystalline order [2]. Surface traps can be caused by chemical impurities, specific surface defects caused by oxidation products, broken chains and adsorbed molecules [3]. The predominance of surface or volume traps varies from polymer to polymer. Teflon, for example, is known to have a high proportion of surface traps. The depth of the electron traps in a polymer like polyethylene can vary from 0.4 to 1 eV [4]. In Teflon-FEP, one of the most important electret materials, the deepest traps are 1.8 to 1.9 eV [5]. The release of electrons from deep traps via activated states is only possible at elevated temperatures, while the release from shallow traps can occur at room temperature. Electrons in volume traps tend to require higher release temperatures than those in surface traps (Table 4-1).

Table 4-1. Distribution of traps for negative charges in 25 μm Teflon-FEP-A [1].

Peak release temperature [°C]	Location relative to charge surface [μm]	Kind of trap
95	0-25	Energetically shallower trap active under trap-filled limit conditions
155	0-0.5	Surface trap
170	0.5-1.8	Near-surface trap
200	1.8-25	Bulk trap

The ability to convert normal dielectrics into electrets is not a modern development. In 1732, Gray had already referred to electrets when he described the generation of an attractive electrostatic force due to the cooling of naturally occurring waxes, rosins and sulfur in iron ladles [6]. The term "electret" was first coined by Heaviside in 1892, when he hypothesized the existence of permanently polarized dielectrics [7]. However, it was not until the beginning of the 20th century that systematic scientific studies were conducted on electrets. The first to do so was Eguchi in 1919 [8, 9]. He formed electrets from similar materials as Gray, namely Carnauba wax and resin with the addition of beeswax. The electrets were formed by cooling the heated wax in the presence of a strong electric field. From his experiments, Eguchi not only presented the results of measurements of surface charge densities, but he also formed the first hypothesis explaining the existence of a permanent polarization in waxes and resins.

After Eguchi's initial research on electrets, other scientists produced electrets using other materials and charging techniques. In 1928, Selenyi pioneered the injection of electrons or ions into insulators [10]. In 1937, Nadjakoff investigated the formation of electrets through illumination of light [11]. In the 1950s, research was conducted on the breakdown and thermal charge release of electrets formed by high-energy ionizing radiation such as electron beams [12, 13]. During the next few decades, experiments on charging dielectrics with gamma radiation [14], corona discharge [15], magnetic fields [16] and liquids [17] were demonstrated.

Prior to 1960, electrets were more of a scientific curiosity. It was not until afterwards that the first electrets were put to practical use. This started with the application of electrets in xerography [18] and the use of polymer electret films in condenser microphones [19] in the early 1960s. Today, stable electrets (mostly based on fluoropolymers) are used in wide range of scientific and commercial applications. These include: electroacoustic transducers, xerography, electromechanical transducers, electrostatic recorders, air filters, motors, generators, dosimeters, pyroelectric detectors, and relay-type switching devices [1].

4.2 Electret Formation

There are three main practical methods by which stable electrets can be formed. Each produces different kinds of charges in the electret and is more suitable for use with certain dielectrics materials. Table 4-2 summarizes these electret formation methods.

Table 4-2. Electret forming techniques [2].

Electret Type	**Thermoelectrets**	**Photo- and Radioelectrets**	**Charge-Implanted Electrets**
Source and types of charges	Internal source: Dipole charges Heterocharges Some homocharges injected from polarization electrodes	Internal source: Heterocharges	External source: Homocharges
Methods of formation	Dielectric heated to excite dipoles Cooled in the presence of an externally applied electric field to freeze ordered dipoles in place	Excitation of electrons from the valance band or deep trapping levels to the conduction band through light illumination or radiation exposure in the presence of an external electric field Electric field causes charge migration to electrodes	1. Irradiation with low energy electrons 2. Injection of electrons and ions during stabilized breakdown 3. Irradiation with electrons and ions during corona discharge in air 4. Transfer of charge from liquid to dielectric surface
Most suitable dielectric	Dipolar materials: Carnauba wax, Bees wax mixture, rosins	Selenium, Sulfur	Polyolefine films: Teflon-PTFE Teflon-FEP Teflon-PFA etc.
Usefulness in electret microphone	Low	Low	High

It can be seen from Table 4-2 that thermoelectrets and photo- or radioelectrets are not suitable for electret microphone applications because they only contain dipole and/or

heterocharges. As described in section 2.1.2, electret microphone operation depends on the presence of homocharges at or near the electret-air interface. Thus, electret formation by charge implantation seems the obvious choice.

In choosing from the four possible charge implantation methods: low energy e-beam, stabilized breakdown, corona discharge and liquid transfer, one must keep in mind the compatibility of each process with the features of a MEMS device. The desire to integrate microelectronics with MEMS electret microphones will immediately eliminate the stabilized breakdown and corona discharge methods. This is because placing several kV of electric potential a few millimeters above the microphone chip will most likely damage any integrated electronics (e.g., due to breakdown of gate oxide). The liquid transfer method can also be eliminated since it only forms very shallow surface charges that may be too sensitive to environmental factors such as moisture and dust. Furthermore, only a number of liquids can be used to charge certain dielectrics and these liquids may not be compatible with the MEMS materials used in an electret microphone.

This leaves only electret formation by irradiation with low-energy electron beams. This technique not only allows for control of electron dose and energy, but the dielectric material of choice for this method, thin film fluoropolymers, can also be used as a diaphragm material. Since the implantation depth of the electron beam is adjustable, simple electron barriers such as photoresist can be used to mask integrated electronics during the electret charging process.

4.2.1 Back-Lighted Thyratron

The most obvious and widely available electron beam source in most research facilities is a scanning electron microscope (SEM). When using this technologically complex apparatus, the dielectric sample is placed in a vacuum chamber and a uniform beam of monoenergetic electrons is scanned over the sample. The disadvantages of a SEM are that it is too expensive and complicated to maintain, and too cumbersome to operate for the simple task of charging dielectrics. Furthermore, the setup cannot accommodate entire 4" or 6" wafers, the scanning area of the beam is limited to only a few mm^2, the electron beam has only a set energy range, other users will resist modifications to the instrument, and the rastoring of the electron beam cannot be turned

off (otherwise the dielectric sample cannot be observed in the vacuum chamber). In light of these limitations, a need existed for a simple, low cost, high throughput, wafer compatible, energy adjustable, non-scanning electron beam source. With help from Dr. Tseng-Yang Hsu in 1995, a custom wide-beam electron source was constructed according to the above criteria.

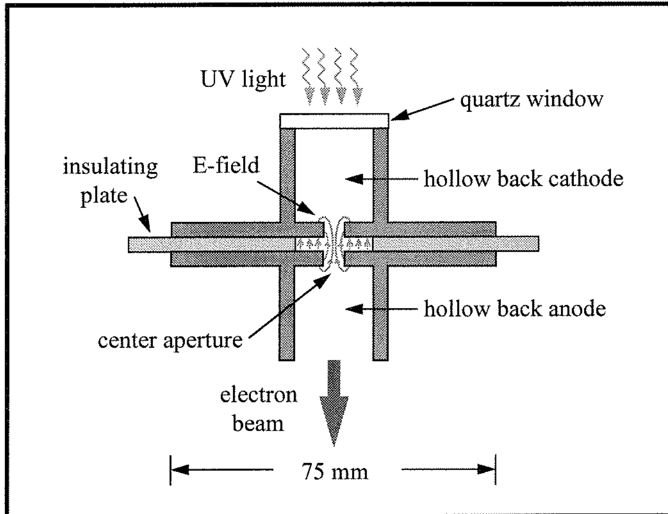

Figure 4-3. The Back-Lighted Thyratron.

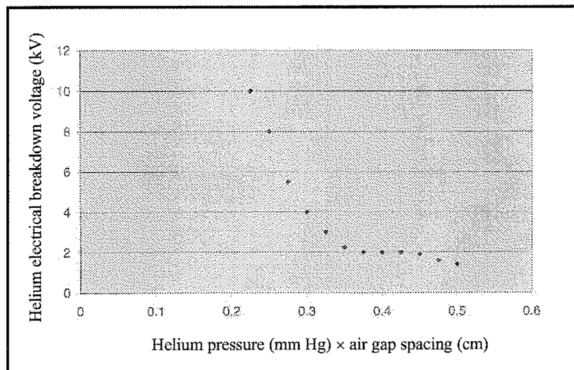

Figure 4-4. Helium electrical breakdown curve for the BLT.

To form electrets from thin film dielectrics, the use of a Back-Lighted Thyratron (BLT) was investigated. The BLT [20, 21] structure consists of two electrode plates with a hollow back cathode and hollow back anode (Figure 4-3). The two brass electrodes facing each other have a diameter of 75 mm and a center aperture of 5 mm. The

electrodes are separated by a 5 mm thick insulating Plexiglas plate. The structure is filled with helium to a pressure of 300 to 1000 mTorr. The breakdown voltage of helium between the parallel plate electrodes is a function of the product of distance between the electrodes and helium pressure (Figure 4-4). This is described by the well-known Paschen curve.

The BLT is triggered optically by an ultraviolet light pulse applied to the back of the cathode. The ultraviolet light passes through a quartz window into the back of the cathode, generating free electrons near the center aperture. The electrons are subsequently drawn by the strong electric field towards the anode. Since the BLT is operated on the left-hand side of the helium Paschen curve, the breakdown occurs along the longest possible path between the cathode and anode. As the low current predischarge travels along this path, it increases rapidly by charge-carrier multiplication. During and briefly before voltage breakdown, an energetic beam of runaway electrons is formed. Part of this electron current becomes an electron beam that is ejected from the anode center aperture and is directed towards the grounded dielectric sample. The beam propagates in a self-focused manner over a length of several tens of centimeters.

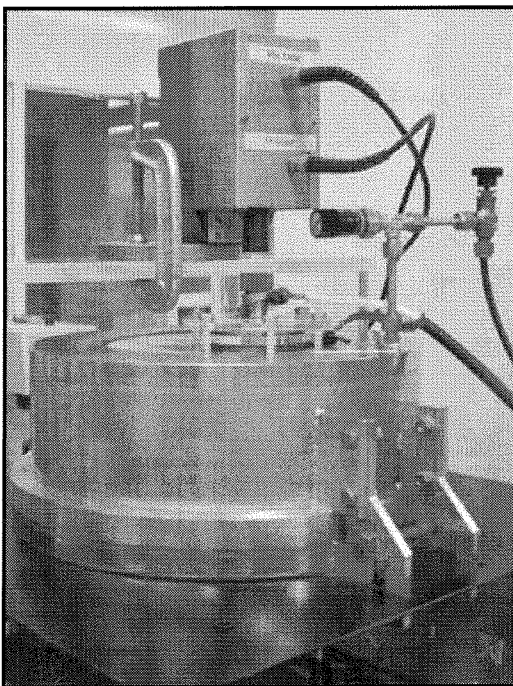

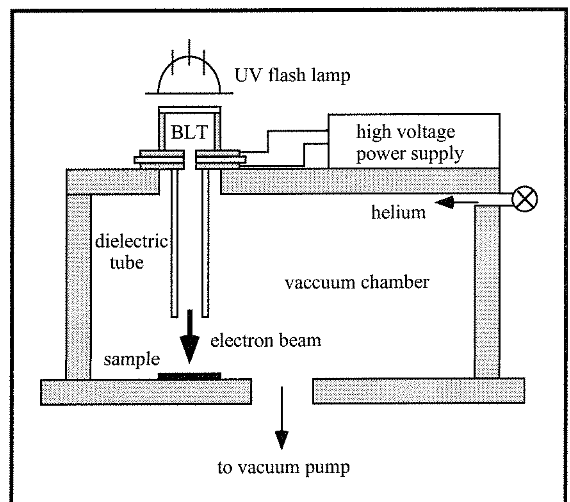

Figure 4-5. Picture and schematic of the BLT charge implantation chamber.

The in-house BLT was constructed on top of a vacuum chamber with a triggering UV flashlamp at a distance of 2 cm away from the quartz window as shown in Figure 4-5. The BLT cathode is biased at a high negative potential for beam acceleration. The electron beam pulse is directed to the sample which is 12 cm away from the beam exit. With a beam divergent angle of 6°, the beam diameter is 1.75 cm at the sample surface [21]. Integrating a dielectric tube at the beam exit has the effect of collimating and focusing the electron beam [22]. The bias potential is adjusted according to the desired range of electrons in the dielectric film. The use of the BLT is favorable because:

- it operates at room temperature
- the electron beam energy can be easily varied from 2 to over 10 keV
- the electron beam duration can be controlled by an external RC circuit
- it has a large beam size (several millimeters in diameter)
- it can deliver high electron doses (10^{-9}-10^{-6} C)
- it has a high throughput
- it is rugged, low cost and has a long life
- it can be instantaneously started up

and with an internal motorized XY stage it can step through individual dies on a whole wafer.

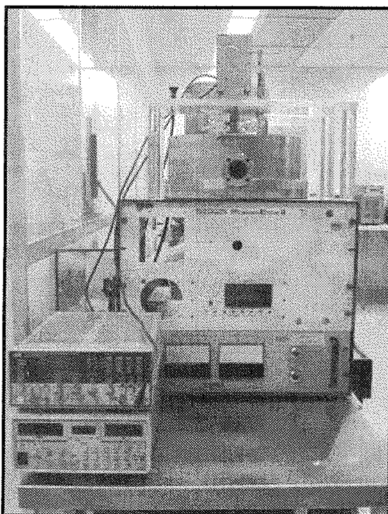

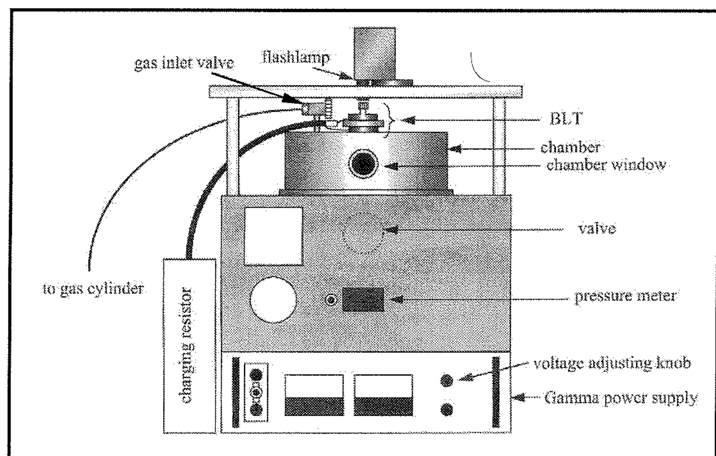

Figure 4-6. Picture and drawing of the BLT charge implantation system.

Figure 4-6 is a picture and drawing of the BLT system. By adjusting the helium pressure in the chamber to a level slightly below the illustrated electrical breakdown points in Figure 4-4, the electron beam energy can be varied from 2 to over 10 keV. Since the range of monoenergetic electrons is strictly defined by their energy, this allows the operator to ensure that the maximum electron beam range is smaller than the dielectric thickness.

4.3 Charge Measurement

In order to determine the effectiveness of the BLT, as well as the suitability of different electret materials, the electret charge must be measured. This is done by measuring the effective surface charge density of an electret sample. The term 'effective' means that surface and bulk homocharges are not distinguished in the measurement, but only their total contribution to the surface potential of the electret is determined.

Two different test instruments were set up to accomplish this task. Both are able to make contact-less measurements. The custom-made instrument was built in 1995 and is referred to as the 'PZT-shaker.' The commercially available instrument was purchased in 1998 and is called a 'Monroe Isoprobe Electrostatic Voltmeter.' The theory of operation and configuration of each instrument will be discussed below.

4.3.1 PZT-shaker

The PZT-shaker setup consists of a PZT stack and a micrometer-controlled stationary electrode (Figure 4-7). To confine displacement in the Z-direction only, the PZT is integrated into a 304 stainless steel flexure hinge that is machined by electrical discharge machining (EDM). The movable part of the flexure hinge weighs 30 g and has a spring constant of 1.53×10^6 N/m. The PZT driver deforms 15 μm at 100 V and can be driven by a maximum voltage of 150 V. The linearity of the PZT displacement caused by hysteresis is 10%. The PZT is driven by a unit consisting of a periodic source and an amplifier. The amplifier is a class-B push-pull type amplifier specially designed for capacitive loads. An eddy-current sensor is integrated into the stationary electrode assembly to monitor the dynamic and static displacement of the vibrating electrode. The

test samples are typically 1.2 cm × 1.2 cm silicon dies, evaporated with 2000 Å of Cr/Au on one surface. The Au surface is then coated with the electret material under test and the BLT is used to implant electrons with different energies into the material.

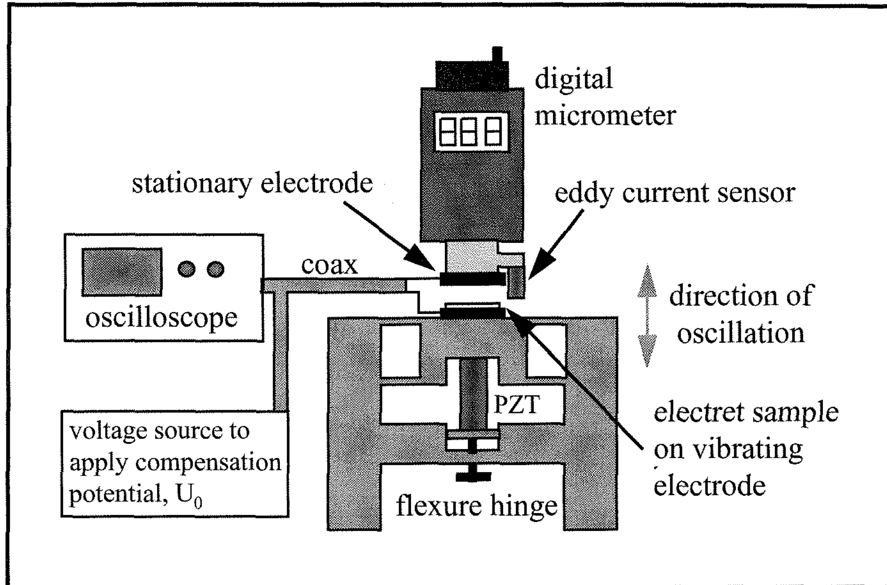

Figure 4-7. Schematic of the PZT-shaker.

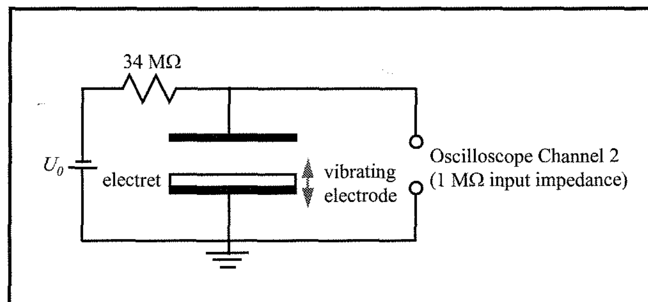

Figure 4-8. Schematic of the electric field compensation circuit.

The electret sample is fixed on top of the vibrating flexure hinge by vacuum and is then positioned about 1 mm away from the surface of the stationary electrode. When the PZT is turned on, an AC signal (generated by induced charges on the stationary electrode due to the vibrating electret) can be observed on an oscilloscope (Figure 4-8). By applying a compensation potential, U_0, between the two electrodes, the net electric field

in the air gap between the vibrating and stationary electrode can be reduced to zero. The AC signal generated by the induced charges then also becomes zero. This is called the 'electric field compensation method' of electret charge measurement. The effective surface charge density, σ_e, of the electret sample is then given by [1]:

$$\sigma_e = \frac{\varepsilon_e \varepsilon_0 U_0}{s_e} \quad [\mathrm{C/m^2}] \tag{4-1}$$

where:

σ_e: electret surface charge density [C/m^2]

ε_e: relative dielectric constant of electret [unitless]

ε_0: permittivity of free space [8.85×10^{-12} F/m]

U_0: compensation potential [V]

s_e: electret thickness [m]

Figure 4-9a shows a typical PZT driving signal at 100 Hz and the AC signal generated by an electret sample, as viewed on an oscilloscope. Figure 4-9b shows the generated AC signal being compensated to zero by the application of a compensation potential, U_0. Figure 4-10 shows a picture of the actual PZT-shaker setup.

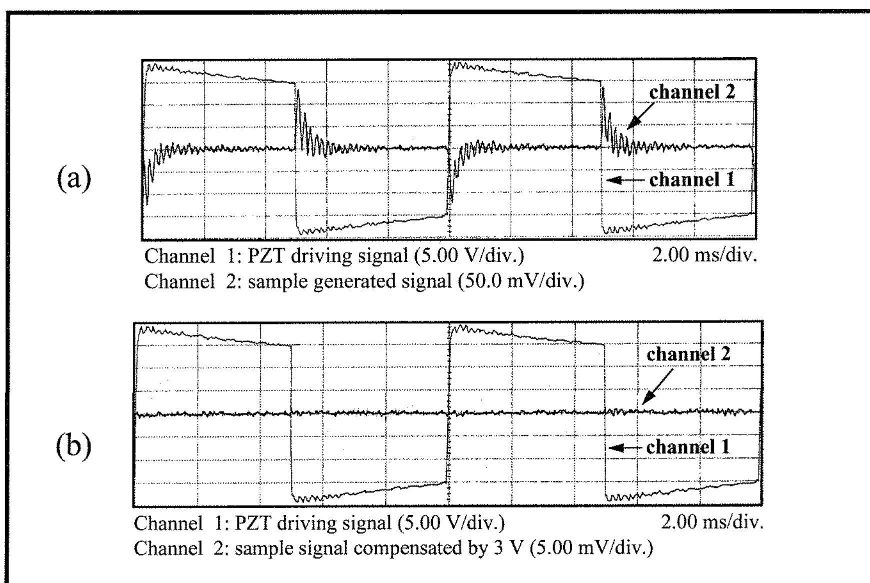

Figure 4-9. Oscilloscope screen views. (a) A PZT driving signal and the induced AC signal. (b) The same PZT signal and the compensated AC signal.

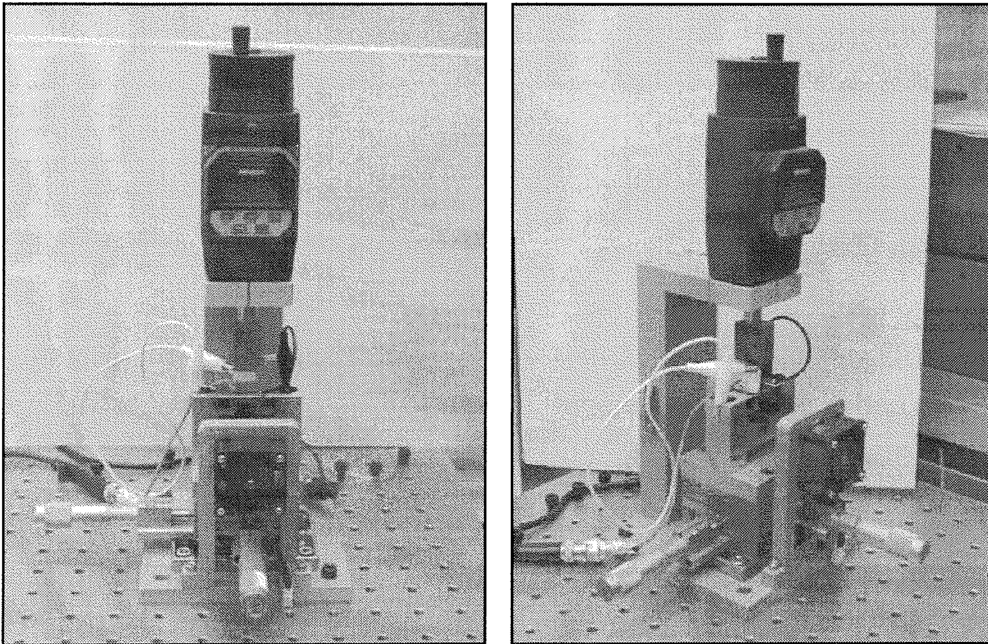

Figure 4-10. Pictures of the PZT-shaker setup.

4.3.2 Monroe Isoprobe Electrostatic Voltmeter

Although the PZT-shaker can accurately measure the surface charge density of electret samples with solid substrates, it cannot be used to measure the electret charge on diaphragms since the entire sample must be held in place by a vacuum pickup and then shaken vigorously. Consequently, a commercial electrostatic voltmeter and probe was purchased from Monroe Electronics in 1998. A simplified block diagram of the Monroe voltmeter Model 244A and probe Model 1017 Type AEH is shown in Figure 4-11.

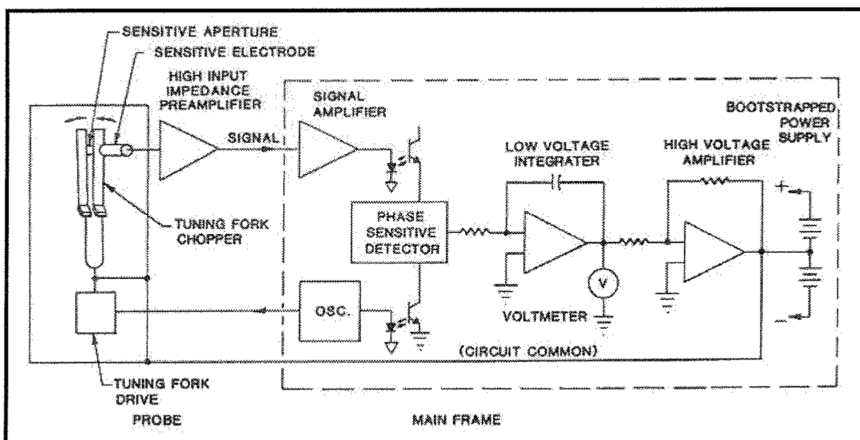

Figure 4-11. Simplified block diagram of the Monroe voltmeter and probe [23].

The probe is usually placed about 1 mm away from the electret surface under test. The sensitive probe electrode looks at the electret surface through a small aperture at the base of the probe assembly. The chopped AC signal induced on this electrode is proportional to the potential difference between the electret surface and probe. By minimizing the induced chopped AC signal, the internal amplifiers drive the probe to the same potential as the electret surface. In effect, this is the same electric field compensation principle as used in the PZT-shaker. For a 1 mm probe-to-surface spacing, the mismatch between electret and probe potential is within 0.1% [23]. By simply metering the output of the high voltage amplifier (up to 3000V), the electret surface potential can be read out. The effective surface charge density of the electret can then be calculated from equation (4-1), by replacing the compensation potential, U_0, with the read out potential of the Monroe voltmeter.

Figure 4-12 shows a picture of the Monroe Isoprobe Electrostatic Voltmeter setup. Surface charge density measurements using this instrument are in close agreement with the values obtained with the PZT-shaker. The main advantages of the Monroe system over the PZT-shaker are: quietness (the PZT makes tons of noise), ease of use, accuracy, reliability and portability. The disadvantage is that electrical arching can sometimes occur between the probe and the very closely positioned electret diaphragm under test. The spark that is generated can sometimes rupture the thin diaphragm.

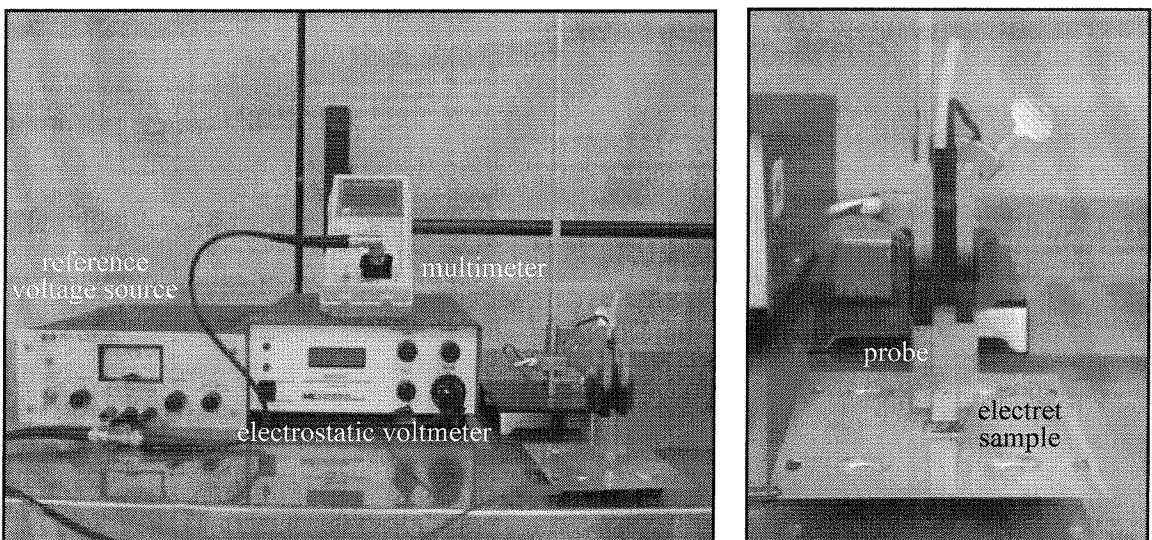

Figure 4-12. Pictures of the Monroe voltmeter and probe setup.

4.4 Electret Materials

In a MEMS electret microphone, the criteria that must be satisfied when choosing a dielectric that can be used as both an electret and diaphragm material are:

1. exhibit fairly high charge densities (10^{-5} to 10^{-4} C/m^2) that are stable over time in the temperature range -20 to 100°C
2. have a glass transition temperature, T_g, well above 100°C, the upper operating temperature of the microphone
3. have the mechanical properties: low to medium density, high elasticity, residual tensile stress and pinhole-free
4. should be non-hygroscopic
5. can form an electret by electron implantation using the BLT
6. should be deposited at low temperatures (to allow for post-IC processing)
7. ability to form thin film membranes with controllable thickness
8. are compatible with MEMS fabrication processes

Table 4-2 showed that polyolefines are the most suitable materials for charge-implanted electrets. Table 4-3 lists the electret discharge and glass transition temperature of various polyolefines materials. Criteria 1 and 2 are only satisfied by three polyolefines: polytetrafluoroethylene (PTFE), polyfluoroethylenepropylene (FEP) and polystyrene (PS). Since it is nearly impossible to form any type of PS membrane, only PTFE and FEP satisfy criteria 3 through 7. These two materials belong to the family of DuPont fluoropolymers and are know by the trade names: Teflon-PTFE and Teflon-FEP. Both exhibit extreme chemical inertness, have melting points above 250°C, exhibit low water absorption (< 0.03%) and are very elastic. They have extremely high resistivities (> 10^{18} Ω-cm) and are excellent at storing negative homocharge.

The only drawback of these two polymers is their incompatibility with MEMS fabrication processes (criterion 8). Since both PTFE and FEP and are insoluble at temperatures below 300°C, they cannot be spin-cast as a polymer suspension, dried and patterned by standard lithographic processes. Although these fluoropolymers are commercially available in films that are 12.5 or 25 μm thick, adhesion to foreign surfaces

usually requires the use of a chemical adhesive, a process that will not produce films a few microns in thickness. Clearly, another polymer dielectric that has similar mechanical, chemical and electrical properties as PTFE and FEP, but can be selectively deposited and removed as a very thin film using MEMS compatible processes, is needed. This polymer dielectric is Teflon AF, an amorphous fluoropolymer from Du Pont.

Table 4-3. Discharge and glass transition temperature of various polyolefine electrets [5].

Material Name (Abbreviation)	Discharge Temp [°C]	Glass Transition Temp [°C]
High density polyethylene (PE/HD)	150	~ -125
Polyvinyl fluoride (PFV)	40	-20
Polyvinyl chloride (PCV)	55	65
Polyvinylidene fluoride (PF_2V)	90	-45
Chlorinated polyvinyl chloride (CPCV)	95	NA
Polytetrafluoroethylene (PTFE)	230	127
Polyfluoroethylenepropylene (FEP)	NA	130
Trifluorochloroethylene (TFCE)	120	45
Polystyrene (PS)	125	100
Polypropylene (PP)	155	-20
High density polyethylene w/ large crystallites (PE/HD,LC)	150	~ -125
High density polyethylene w/ small crystallites (PE/HD,SC)	130	~ -125
Medium density polyethylene (PE/MD)	120	~ -125
Low density polyethylene (PE/LD)	85	~ -125

4.4.1 Teflon AF

Teflon AF is a copolymer of 2,2-bistrifluoromethyl-4,5-difluro-1,3-dioxole, (PDD) with tetrafluroethylene (TFE), where PDD is the principle monomer (Figure 4-13). There are two general-purpose grades of Teflon AF: AF 1600 which has 65 mol% PDD and a T_g of 160°C, and AF2400 which has 87 mol% PDD and a T_g of 240°C. Since the MEMS electret microphones in this paper incorporate other low temperature

polymers (Parylene and photoresist) as structural materials, in order to keep processing temperatures as low as possible, only Teflon AF 1600 is used.

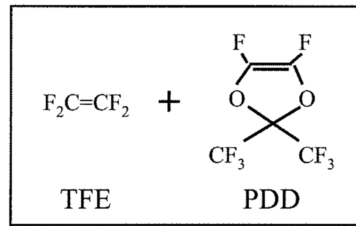

Figure 4-13. Monomers of Teflon AF [24].

Table 4-4. Solvents for Teflon AF [24].

Designation	Boiling Point [°C]	Manufacturer
Fluorinert		
FC-72	56	3M
FC-77	97	3M
FC-75	102	3M
Flutec		
PP50	29	Rhone-Poulenc
PP2	76	Rhone-Poulenc
PP6	142	Rhone-Poulenc
Galden		
HT-110	110	Ausimont
HT-135	135	Ausimont
DO2, DO-2-TS, DO3, DO5	165-230	Ausimont

Because Teflon AF is completely amorphous, it is soluble in several perfluorinated solvents at room temperature (Table 4-4). The electrets fabricated in this thesis are made from Teflon AF 1601S-6 solution (6% solid Teflon AF by concentration suspended in FC-75 solvent). This particular mixture ratio was chosen because its viscosity (80 cP at 23°C) allows 0.5 to 2.5 μm thick films to be spin-cast using conventional photoresist spinners (Figure 4-14). The FC-75 solvent was chosen because its 102°C boiling point

allows the drying and sintering of the film to occur in normal convection ovens. Table 4-5 shows more property data for Teflon AF 1601S. Teflon AF is stable in air up 360°C, after which it decomposes. Teflon AF 1601S-6 costs $280 per 100 mL bottle (1/1/98).

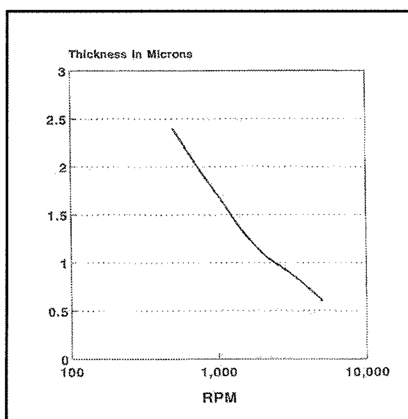

Figure 4-14. Spin curve of Teflon AF 1601S-6 solution [24].

Table 4-5. Typical property data for Teflon AF 1601S [24].

Property	ASTM Method	Unit	Value
Physical and Mechanical Properties			
Glass Transition Temperature	D3418	°C (°F)	160 (320)
Tensile Strength	D638	MPa	27
Ultimate Elongation	D638	%	15
Tensile Modulus	D638	GPa	1.55
Volume Coefficient of Thermal Expansion	E831	ppm/°C	260
Specific Gravity	D792		1.78
Melt Viscosity	D3835	Pa·sec	5000 at 250°C (482°F), 100 sec^{-1}
Electrical Properties			
Dielectric Constant	D150	at 1 MHz	1.934
		at 3.5 MHz	1.933
		at 9.5 MHz	1.933
		at 100 MHz	1.933
		at 1 GHz	1.930
		at 3 GHz	1.928
		at 8.5 GHz	1.927
		at 13.6 GHz	1.927
Dissipation Factor	D150	at 1 MHz	0.00012
		at 3.5 MHz	0.00012
		at 9.5 MHz	0.000073
		at 100 MHz	0.000099
		at 1 GHz	0.00018
		at 3 GHz	0.00022
		at 8.5 GHz	0.00015
		at 13.6 GHz	0.00020
Other Properties			
Optical Transmission	D1003	%	>95%
Refractive Index	D542	-	1.31
Contact Angle with Water		degrees	104
Critical Surface Energy		dynes/cm	15.7
Brookfield Viscosity in Fluorinert FC-75		Pa·sec	5500 at 18 wt%
Water Absorption	D570	%	<0.01
Solubility in Fluorinert FC-75		%	25–30 wt% at RT

4.5 Working Process

The Teflon AF electret is prepared according to the following procedure:

Dielectric preparation

1. The substrate (cleaned of dusts, organic contaminants and weakly adhering oxide) is baked at 130°C for 30 minutes to drive off any residual water from its surface.
2. The substrate is then cooled to room temperature and Teflon AF is spun onto the substrate surface to the desired thickness (using the spin curve in Figure 4-14 as a guide). A thickness measurement using an Alpha-step profilometer can be obtained at this point.
3. The coated substrate is then air-dried for 10 minutes at 25 to 50°C to remove most of the solvent.
4. The coated substrate is then baked at 10°C above the boiling point of the solvent (for FC-75, b.p. is 102°C) for 45 minutes. At this point less than 1% of solvent remains.
5. To remove the last trace of solvent, the coated substrate is heated to 5°C above the T_g of the Teflon AF (for AF 1600, T_g is 165°C) for 15 minutes.
6. For maximum uniformity of coating thickness and enhanced adhesion, the coated substrate can be heated to 330°C for 10 to 15 minutes. This allows the polymer to spread uniformly over the substrate and level any uneven contours formed during previous drying steps. The thickness of the electret should be measured again at this point. Note: This final step cannot be performed when Teflon AF is spun onto other low temperature polymers (e.g., Parylene C) whose melting points are below 330°C!
7. Steps 2 through 6 can be repeated if films thicker than 2 μm are desired.

Electret Formation

8. The coated substrate is placed into the BLT, and the chamber is adjusted to the desired helium pressure as set by the electrical breakdown curve in Figure 4-4.
9. The BLT bias voltage is set slightly below the helium breakdown point as determined by the pressure in step 8.
10. The BLT is triggered once with a UV light pulse, resulting in the delivery of one electron 'shot.' Multiple shots can be applied to increase the charge in the electret.

11. The electret is then removed and the effective surface potential is measured by the PZT-shaker or Monroe Isoprobe Electrostatic Voltmeter to make sure that the BLT was effective.
12. The electret is then aged at 100°C for 3 hours in a convection oven to drive off electrons from energetically shallow traps. It helps to place the electret substrate on a conductive surface during this step to allow electrons that are freed from their traps to move out of the Teflon AF dielectric.
13. The stabilized effective surface potential is then measured again. The effective surface charge density of the electret is calculated using equation (4-1) of section 4.3.1.

The above process can be applied to solid substrates as well as free-standing diaphragms. The desired temperature set-points should be reached by gradual ramping to minimize thermal shock. Good ventilation must be provided since the residual gasses that out-diffuse from Teflon AF (e.g., FC-75, HF, COF_2, CO and HFA) may be harmful.

4.6 Teflon AF Physical Characteristics

Since Teflon AF is essentially nonpolar, contains no reactive chemical functionality and is highly resistant to chemical attack, adhesion to various substrates depends primarily on physical, rather than chemical interactions. For time spans comparable to usual processing times (less than ten minutes), the adhesion of Teflon AF to different material surfaces such as silicon, silicon dioxide, silicon nitride, gold, chrome and Parylene is satisfactory in the presence of chemicals frequently used in MEMS fabrication, such as water, photoresist developers, isopropanol, HF, BHF, Cr etch and Au etch. Teflon AF was found to adhere well to titanium, aluminum and electrolytic copper, and poorly to any substrate when soaked for over 10 minutes in KOH or acetone. The application of fluorosilanes onto glass or silicon substrates (followed by 10 minutes at 110°C) before coating with Teflon AF has been found to improve adhesion. Chemical or mechanical roughening of the substrate has the same effect.

If necessary, the Teflon film can be patterned with oxygen plasma using a metal or photoresist mask. To ensure good adhesion to photoresist, the Teflon surface is roughened by bombardment with low energy oxygen plasma for a few tens of seconds. Since the (high) etch rates of Teflon AF and photoresist in oxygen plasma are very similar, significantly thicker photoresist should be used when etching Teflon AF films down to the substrate. No measurable etching was observed for Teflon AF in SF_6 plasma, CF_4 plasma, BrF_3 or XeF_2 gas.

The Teflon AF 1601S film that is deposited according to the aforementioned working process (minus the 330°C annealing step) is a transparent film that has a surface roughness of approximately ± 0.10 μm. Figure 4-15 shows pictures of the Teflon surface over evaporated gold. Annealing at 330°C reduces the surface roughness to less than ± 0.03 μm. However, as previously mentioned this high temperature annealing step is not suitable for all processes. As expected from a fluoropolymer, the resulting film is also extremely hydrophobic.

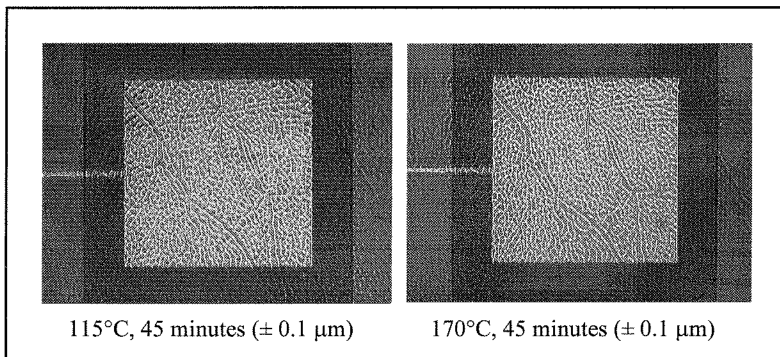

115°C, 45 minutes (± 0.1 μm)   170°C, 45 minutes (± 0.1 μm)

Figure 4-15. Surface of Teflon AF 1601S film on gold annealed at 115°C & 170°C.

4.7 Teflon AF Electret Characteristics

Depending on the number of BLT shots, stable effective surface charge densities on the order of 10^{-5} to 10^{-4} C/m^2 have been obtained using Teflon AF 1601S. These charges are always negative. The charge density magnitude is comparable to what has been reported for Teflon films [1, 2, 25]. Multiple BLT shots have the effect of increasing the overall charge density (Figure 4-16). However, this cumulative effect is only limited to a

maximum of 3 to 4 shots, after which the charge density saturates (to around 10^{-4} C/m^2). Electrons with energies between 7 to 10 keV are typically used with Teflon AF 1601S electrets. Lower energies do not seem to impart any significant stable charge to the Teflon AF (<10^{-5} C/m^2). The measured electret surface potentials have been found to be slightly higher for 7 keV electrons than for 10 keV electrons. A reasonable explanation for this is that lower energy electrons are implanted closer to the electret-air interface, where they contribute more to the measurable effective surface potential. The saturated charge density that can be achieved for a given electron energy is rather repeatable (± 15%), but the amount of charge implanted per shot varies from sample to sample.

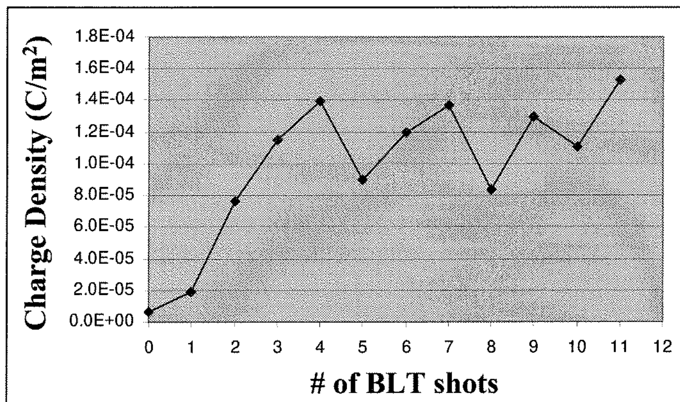

Figure 4-16. Charge saturation with number of BLT shots using 10 keV electrons.

Electrons that are implanted into Teflon AF electrets do not remain indefinitely and under any conditions. Changes in environmental factors such as temperature, humidity and exposure to chemicals can quickly change the number and distribution of these charges. In polymer electrets containing bulk or surface trapped electrons, there are three main mechanisms to charge decay [26]. These mechanisms determine the degree of charge stability in an electret. One is due to the attraction of positively charged ions or other charged particles from the environment. If these foreign charges become trapped at the electret surface, they can negate surface trapped electrons or terminate the electric fields emanating from bulk trapped electrons. The second mechanism of decay is due to the ability of electrons to move by conduction through the body of the electret. This is determined by the bulk conductivity and permittivity of the electret material. The last mechanism of decay is a result of lateral conductivity at the electret-air interface. The

adsorption of environmental polar gases or contaminants can contribute to this surface conductivity. Stable electrets should have surface conductivities that are as low as possible.

This thesis will not delve into the exact mechanisms by which Teflon AF electrets trap or de-trap charge, as this is by itself a Ph.D. thesis topic. We will, however, present the results of our observations on the net influence of different environmental factors on the effective surface charge density (hereafter simply referred to as 'charge density'). These stability trends will obviously affect the performance of MEMS electret microphones fabricated using this technology.

4.7.1 Thermal Stability

Experimental data has shown that at room temperature (25°C), Teflon AF 1601S electrets initially undergo a drop in charge density a few hours after implantation, but then stabilize afterwards (Figure 4-17). Some samples were monitored at room temperature over a period of three years (the longest observation period to date) and no significant charge decay has been observed. Samples have also been tested for charge decay at elevated temperatures in air. Curve (a) of Figure 4-18 shows the charge density of a sample at 100°C for 16 hours. The 40% drop in charge density is due to the elevated temperature. However, even at 100°C, the charge stabilizes after this initial drop to a rate that is not measurable within the time span of the experiment. The same electret sample is then monitored for charge decay at 120°C as shown by curve (b) of Figure 4-18. Again there is an initial drop in charge density, but the charge stabilizes after a few hours. The same trend is observed for the same sample at 140°C, as illustrated by curve (c) in Figure 4-18. Further tests at 130°C and 160°C with different samples confirm the same decay-then-stabilize behavior (Figure 4-19). Using this data trend, a procedure was devised to stabilize the Teflon AF electret by thermally 'aging' it at 100°C in air for 3 hours (immediately after charge implantation). After thermal annealing, electrons that occupy energetically shallow traps are released, thus resulting in a less charged, but more stable electret at room temperature.

It was also discovered that at 190°C, Teflon AF 1601S electrets loses more than 80% of their charge within a few hours (Figure 4-19). This is not surprising since its T_g is only

160°C. This is also consistent with the Teflon-FEP-A data presented in Table 4-1, which shows that at around 200°C the electrons from surface, near-surface and bulk traps all become released.

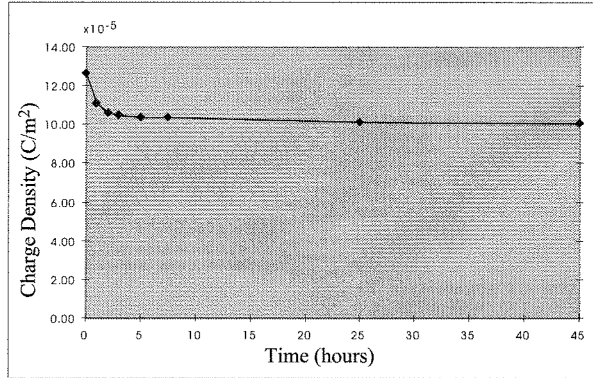

Figure 4-17. Charge density of Teflon AF electret at 25°C.

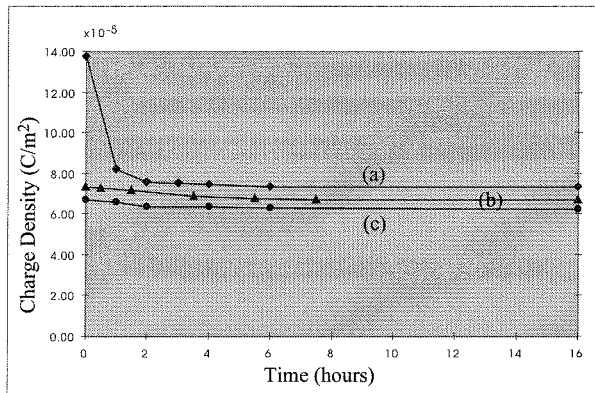

Figure 4-18. Charge density of Teflon AF electret at elevated temperatures.

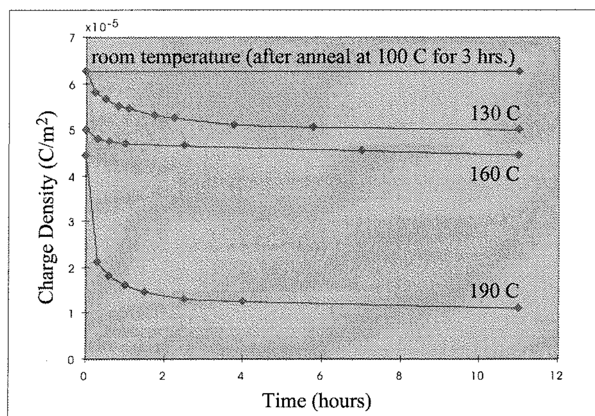

Figure 4-19. Significant charge loss in Teflon AF electret at 190°C.

The charge decay time constant, τ, at various elevated temperatures can provide valuable information about the lifetime of stabilized electrets at room temperature. If we assume the charge decay can be approximated by the exponential function:

$$\sigma_e(t,T) = \sigma_e(0,T)\exp\left(\frac{-t}{\tau}\right) \quad [\mathrm{C/m^2}] \tag{4-2}$$

where:

σ_e: electret effective surface charge density [C/m^2]

t: time [s]

T: absolute temperature [K]

τ: charge decay time constant [s]

By measuring the decay in surface potential over time at many constant elevated temperatures and performing an exponential fit to these sets of data, values for the charge decay time constant, τ, can be obtained for different temperatures, T. Since it turns out that for electrets the temperature dependence of the charge decay time constant, τ, is of the Arrhenius type [2]:

$$\tau(T) = \tau_0 \exp\left(\frac{W}{kT}\right) \quad [\mathrm{s}] \tag{4-3}$$

where:

W: activation energy [J]

k: Boltzmanns constant [1.38×10^{-23} J/K]

τ_0: reference charge decay time constant [s]

values for the activation energy, W, and reference charge decay constant, τ_0, can be obtained using corresponding values of τ and T. The charge decay time constant at room temperature can then be obtained for the test electret. Using this method of calculation, room temperature lifetimes on the order of 5 to 50 years have been obtained for aged Teflon AF 1601S electrets. Although the spread of these lifetime values is wide, the magnitudes are sufficiently large to be useful in electret microphone applications.

4.7.2 UV Stability

When an aged (100°C anneal for 3 hours) electret sample was exposed to UV light (365 nm at 3.85 mW/cm^2, 400 nm at 8.5 mW/cm^2) for one hour, no charge decay was observed (Figure 4-20). Although only short-term data has been available, the lack of charge decay at room temperature and in the presence of UV light suggests that a stable and photolithographic-compatible electret can be formed using Teflon AF and the BLT. This opens up the possibility of patterning Teflon AF after it has been charged by the BLT.

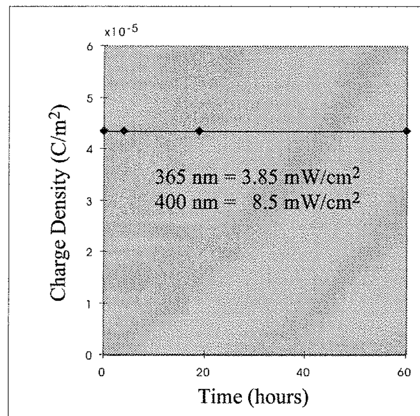

Figure 4-20. Charge density of Teflon AF electret under UV light exposure.

4.7.3 Humidity Stability

Experiments have shown that relative humidity levels as high as 100% at 25°C have negligible effect on the charge storage of aged Teflon AF 1601S electrets. This is true for samples with charge densities ranging from 10^{-4} to 10^{-5} C/m^2. A plausible explanation for this observation is that the BLT implants electrons below the electret surface (higher degree of volume- vs. surface-trap filling) where they are not prone to charge-reducing surface contaminants such as water molecules. This characteristic will undoubtedly improve the humidity stability of MEMS electret microphones that use Teflon AF technology.

4.7.4 Chemical Stability

Of all the chemicals used in MEMS fabrication processes, both acetone and AZ photoresist developer have been found to impart a sizeable negative charge to Teflon AF

1601S electrets. Charge densities as high as 10^{-4} C/m^2 have been measured. The magnitude of these charges are, however, extremely unpredictable. Exposures to these chemicals under identical conditions do not yield similar electret surface potentials. Similarly, the effect of high temperature exposure will quickly eliminate the charges on some electrets, while leaving the charges on others relatively unaffected. Due to the lack of predictability and control of this liquid-charging process, this type of electret formation should be avoided at all times. Thus during MEMS microphone manufacturing, the charging of the Teflon AF polymer should only be done after all the wet fabrication processing steps have been completed. This phenomena is also rather mysterious and somewhat contradictory because DuPont purports that acetone and NaOH (a base similar to the one in AZ developer) have essentially no chemical effect on Teflon AF 1601S [24].

4.8 Summary

This chapter has provided a brief lesson on the theory and history of electrets, while reviewing various types of dielectric materials, formation techniques and charge measurement instruments. Teflon AF 1601S, a brand of Du Pont fluoropolymers, was chosen as the MEMS microphone electret material because it can be spin-cast at room temperature to form micron-thick films. This allows it to be used as a diaphragm material. Teflon AF's excellent charge storage characteristics, chemical inertness, good adhesion and high temperature stability also makes it an effective electret material.

A custom-built Back-Lighted Thyratron charge implantation system has been chosen as the method for transforming the thin film Teflon AF into an electret. The use of the BLT is favorable because it operates at room temperature, the electron beam energy can be easily varied, it has a large beam size, it can deliver high electron doses, it has high throughput, it is robust, it is wafer compatible and it is low cost. By combining the Teflon AF polymer with the BLT system, an effective MEMS compatible thin film Teflon electret technology has been developed.

4.9 References

[1] G.M. Sessler, "Topics in Applied Physics, Vol. 33: Electrets," Springer-Verlag, New York, 1987

[2] B. Hilczer and J. Malecki, "Studies in Electrical and Electronics Engineering 14: Electrets," Elsevier Science Publishing Co. Inc., 1986

[3] H. Fuhrmann, J. Electrostatics, 4, pp. 109, 1978

[4] H. Bauser, "Ladungsspeicherung in Elektronenhaftstellen in Organischen Isolatoren," Kunststoffe, 62, pp. 192, 1972

[5] R.A. Creswell, M.M. Perlman and M. Kabayama, "Dielectric Properties of Polymers," Plenum Press, New York, pp. 295, 1972

[6] S. Gray, Philos. Trans. R. Soc. London, Ser. A, 37, pp. 285, 1732

[7] O. Heaviside, "Electrization and Electrification. Natural Electrets," Electrical Papers, London, Macmillan, 1, pp. 488, 1892

[8] M. Eguchi, "Variation of Electrical Conductivity of Oils and Waxes," Proc. Phys.-Math. Soc. Japan, 1, pp. 320, 1919

[9] M. Eguchi, "On Dielectric Polarization," Proc. Phys.-Math. Soc. Japan, 1, pp. 326, 1919

[10] P. Selenyi, Z. Tech. Phys., 9, pp. 451, 1928

[11] G. Nadjakov, "On a New Type of Permanent Polarization of Dielectrics. A New Type of Electret: Photoelectrets," Tobinnik Fiz. Mat, Sofijskij Univ., 33, pp. 409, 1936/37

[12] L.G. Brazier, Engineer, 196, pp. 637, 1953

[13] B. Gross, J. Polym. Sci., 27, pp. 135, 1958

[14] B. Gross, Z. Phys., 155, pp. 479, 1959

[15] R.A. Creswell and M.M. Perlman, J. Appl. Phys., 41, pp. 2365, 1970

[16] C.S. Bhatnagar, Indian J. Pure Appl. Phys., 2, pp. 331, 1964

[17] P.W. Chudleigh, Appl. Phys. Lett., 21, pp. 547, 1972

[18] J.H. Dessauer, "Xerography - A New Method of Image Recording," Internationales Kolloquium uber wissenschaftliche Photographie, Zurich, pp. 93, 1961

[19] G.M. Sessler and J.E. West, "Self-Biased Condenser Microphone with High Capacitance," J. Acoust. Soc. Am., 34, pp. 1787, 1962

[20] G. F. Kirkman and M. A. Gundersen, "A Low Pressure Light Initiated Glow Discharge Switch for High Power Applications," Appl. Phys. Lett. 49, pp. 494 1986

[21] T-Y Hsu, "A Novel Electron Beam Source Based on the Back-Lighted Thyratron," Ph.D. Thesis, University of Southern California, 1992

[22] T-Y Hsu, K. Frank, and M. A. Gundersen, "Collimating Structure for Intense Pseudospark Electron Beams," IEEE International Conference on Plasma Science, New Mexico, June 6-8, 1994

[23] "Instruction Manual: Isoprobe® Electrostatic Voltmeter Model 244A," Monroe Electronics, New York, 1991

[24] W.H. Buck and P.R. Resnick, "Properties of Amorphous Fluoropolymers Based on 2,2-Bistrifluoromethyl-4,5-Difluro-1,3-Dioxole," 183rd Meeting of the Electrochemical Society, Honolulu, USA, May 1993

[25] Y. Tada, "Experimental Characteristics of Electret Generator, using Polymer Film Electrets," Japan J. Appl. Phys. 31, pp. 846, 1992

[26] J.A. Voorthuyzen, W. Olthuis, P. Bergveld and A.J. Sprenkels, "Research and Development of Miniature Electrets," IEEE Transaction on Electrical Insulation, Vol. 24, No. 2, pp. 255-266, April 1989

Chapter 5
MEMS Electret Microphones with Nitride Diaphragms

5.1 Preface

An electret acts as a permanent charge source, thus an electret microphone can produce a signal without the need for external biasing. This reduces system volume and complexity (Chapter 2). Due to the superior charge storage characteristics of fluorocarbon polymers, almost every conventional electret microphone uses fluorocarbon electrets, such as Teflon. However, previous research on MEMS electret microphones has mainly focused on the use of silicon dioxide as the electret material, rather than Teflon (Chapter 3). The extremely poor adhesion of Teflon, difficulty in applying it in thin film form (< 5 μm) and inability to pattern it using standard lithographic processes are the main reasons why its use as an electret in MEMS microphones has been limited.

Using a new amorphous thin film Teflon technology that overcomes most of the aforementioned problems (Chapter 4), a proven electret material can now be combined with the advantages of MEMS fabrication processes. This is demonstrated in three different types of MEMS electret microphones that combine silicon nitride diaphragms with silicon, glass and Parylene C/silicon nitride backplates.

5.2 Silicon Nitride Diaphragms

Silicon nitride is a relatively attractive microphone diaphragm material because it has the following chemical, mechanical, electrical and process-compatibility properties:

- It is very resistant to attack by anisotropic silicon etchants frequently used in bulk micromachining such as KOH and TMAH [1]. This allows it to be used as an etch-stop when deposited onto silicon substrates.

- It has a controllable residual tensile stress [2]. Since most MEMS microphone diaphragms are modeled as membranes (section 2.3.1), it is the residual tensile stress that affects mechanical sensitivity, rather than the Young's Modulus of the diaphragm material.
- It is a good insulator, so metal electrodes can be deposited onto its surface without shorting to the conductive silicon substrate.
- Its deposition can be precisely controlled to submicron or micron thicknesses with good uniformity across a wafer and from wafer-to-wafer. This is important for device uniformity and reproducibility.
- Teflon AF 1601S adheres relatively well to its surface.

There are two main methods by which silicon nitride films can be deposited onto silicon substrates. One is plasma-enhanced chemical vapor deposition (PECVD) and the other is low pressure chemical vapor deposition (LPCVD). Although PECVD silicon nitride films can be grown at 300°C (such that it can be deposited in the presence of some metals or microelectronics) it has inferior chemical, mechanical and electrical properties when compared to LPCVD silicon nitride films that are deposited at 835°C. For PECVD films it has been reported that the degree of tensile stress is unstable over time and difficult to reproduce from run to run. Its etch rate in KOH is about 60 times higher than that of LPCVD films and leakage currents are higher and the buckling strengths are lower than similarly sized LPCVD films [3]. Consequently, LPCVD silicon nitride is the better choice of diaphragm material for use in MEMS electret microphones.

The LPCVD deposition parameters used for the devices in this thesis are:

- Deposition temperature: 835-837°C
- SiH_2Cl_2/NH_3 ratio: 4.0-4.3
- Deposition pressure: 340 mTorr

These conditions were chosen because it produces silicon nitride films with relatively low tensile stress (70-150 MPa). This is consistent with reports in literature that for

deposition temperatures in the range 835 to 850°C, the residual tensile stress decreases with increasing deposition temperature and increasing SiH_2Cl_2/NH_3 ratios [2].

5.3 Silicon Nitride/Teflon AF Composite Diaphragm Characteristics

The MEMS electret microphone diaphragms described in this chapter are all silicon nitride, Cr, Au and Teflon AF composite structures. The nitride is typically 0.5 to 1 μm thick and acts as the main stress-determining material. The evaporated 100 Å Cr and 1000-2000 Å Au layers form the diaphragm electrode. The Teflon AF film serves as the electret layer and is usually about 1 μm thick.

By measuring the resonant frequency, f_0, of these composite diaphragms with a Laser Doppler Vibrometer (LDV) and by applying the membrane model, the residual tensile stress can be approximated by equation (2-13) [4]:

$$f_0 = \sqrt{\frac{\sigma}{2a^2\rho}} \qquad \text{[Hz]}$$

where:

σ: residual tensile stress of the composite diaphragm [N/m^2]

ρ: density of the main stress-contributing diaphragm material [kg/m^3]

a: length of one side of square diaphragm [m]

Figure 5-1 shows pictures of the LDV setup. At the right is a small PZT actuator on top of which is mounted the diaphragm chip (using double-side stick tape). The PZT is used to excite the diaphragm across a range of frequencies. On the left is a commercially available LDV that consists of a frequency stabilized HeNe laser and an acoustooptical modulator for upshifting the laser frequency to 40 MHz. The shifted signal beam emitted by the LDV is redirected and focused onto the center of the composite diaphragm. The beam is reflected off the Cr/Au diaphragm layer and is collected by the LDV and recombined with the reference beam to provide a frequency-modulated signal with a carrier of 40 MHz and a modulation signal proportional to the velocity of excitation motion of the diaphragm. This signal is then fed to a FM demodulator and the output is

connected to a spectrum analyzer that also provides the excitation signal to the PZT. Figure 5-2 shows the frequency response of an individual PZT and that of a composite diaphragm mounted on top of a PZT. The fundamental resonant frequency, f_0, of the diaphragm is the first peak that is present in its frequency response graph.

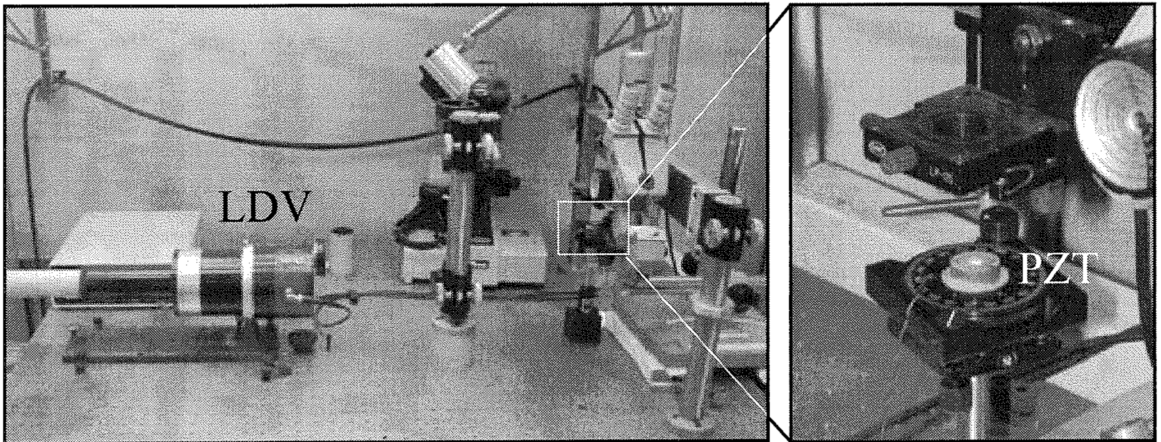

Figure 5-1. Laser Doppler Vibrometer setup for resonant frequency measurements.

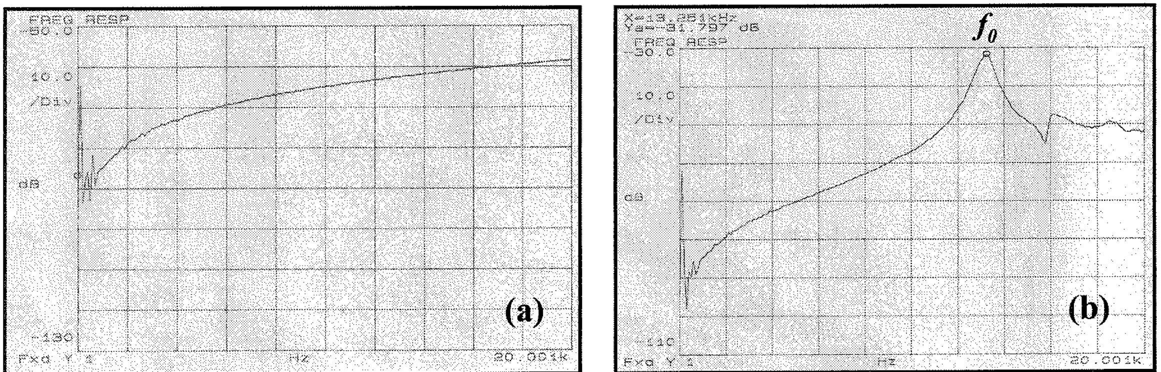

Figure 5-2. Frequency response of (a) PZT and (b) a composite diaphragm on PZT.

Experiments were performed on several silicon nitride/Teflon AF composite diaphragms to study their mechanical stability under different environmental conditions. Table 5-1 shows a typical set of results. All resonant frequency data was obtained at room temperature by the LDV. The data indicates that relative humidity and temperature levels as high as 99% and 85°C, respectively, result in less than 3.5% change in the

resonant frequency (residual tensile stress) of these composite diaphragms. Since the typical measurement error associated with removing and remounting a diaphragm sample onto the LDV PZT is about 1-2%, the measured change is not significant. This is not surprising since silicon nitride is the dominant tensile stress contributor. Its 835°C deposition temperature allows its residual stress to remain unaffected at lower temperatures. The adhesion of Teflon AF to Au and silicon nitride was also found to be favorable under 99% RH and 85°C conditions. No bubble formation or delaminating of the Teflon AF film was observed. These are promising results since a high degree of diaphragm mechanical stability will ultimately translate into more stable MEMS electret microphones.

Table 5-1. Environmental influences on silicon nitride/Teflon AF diaphragms.

8mm × 8mm × 0.5 μm nitride diaphragm 5mm × 5mm 100Å Cr, 1000Å Au 1 μm Teflon AF 1601S	***f₀* right after diaph. fabricat. [kHz]**	***f₀* after 24 hours @ 23°C, 99% RH [kHz]**	***f₀* after 24 hours @ 85°C, room RH [kHz]**	***f₀* after 72 hours @ 85°C, room RH [kHz]**	***f₀* after 7 days @ 85°C, 99% RH [kHz]**
Sample 1	13.68	13.58	14.06	14.06	13.70
Sample 2	13.25	13.12	13.50	13.51	13.25
Sample 3	13.42	13.31	13.79	13.79	13.42

5.4 Silicon Backplate Microphone

The first MEMS electret microphone to be fabricated using the new thin film Teflon AF electret technology is a two-chip device. The substrates of both chips are made from single crystal silicon. One chip contains the silicon nitride/Teflon AF diaphragm, while the other forms a cavity-riddled silicon backplate.

5.4.1 Fabrication and Packaging

Fabrication of the microphone diaphragm begins with a <100> silicon wafer coated with 1 μm thick low-stress LPCVD silicon nitride (SiH_2Cl_2/NH_3=4, 835°C). It is then anisotropically back-etched with KOH to form a 3.5 mm × 3.5 mm free standing nitride diaphragm. The front side of the diaphragm is evaporated with 2100 Å thick Cr/Au

through a physical mask to form the diaphragm electrode. 1 μm thick Teflon AF 1601S is then deposited onto the gold and two shots of 10 keV electrons are implanted into the Teflon using the BLT.

The backplate electrode is fabricated from a wafer coated with 3 μm thermal oxide. Portions of the oxide layer are etched to create etching windows that extend to the silicon substrate. A timed KOH etch follows, creating a 3 μm deep recess in the silicon substrate that defines the air gap of the microphone. A 3 μm thick thermal oxide is then grown. A 40 × 40 array of cavities for reducing the air streaming resistance is then formed by anisotropic followed by isotropic etching through the patterned oxide. Each cavity has a 30 μm diameter opening and a half-dome shaped hole 80 μm in diameter and 50 μm deep. Lastly, a 2100 Å thick Cr/Au electrode is evaporated onto the backplate using a physical mask.

Figure 5-3 shows the process flow of the MEMS electret microphone. Using the LDV, the fundamental resonant frequency of the composite diaphragm was found to be above 30 kHz. Pictures of the microphone membrane and backplate are shown in Figure 5-4. A blow-up of a portion of the backplate cavity array with conducting gold is also presented. The hybrid microphone package schematic is illustrated in Figure 5-5. The two halves of the microphone are mechanically clamped together and are enclosed in a metal box that provides electromagnetic shielding.

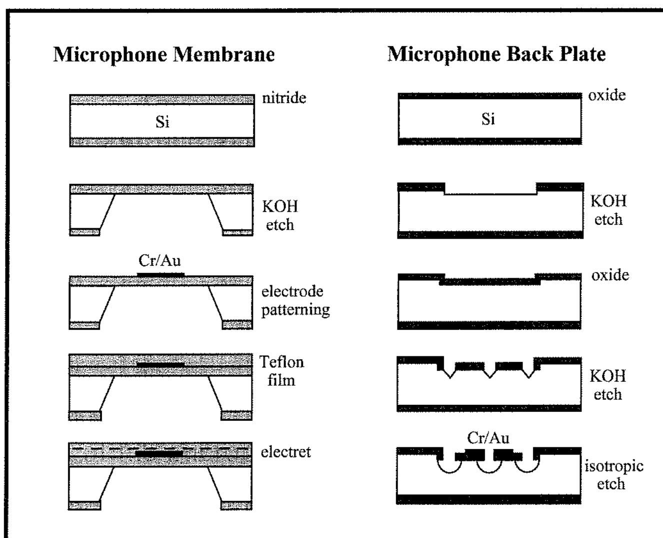

Figure 5-3. Process flow of a MEMS electret microphone with silicon backplate.

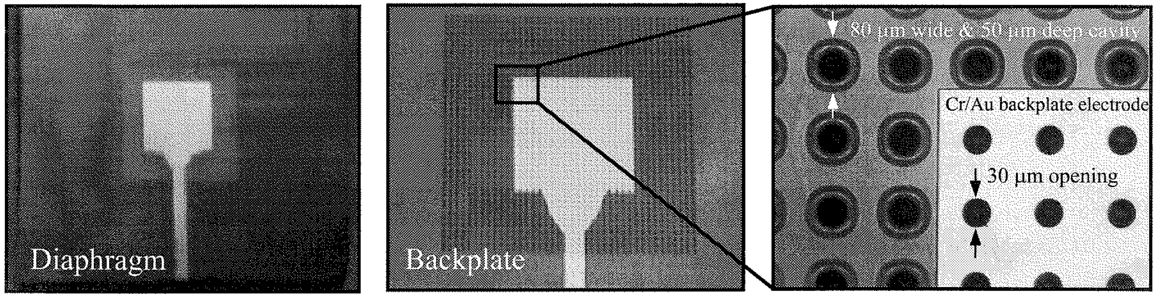

Figure 5-4. Pictures of silicon nitride diaphragm and silicon backplate.

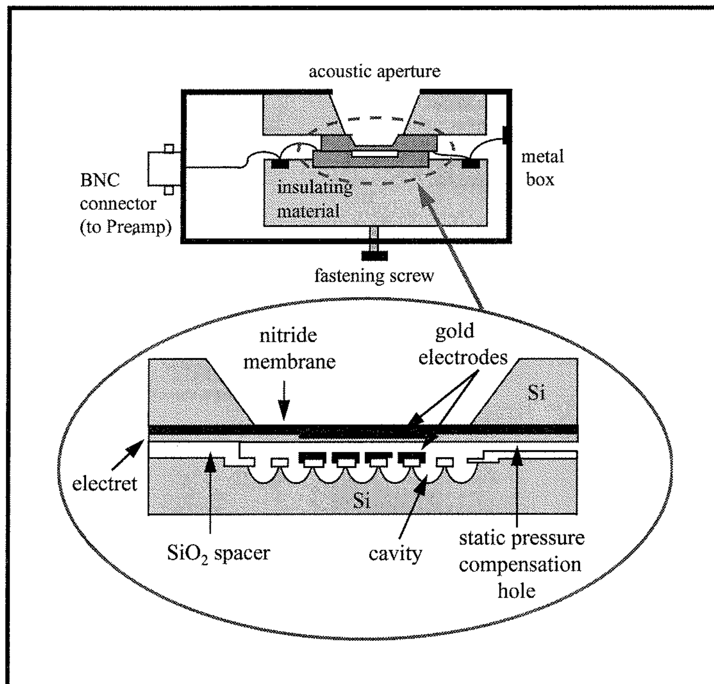

Figure 5-5. The assembled silicon nitride diaphragm and silicon backplate package.

5.4.2 Testing and Performance

To reduce stray capacitance, the electrode area was designed so that it only covered a fraction of the membrane and backplate area [5]. Thus, a 2 mm × 2 mm square Cr/Au electrode was used to cover the center part of the 3.5 mm × 3.5 mm diaphragm and 4 mm × 4 mm perforated backplate. The fraction of backplate area occupied by cavity openings is 0.07. The air-streaming resistance, R_a, is calculated to be 0.03 Ns/m (equation 2-14). The cut-off frequency due to R_a is given by $f_{streaming} = 13.57\ \sigma\ t\ /\{2\pi\ R_a\}$, where $\sigma = 100$

MPa is the composite diaphragm stress and t = 1 μm is the diaphragm thickness. $f_{streaming}$ is calculated to be approximately 7.6 kHz. This is clearly the upper limit of the actual cut-off frequency because equation (2-14) assumes the acoustic holes in the backplate lead to a back chamber with infinite volume. This is not the case here since no back chamber exists and the acoustic holes are actually cavities with finite volume. Unfortunately, the microphone frequency response could not be measured at the time because the necessary equipment was not yet available.

With a 4.5 μm air gap, 1 μm thick Teflon electret and an electrode area of 4 mm^2, the theoretical capacitance of the microphone is 7 pF. Using a Hewlett Packard 4192 LF Impedance Analyzer the measured capacitance of the microphone package was 30 pF. The large discrepancy in capacitance values can be attributed to the stray capacitance formed between the Cr/Au electrodes and silicon substrates and between the two clamped halves of the microphone.

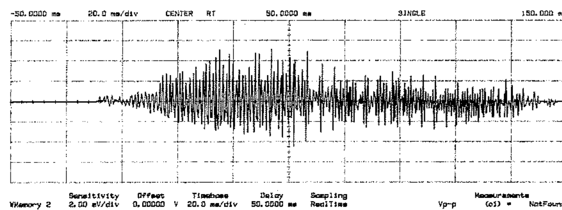

Figure 5-6. An oscilloscope display of a human voice detected without an amplifier.

The microphone was barely able to detect sound from a loud human voice without the use of an amplifier (Figure 5-6). When the microphone was connected to an EG&G PARC Model 113 Pre-amp (gain set at 1000) and was excited by a Brüel & Kjaer (B&K) Type 4220 Pistonphone operating at 250 Hz and 123.9 dB SPL (re. 20 μPa), the oscilloscope displayed a 250 Hz, 190 mV peak-to-peak amplitude signal. The measured open-circuit sensitivity of the microphone at this frequency is about 14 μV/Pa! Taking into account the 15 pF input capacitance of the pre-amplifier and the 20+ pF stray capacitance of the assembled microphone, this is not at all surprising.

5.4.3 Analysis

This prototype MEMS electret microphone was the first to demonstrate the feasibility of using a Teflon AF electret in a MEMS acoustic sensor. However, the actual

performance of the microphone itself, in particular the open-circuit sensitivity, leaves a lot to be desired. The high stray capacitance of the microphone needs to be eliminated and a preamplifier with a significantly lower input capacitance must be used to reduce electrical loading. Furthermore, since the PZT-shaker could not measure the surface potential of the Teflon electret because it resides on a nitride diaphragm, the actual electret surface charge density was not determined. Perhaps the two BLT shots did not implant any significant charge into the Teflon AF, thereby contributing to the abysmal open-circuit sensitivity. Another plausible explanation for the poor microphone performance could be that 10 keV electrons are implanted too deep into the 0.9 μm thick Teflon, causing a reduction in the effective electret surface charge density.

5.5 Glass Backplate Microphone

The second MEMS electret microphone to be fabricated from the new thin film Teflon AF electret technology also consist of two chips. This microphone presents the first opportunity to correct design flaws found in the first version. Here a cavity-riddled glass substrate is used to form the microphone backplate. The purpose of the insulating glass is to reduce stray capacitance formed between the electrode and substrate and between the two clamped halves of the microphone. As in the first MEMS electret microphone, the diaphragm is made of silicon nitride and Teflon AF. In this case, a slightly thicker Teflon film is used with lower BLT energy to try to increase the electret surface charge density.

5.5.1 Fabrication and Packaging

The fabrication steps for this electret microphone are shown in Figure 5-7. The microphone diaphragm is made by anisotropically back-etching a <100> silicon substrate coated with 0.91 μm thick LPCVD silicon nitride (SiH_2Cl_2/NH_3=4, 835°C). This forms a 3.5 mm × 3.5 mm free-standing nitride membrane. The front side of the membrane is then evaporated with 2000 Å Cr/Au through a physical mask to form one electrode. Teflon AF 1601S-6 solution is then spin-cast over the front surface of the membrane and baked at 250°C for 3 hours to drive off solvents. The resulting thickness is 1.2 μm.

Electrons with 7 keV energy are then implanted into the Teflon using the BLT, followed by annealing in air at 100°C for 3 hours to age the electret. For this MEMS electret microphone, a charge density on the order of 10^{-5} C/m^2 was obtained. This value was inferred from measurements by the PZT-shaker on non-diaphragm substrates that had undergone the exact electret forming processes.

The backplate of the microphone is fabricated from a glass substrate coated with 2500 Å Cr/Au on one side. The Cr/Au layer is patterned and etched to form a backplate electrode that has 20 holes across its 2 mm diameter. A 5 μm thick photoresist spacer is then applied and patterned to define the air gap between the diaphragm and backplate electrodes. A timed BHF etch follows, creating a cavity array and static pressure equalization hole in the glass substrate. Each cavity has a 40 μm diameter opening and a half-dome shaped hole 70 μm in diameter and 15 μm deep beneath the opening. These cavities serve to increase the high frequency cut-off of the microphone by reducing the air-streaming resistance in the air gap. The static pressure equalization hole extends across the entire glass backplate chip and has a 20 μm × 5 mm cross-sectional area. Pictures of the microphone diaphragm and backplate are shown in Figure 5-8.

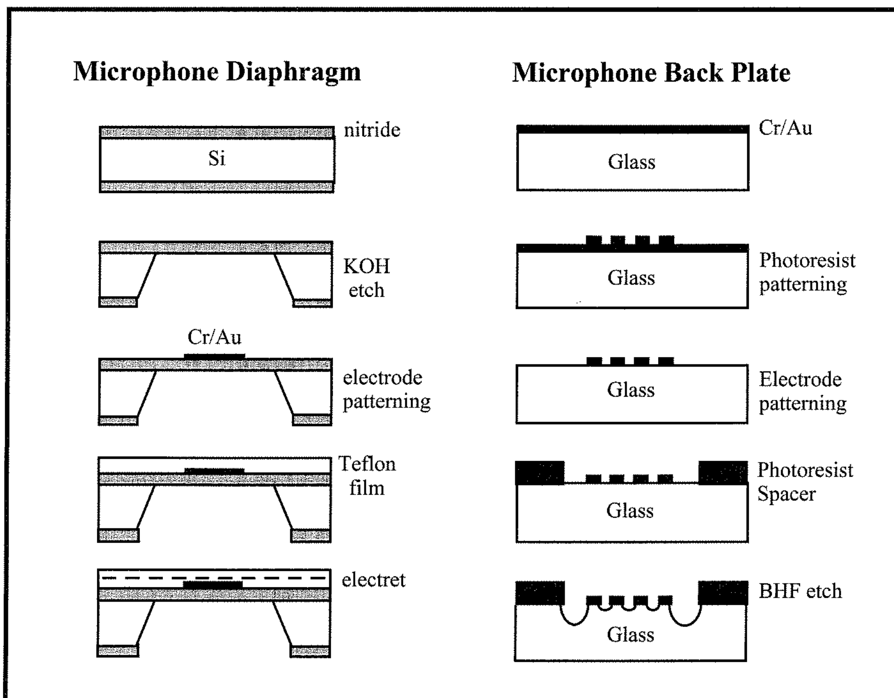

Figure 5-7. Process flow of a MEMS electret microphone with glass backplate.

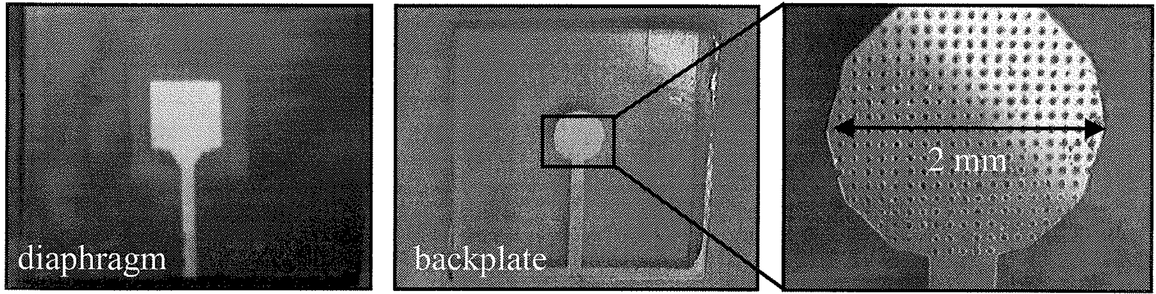

Figure 5-8. Pictures of silicon nitride diaphragm and glass backplate.

The two halves of the microphone are mechanically clamped together and are enclosed in a metal box that provides electromagnetic shielding. Figure 5-9 shows the microphone structures and package. To reduce stray capacitance, the electrode area of the microphone diaphragm was designed so that it only covered a fraction of the diaphragm and backplate area [5]. Thus, a 2 mm × 2 mm square Cr/Au electrode was used to cover the center of the 3.5 mm × 3.5 mm nitride diaphragm. A 2 mm diameter circular electrode (originally planned to facilitate future circular diaphragms) was used on the perforated glass backplate.

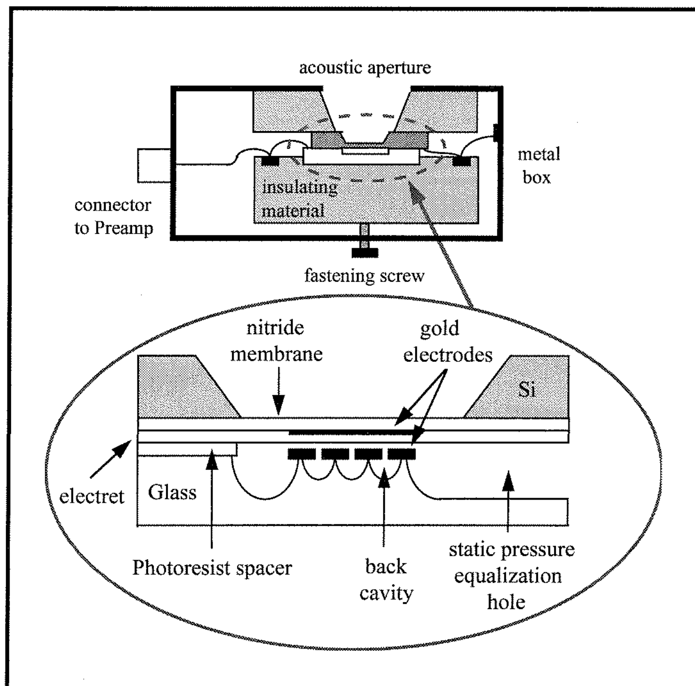

Figure 5-9. The assembled silicon nitride diaphragm and glass backplate package.

Using a LDV, the resonant frequency of the free-standing composite nitride/Teflon AF diaphragm (with 2500 Å Cr/Au) was determined to be 38 kHz. From the fundamental resonant frequency equation (2-13), $f_0 = (\sigma/2a^2\rho)^{0.5}$, for a square nitride diaphragm with tensile stress, where: f_0 = 38 kHz, nitride density, ρ = 3100 kg/m^3 and length of one side of the square diaphragm, a = 3.5 mm, the residual tensile stress, σ, is about 110 MPa.

For a 5 μm air gap, a 1.2 μm thick Teflon electret and an electrode area of 3.14 mm^2, the theoretical capacitance of the microphone is 4.9 pF. The measured capacitance was 5.2 pF. The close agreement between the theoretical and experimental values can be attributed to the glass substrate, which practically eliminates all stray capacitance between the Cr/Au electrode and silicon substrate, and between the two clamped halves of the microphone.

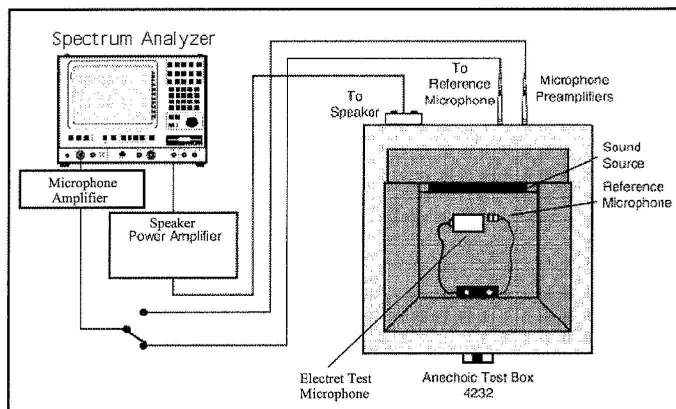

Figure 5-10. Microphone measurement test setup.

5.5.2 Testing and Performance

The thin film Teflon electret microphone was tested in a B&K Type 4232 anechoic test chamber (Figure 5-10). An integrated speaker in the test chamber served as the acoustic source. A B&K Type 4189 1/2-inch reference microphone was used to measure the sound pressure level at the test position. The reference microphone was connected to a B&K Type 2669 preamplifier and a B&K Type 5935 dual channel amplifier/power supply. The electret microphone under test was also connected to a B&K Type 2669

preamplifier and it shared the same B&K dual channel amplifier/power supply with the reference microphone. This ensured that the only variable in the entire test system was the MEMS electret microphone and that the other components were kept constant. The schematic representation of the electret microphone-preamplifier circuit is shown in Figure 5-11. The electrical response of the circuit is given by equation (2-9):

$$H_e(\omega) = \frac{v_{out}}{v_{oc}} = \frac{j\omega R_i C_m}{1 + j\omega R_i (C_s + C_m + C_i)}$$

where ω is the frequency in rad/s. For an electret microphone capacitance, $C_m = 5.2$ pF, package stray capacitance, $C_s = 2$ pF, preamplifier input capacitance, $C_i = 0.45$ pF, preamplifier input resistance, $R_i = 15$ GΩ and preamplifier output resistance, $R_o = 25$ Ω, $H_e(\omega)$ is a constant and equal to 0.68 over the frequency range of interest (100 Hz - 10 kHz). The electrical low-frequency roll-off is less than 10 Hz, and the preamplifier high frequency cut-off is much greater than 20 kHz. Thus, the electrical response is well suited for acoustic signals in the audible range.

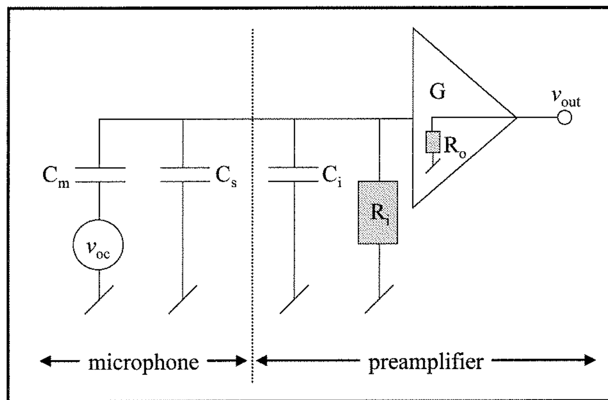

Figure 5-11. Schematic of microphone-preamplifier circuit.

When the electret microphone was excited by a 650 Hz, 2 Pa RMS sinusoidal acoustic signal, a clear, undistorted sinusoidal output signal was observed on the oscilloscope (Figure 5-12). Using a Stanford Research Systems Model SR780 Network Signal Analyzer to apply an input sinusoidal signal of known sound pressure from 100

Hz to 10 kHz (Figure 5-13), the frequency response of the electret microphone was obtained. Sound pressure levels with higher frequencies were not used because the output of the built-in speaker in the anechoic sound chamber is attenuated above 10 kHz. The microphone frequency response data shows that the measured open-circuit sensitivity of the microphone is approximately 0.2 mV/Pa and the bandwidth of the microphone is greater than 8 kHz (Figure 5-14). For diaphragm deflections smaller than the air gap thickness and assuming a square nitride membrane with large initial stress, a first-order calculation of the theoretical microphone open-circuit sensitivity, S_{oc}, is given by equation (2-7):

$$S_{oc} = \left(\frac{a^2}{3.04 t \sigma 2} \right) \left(\frac{\dfrac{\sigma_e s_e}{\varepsilon_0 \varepsilon_e}}{\dfrac{s_e}{\varepsilon_e} + s_a} \right) \approx 1.1 \text{ mV/Pa}$$

where: electret thickness, s_e = 1.2 μm, electret surface charge density, $\sigma_e = 1\times10^{-5}$ C/m^2, air gap thickness, s_a = 5 μm, permittivity of free space, $\varepsilon_0 = 8.85\times10^{-12}$ F/m, relative permittivity of the Teflon electret, ε_e = 1.9, length of one side of the square diaphragm, a = 3.5 mm, nitride membrane thickness, t = 2.1 μm (effective thickness of a pure silicon nitride diaphragm that would result in the same mass as the composite diaphragm), and stress in the nitride membrane, σ = 110 MPa. Because this equation ignores squeeze film damping effects in the air gap, ignores the absence of a back chamber behind the backplate acoustic holes, ignores the severely-reduced electrode area (only about 20% of total diaphragm area), and ignores the effect of the Cr/Au electrode and Teflon film on lowering the diaphragm mechanical sensitivity, it is expected that this theoretical open-circuit sensitivity will be an over-estimate of the measured open-circuit sensitivity.

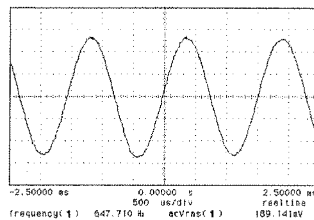

Figure 5-12. Microphone output for a 2 Pa RMS, 650 Hz input signal (Gain = 50 dB).

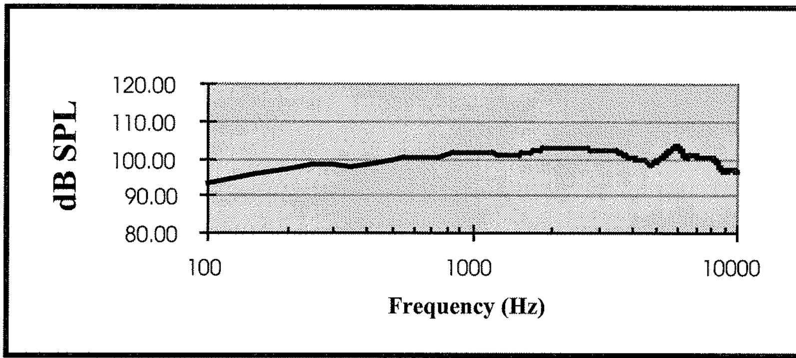

Figure 5-13. Input sound pressure level for frequency response measurements.

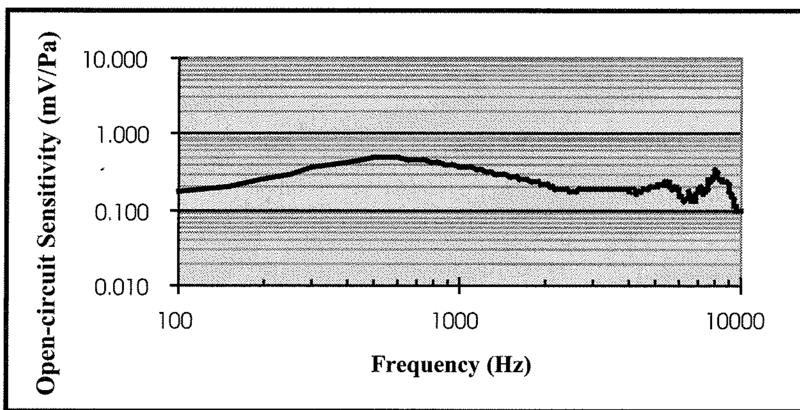

Figure 5-14. Frequency response of MEMS electret microphone with glass blackplate.

The 600 Hz peak in the frequency response is most likely caused by acoustic resonance in the microphone package in conjunction with the large static pressure equalization hole in the clamped two-chip microphone structure (Figure 5-9). This low frequency resonance cannot be attributed to the diaphragm resonance (38 kHz), nor to the electrical low-frequency cut-off (<10 Hz) of the microphone-preamplifier system. The above explanation is further supported by the observation that physically modifying parts of the microphone package and static pressure equalization hole has the effect of shifting the position and amplitude of this low frequency resonance peak. Consequently, future designs will require simpler packaging structures and smaller static pressure equalization holes for which the acoustic impedance can be easily modeled and calculated so that the low frequency cut-off can be better predicted and placed.

The peaks in the frequency response between 5 - 8 kHz are most likely due to two factors. The first possibility is sub-harmonic resonance in the diaphragm-air gap-backplate system. The second possibility is squeezed-film damping in the air gap (see section 2.4.2). The presence of squeezed-film damping is supported by the finite downward slope in the response curve above 600 Hz. The magnitude of the response attenuates towards higher frequencies because the spring-force of the air gap increases as the air in the gap becomes compressed at higher frequencies. It is apparent that to reduce squeezed-film damping, future microphone designs must incorporate a higher density of holes in the backplate as well as a much larger back chamber volume.

The lower limit of dynamic range is fixed by the inherent noise level of the electret microphone. There are two noise sources in the microphone itself: the diaphragm damping resistance and the static pressure equalization resistance. In practice, for large static pressure equalization holes, as is the case here, the diaphragm damping noise is dominant. The measured noise level of this MEMS electret microphone (with B&K Type 2669 preamplifier) is 60 dB SPL at 20°C. In comparison, a B&K Type 4189 1/2-inch electret microphone with the same preamplifier and at the same temperature has a noise level of 17 dB SPL. Since the noise pressure produced by an acoustic damping resistance is inversely proportional to the 3/2 root of air gap thickness and inversely proportional to the length of the square diaphragm, the high noise floor of the MEMS microphone is not surprising, given its micron-sized air gap and millimeter-sized diaphragm (see section 2.5.1).

The distortion limit of the MEMS electret microphone was found to be above 110 dB SPL (the maximum output of the anechoic sound chamber speaker). This test was conducted at 1 kHz and the measured Total Harmonic Distortion was less than 1% at 110 dB SPL. Given that the lowest detectable sound pressure level is 60 dB SPL, this translates into a microphone dynamic range that is greater than 50 dB SPL.

5.5.3 Analysis

A moderately performing MEMS electret microphone was demonstrated using thin film Teflon AF and the BLT. The performance characteristics of this electret microphone are slightly poorer than other similarly sized MEMS condenser microphones (Chapter 3).

Preliminary calculations suggest potentially higher sensitivities, wider dynamic range and flatter frequency responses are achievable through refinement of the microphone structure. The mechanical sensitivity can be increased by using thinner and larger diaphragms with lower tensile stress. The electrical sensitivity can be improved by increasing the electret charge density, and decreasing the air gap spacing. The air-gap streaming resistance can be reduced by using a higher density of acoustic holes in the backplate and having a larger back chamber volume. A high acoustic hole density will not only lower the microphone noise level, since the diaphragm damping resistance will be reduced, but it will also increase the high frequency cut-off. Lastly, to keep the low frequency cut-off as low as possible, the size and shape of the static pressure equalization hole must be carefully designed and the microphone must be properly packaged.

5.6 Parylene C/Silicon Nitride Composite Backplate Microphone

The third MEMS electret microphone to be fabricated from the new thin film Teflon AF electret technology consists of a thin silicon nitride/Teflon AF composite diaphragm combined with a thicker Parylene C/silicon nitride perforated backplate. In order to increase mechanical sensitivity, this microphone has a thinner and larger diaphragm with lower tensile stress. The thickness of the Cr/Au electrode has been reduced to minimize influence on the mechanical sensitivity of the diaphragm. The backplate is highly perforated and a large back chamber is provided to reduce air-streaming resistance in the air gap. The air gap and electret thickness has also been slightly reduced to increase microphone capacitance. The electret surface charge density has been increased to improve electrical sensitivity. Lastly, a new compact brass housing that has better electromagnetic shielding is used to package the microphone structure.

5.6.1 Fabrication and Packaging

The fabrication steps of the third MEMS electret microphone are shown in Figures 5-15 and 5-16. Diaphragm formation (Figure 5-15) begins with a <100> silicon substrate coated with 0.5 μm low-stress LPCVD silicon nitride ($SiH_2Cl_2/NH_3=4.3$ at 837°C). The higher dichlorosilane to ammonia ratio produces less stressed nitride films. The front

side of the nitride is then evaporated with 1100 Å Cr/Au. After patterning with photoresist, this layer of metal forms one of the microphone electrodes. The nitride on the backside of the wafer is then masked with photoresist, patterned and etched with SF_6 plasma to form a back-etch window. A KOH anisotropic back-etch follows, forming an 8mm × 8mm free-standing nitride diaphragm. Teflon AF 1601S-6 solution is then spin-cast over the front surface of the membrane and is baked according to the working process in section 4.5 to completely drive off the Fluoroinert FC-75 solvent and to reflow the Teflon AF. The resulting film thickness is 0.9 μm. Electrons with 7 keV of energy are then implanted into the Teflon using the BLT. The electret is aged by baking at 100°C in air for 3 hours. For this MEMS electret microphone, a stable charge density on the order of 10^{-4} C/m^2 was obtained as measured by the Monroe Isoprobe Electrostatic Voltmeter.

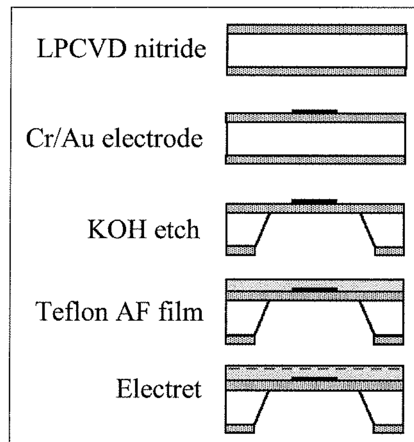

Figure 5-15. Process flow of 8 × 8 mm^2 silicon nitride/Teflon AF diaphragm.

The backplate of the microphone (Figure 5-16) is fabricated from a <100> silicon substrate coated with 1.1 μm thick low stress LPCVD silicon nitride (SiH_2Cl_2/NH_3=4.3 at 837°C). A KOH anisotropic back-etch ensues, until a 20 μm thick silicon diaphragm remains. A 160 × 160 array of acoustic holes is then etched 5 μm deep through the 1.1 μm nitride and into the silicon membrane. Each hole has a diameter of 30 μm and is spaced 50 μm center-to-center. These holes increase the upper cut-off frequency of the microphone by reducing the squeeze-film damping effects in the air gap. A 2.4 μm thick

layer of Parylene C is then deposited onto both sides of the wafer. This serves to structurally reinforce the highly perforated backplate. A 1100 Å thick Cr/Au electrode is then deposited and patterned on top of the front-side Parylene. A 4.5 μm thick hard-baked photoresist spacer is applied to the front side of the wafer to define the air gap between the electrodes. The static pressure equalization hole extends across the entire backplate chip and is defined by a 4.5 μm × 8.3 mm cross-sectional area between the photoresist spacers. The final step involves etching away the Parylene C in the back cavity with oxygen plasma to expose the 20 μm thick silicon, and then BrF_3 etch is used to free the perforated nitride/Parylene C composite backplate. The Parylene C stubs protruding from the 160 x 160 array of holes are removed by oxygen plasma from the backside of the wafer. Figure 5-17 shows pictures of the microphone diaphragm and backplate. To reduce stray-capacitance, both electrode areas (5mm × 5mm) on the diaphragm and backplate cover only a fraction of the diaphragm area (8mm × 8mm) [5].

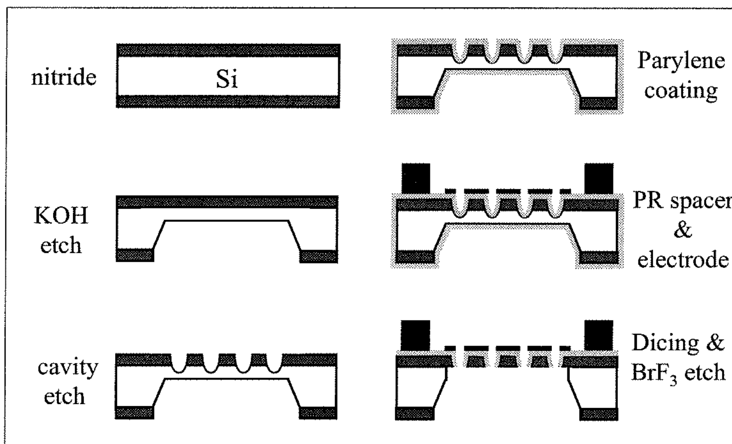

Figure 5-16. Process flow of 8 × 8 mm^2 perforated Parylene C/silicon nitride backplate.

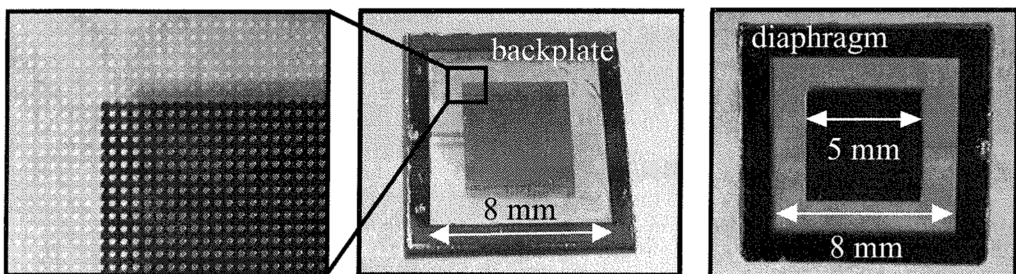

Figure 5-17. Pictures of nitride diaphragm and perforated Parylene C/nitride backplate.

Figure 5-18 shows a schematic cross-section of the assembled microphone. The two halves of the microphone are mechanically clamped together and are enclosed in a brass housing that provides electromagnetic shielding (Figure 5-19). The rear of the housing is threaded so that it will seamlessly screw onto a B&K Type 2669 preamplifier (Figure 5-20). The backplate chip is double-side taped to an electrically insulating surface inside the housing and its electrode is connected to a non-grounded terminal that will be coupled to the preamplifier input. The diaphragm chip is then placed on top of the backplate chip and is held in place by pressure from the top half of the brass housing. The diaphragm electrode is connected to ground.

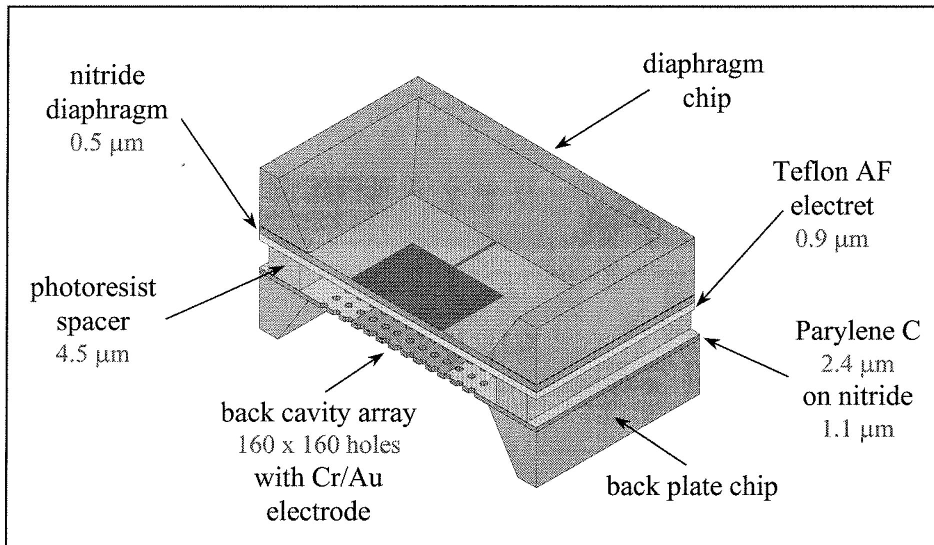

Figure 5-18. Cross-section of MEMS electret microphone with nitride diaphragm.

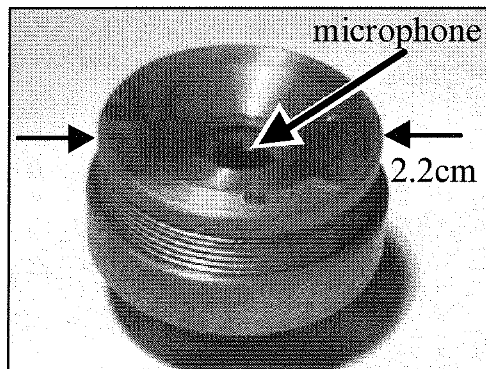

Figure 5-19. Picture of MEMS electret microphone brass housing.

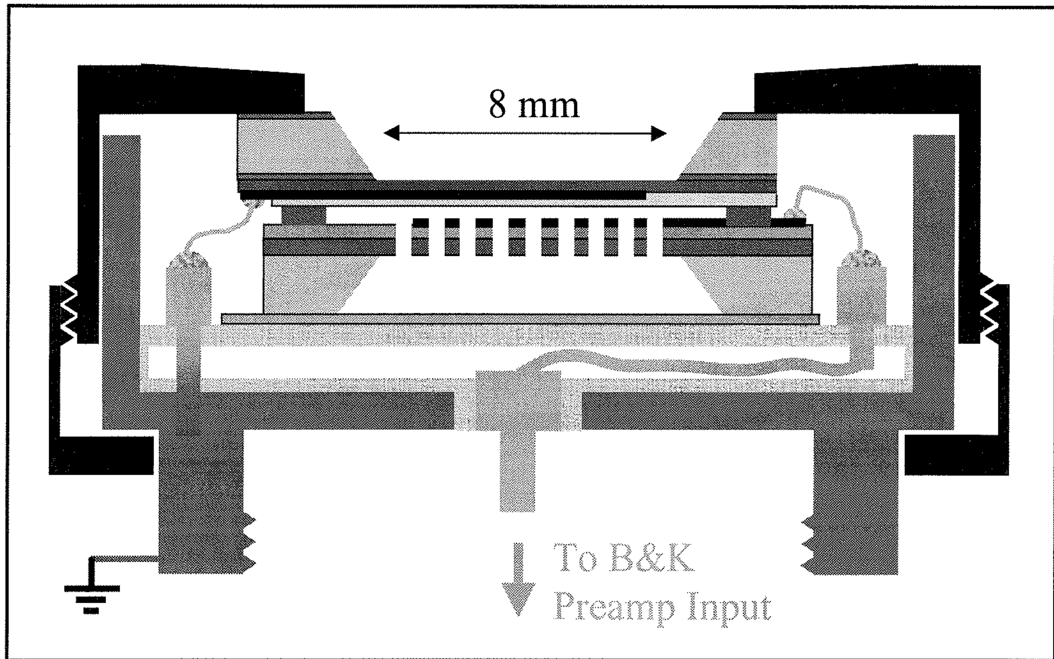

Figure 5-20. Cross-section of MEMS electret microphone housing.

5.6.2 Testing and Performance

Using a LDV the resonant frequency of the nitride diaphragm with 1100 Å Cr/Au and 0.9 μm Teflon AF was determined to be 13.25 kHz (Figure 5-21). From the fundamental resonant frequency equation (2-13), $f_0 = (\sigma/2a^2\rho)^{0.5}$, for a square nitride diaphragm with tensile stress, where: f_0 = 13.25 kHz, nitride density, ρ = 3100 kg/m^3 and length of one side of the square membrane, a = 8 mm, the residual tensile stress of the composite diaphragm, σ, is about 70 MPa. The same measurement was performed for the highly perforated Parylene C/silicon nitride backplate. Its fundamental resonant frequency was measured at 12.88 kHz (Figure 5-21).

For a 4.5 μm air gap, a 0.9 μm thick Teflon electret, a backplate with a hole opening ratio of 0.3 and an electrode area of 25 mm^2, the theoretical capacitance of the microphone is about 31 pF. The measured microphone (minus stray) capacitance was 15 pF. The discrepancy between the theoretical and experimental values can probably be attributed to a larger air gap than designed. This could happen if a small foreign object became trapped in between the two chips when one was placed on top of the other. The corresponding air gap that would result in a 15 pF microphone capacitance is 9 μm.

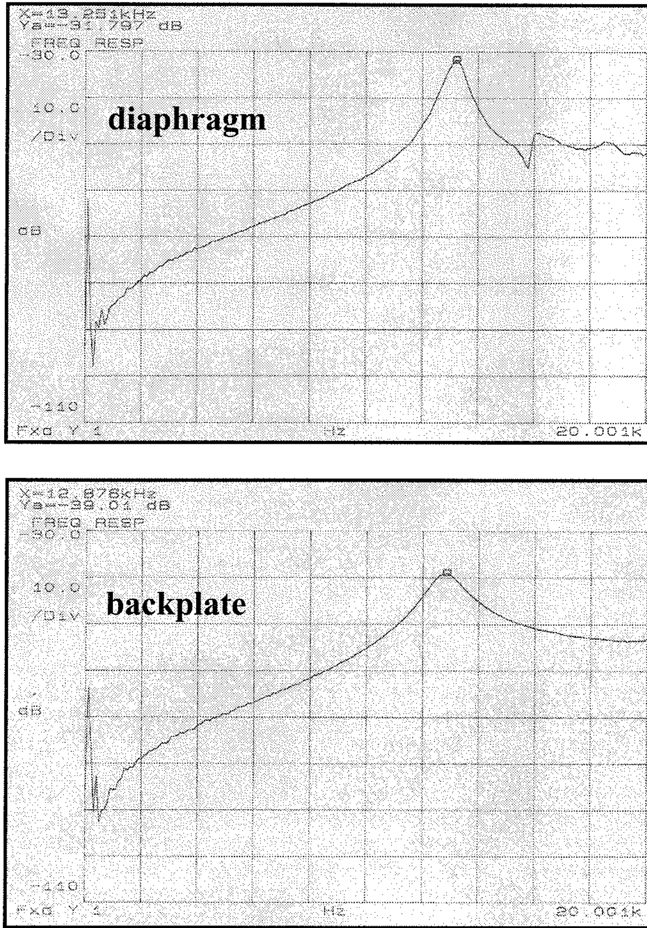

Figure 5-21. Resonance of nitride/Teflon diaphragm and Parylene/nitride backplate.

The electret microphone was tested in a B&K Type 4232 anechoic test chamber (Figure 5-10). An integrated speaker in the test chamber served as the acoustic source. A B&K Type 4189 1/2-inch reference microphone was used to measure the sound pressure level at the test position. The reference microphone was connected to a B&K Type 2669 preamplifier and a B&K Type 5935 dual channel amplifier/power supply. The electret microphone under test was also connected to a B&K Type 2669 preamplifier and it shared the same B&K dual channel amplifier/power supply with the reference microphone. This ensured that the only variable in the entire test system was the MEMS electret microphone and that the other components were kept constant.

The schematic representation of the electret microphone-preamplifier circuit is shown in Figure 5-11. The electrical response of the circuit is given by equation (2-9):

$$H_e(\omega) = \frac{v_{out}}{v_{oc}} = \frac{j\omega R_i C_m}{1 + j\omega R_i (C_s + C_m + C_i)}$$

where ω is the frequency in rad/s. For an electret microphone capacitance, C_m = 15 pF, package stray capacitance, C_s = 2 pF, preamplifier input capacitance, C_i = 0.45 pF, preamplifier input resistance, R_i = 15 GΩ and preamplifier output resistance, R_o = 25 Ω, $H_e(\omega)$ is a constant and equal to 0.86 over the frequency range of interest (100 Hz - 13 kHz). The electrical low-frequency roll-off is less than 1 Hz, and the preamplifier high frequency cut-off is much greater than 20 kHz. Thus, the electrical response is well suited for acoustic signals in the audible range.

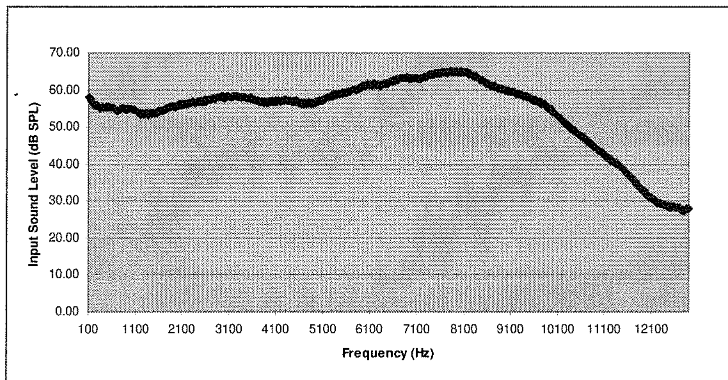

Figure 5-22. Input sound pressure level for frequency response measurement.

Using a Stanford Research Systems Model SR785 Dynamic Signal Analyzer to apply an input sinusoidal signal of known sound pressure level from 100 Hz to 12.896 kHz, the frequency response of the MEMS electret microphone was obtained. Sound pressure levels with higher frequencies were not used because above 13 kHz the output of the built-in speaker in the anechoic sound chamber is severely attenuated to levels below 30 dB SPL (Figure 5-22). The microphone frequency response data shows that the measured open circuit sensitivity of the microphone varies from 3.5 to 16.5 mV/Pa from 1 kHz to 10.5 kHz (Figure 5-23). A peak in sensitivity of 31 mV/Pa occurs at 13 kHz.

There is also an unusual anti-resonance at 11.6 kHz. A plausible explanation for this is that the fundamental resonant frequency of the perforated Parylene C/silicon nitride

backplate (12.88 kHz) is too close to that of the silicon nitride/Teflon AF diaphragm (13.25 kHz). The displacement of the backplate significantly increases around its resonance. The same is true for the diaphragm. If these two events occur around closely spaced frequencies, both the phase and amplitude of diaphragm and backplate vibrations will become identical for a small range of overlapping frequencies. Consequently, the relative displacement between the two microphone electrodes will diminish rapidly, as will the open-circuit sensitivity. This forms a notch in the frequency response around 11.6 kHz.

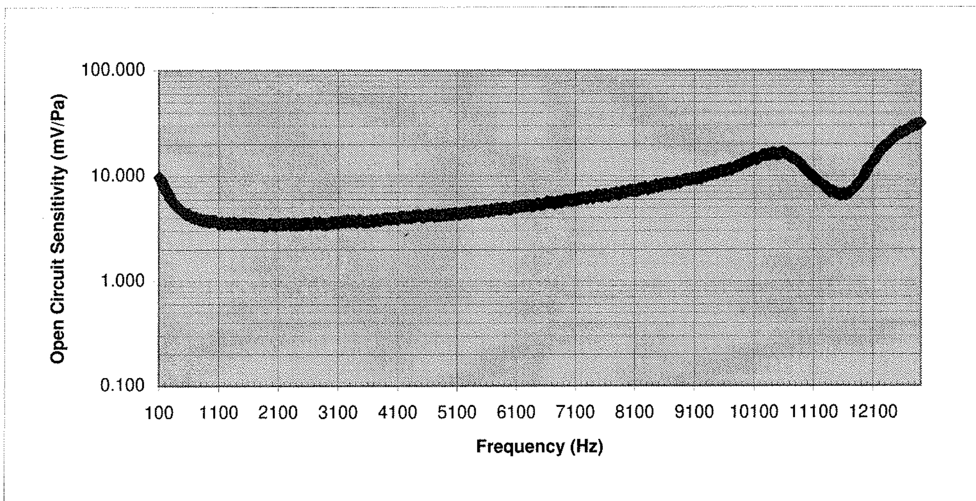

Figure 5-23. Frequency response of MEMS electret microphone w/ nitride diaphragm.

The rise in response for frequencies below 1 kHz is most likely because the microphone pressure equalization hole is not exposed to the sound field (section 2.4.1). As a result, the fraction of stiffness (ratio between air gap stiffness and total diaphragm system stiffness) which is due to the reactive pressure in the internal cavities of the microphone becomes smaller for lower frequencies as this is equalized through the hole. This causes the mechanical sensitivity of the microphone to increase for lower and lower frequencies, until it eventually tapers off.

The upward slope in frequency response at high frequencies is due to the influence of the microphone body on the measured sound pressure in the sound field. The disturbance of a plane sound wave by the microphone body causes the pressure at the position of the diaphragm to deviate significantly from that of the undisturbed field at

higher frequencies (Figure 5-24) [6]. The ratio between the pressure at the diaphragm and that of the undisturbed sound field is a function of the ratio between the microphone diameter and the wavelength. Pressure ratio functions look alike for small and large microphones, but they are shifted within the frequency range depending on the diameter of the microphone body (Figure 5-25). The general trend is for the sound pressure at the diaphragm to be larger than the actual pressure at the same point in an undisturbed sound field. This causes the overall frequency response of the microphone to increase with increasing frequency. The 2.2 cm diameter microphone package (Figure 5-19) of the 8 mm × 8mm MEMS electret microphone approximates the influence of a 1-inch diameter microphone on the sound field (Figure 5-25).

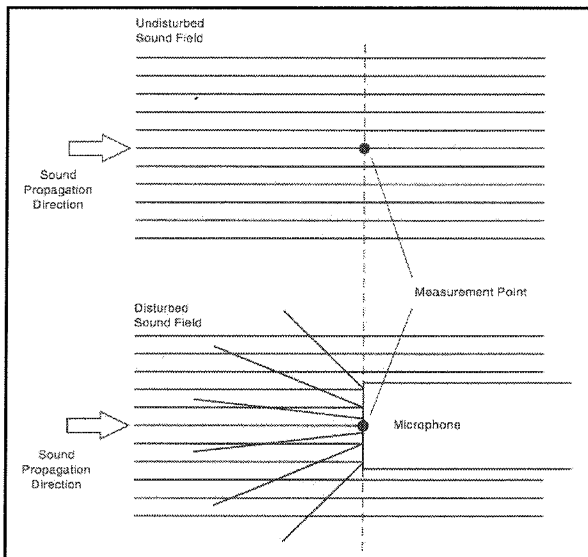

Figure 5-24. Disturbance of a plane sound wave by a microphone body [6].

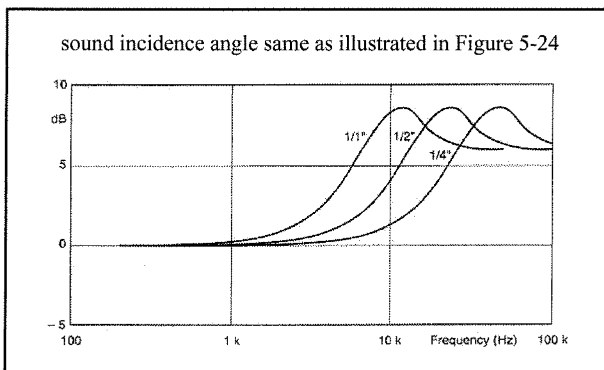

Figure 5-25. Ratio between press. at diaphragm and press. of undisturbed sound field [6].

For diaphragm deflections smaller than the air gap thickness and assuming a square nitride membrane with large initial stress, a first-order calculation of the theoretical microphone open-circuit sensitivity, S_{oc}, is given by a slightly modified form of equation (2-7):

$$S_{oc} = \left(\frac{a^2}{3.04t\sigma 2} \right) \left(\frac{\dfrac{\sigma_e s_e}{\varepsilon_0 \varepsilon_e}}{\dfrac{s_e}{\varepsilon_e} + s_a} \right) (R) \approx 27 \text{ mV/Pa}$$

where: electret thickness, $s_e = 0.9$ μm, electret surface charge density, $\sigma_e = 1.5\times10^{-4}$ C/m^2, air gap thickness, $s_a = 9$ μm, permittivity of free space, $\varepsilon_0 = 8.85\times10^{-12}$ F/m, relative permittivity of the Teflon electret, $\varepsilon_e = 1.9$, length of one side of the square diaphragm, $a = 8$ mm, nitride diaphragm thickness, $t = 1.27$ μm (effective thickness of a pure silicon nitride diaphragm that would result in the same mass as the composite diaphragm), and stress in the nitride diaphragm, $\sigma = 70$ MPa and ratio of Cr/Au electrode area to the total membrane area, $R = 0.273$. Because this equation does not take into account the compliance of the thin perforated nitride/Parylene C backplate, which may cause it to lose relative displacement with respect to the diaphragm or have a DC displacement towards the diaphragm, it is expected that the theoretical open-circuit sensitivity will be an over-estimate of the measured open-circuit sensitivity.

According to equation (2-18) and (2-19), the flexible diaphragm will collapse to the flexible backplate for an electret surface charge density of around 2.8×10^{-4} C/m^2. This assumes the entire diaphragm and backplate areas are covered by metal electrodes. Since the electret surface charge density for this microphone is only 1.5×10^{-4} C/m^2 and the electrodes only occupy 27.3% of the total 8 mm × 8mm diaphragm area, there is little risk of diaphragm collapse due to electrostatic attraction.

The measured noise level of the MEMS electret microphone with B&K Type 2669 preamplifier is less than 30dB SPL at 25°C. In comparison, a B&K Type 4189 1/2-inch electret microphone with the same preamplifier and at the same temperature has a noise level of 17 dB SPL. Using equation (2-14), the theoretical mechanical air-streaming resistance, R_a, of this microphone is a low 0.008 Ns/m. If we plug this value into

equation (2-17) and assume a bandwidth of 14 kHz, the theoretical linear noise pressure of the microphone itself is only 0.5 dB SPL. The low empirical and theoretical noise levels should not be surprising because the backplate has a high acoustic hole density and hole opening ratio.

The 3% distortion limit was found to be above 110 dB SPL (the maximum output of the anechoic sound chamber speaker). This test was conducted at 1 kHz and the measured Total Harmonic Distortion of the MEMS electret microphone was less than 1% at 110 dB SPL. Since the lowest detectable sound pressure level is below 30 dB SPL, this translates into a microphone dynamic range that is greater than 80 dB SPL.

Table 5-2. Characteristics of MEMS electret microphone w/ silicon nitride diaphragm.

	Diaphragm Chip	Backplate Chip
Dimensions & Material	8mm × 8mm × 0.5 μm Silicon Nitride	8mm × 8mm × 1.1 μm Silicon Nitride
Electrode Dimensions	100Å Cr / 1000 Å Au 5mm × 5mm	100Å Cr / 1000 Å Au 5mm × 5mm
Polymer Coating	0.9 μm Teflon AF 1601S	2.4 μm Parylene C
Acoustic Holes	None	160 × 160 array 30 μm diameter 50 μm center-to-center (0.3 opening ratio)
1st Resonant Frequency	13.25 kHz	12.88 kHz
Electret Surface Charge Density	1.5×10^{-4} C/m^2	None
Capacitance	15 pF	
Open-circuit Sensitivity	3.5-16.5 mV/Pa	
Useful Frequency Range	100 Hz - 11.5 kHz	
Dynamic Range	Less than 30 dB - 110+ dB SPL	
Total Harmonic Distortion	<1% @ 110 dB SPL, 1 kHz	

5.6.3 Analysis

A high-performance MEMS electret microphone was demonstrated using thin film Teflon AF and the BLT. A summary of the microphone characteristics is provided in Table 5-2. The open-circuit sensitivity is high enough to allow good sound measurements in the 100 Hz to 11.5 kHz audio frequency range with minimal or no signal amplification. The generous use of acoustic holes in the backplate and the

presence of a large back chamber resulted in a very low noise floor and very little squeezed-film damping at high frequencies. In fact, the upward slope in frequency response at high frequencies implies that the diaphragm is actually a little underdamped.

To prevent the antiresonance seen in Figure 5-23 and to avoid the complex electro-mechanical-acoustic interaction between two deformable diaphragms from occurring, future design improvements should include a very rigid backplate that has a resonant frequency far above that of the diaphragm. This can be accomplished by increasing the backplate thickness or residual tensile stress. Since it is very difficult to grow LPCVD silicon nitride films that are more than 2-3 μm thick, the use of a 10-20 μm thick silicon backplate would be more feasible. To reduce stray capacitance, the backplate electrode could be insulated from the silicon backplate by a thick polymer insulator such as Parylene C. Vertical acoustic holes could be etched through the thicker silicon backplate with a DRIE. These changes should result in a flatter high frequency response, as well as a microphone diaphragm-backplate system that better conforms to the theory provided in Chapter 2 (based on a rigid backplate).

To straighten the response at low frequencies, a small pressure equalization hole that is exposed to the sound field must be designed into the microphone housing so that the low frequency sensitivity can be lowered. The pressure equalization hole of the microphone itself must also be simultaneously made smaller to keep the low frequency cut-off below 50 Hz. The diaphragm area can also be made smaller so that higher electret charge densities can be used without the diaphragm collapsing to the backplate. The loss in mechanical sensitivity can be offset by a smaller air gap and/or thinner diaphragm.

To compensate for the upward slope in frequency response at high frequencies, the diaphragm can be more heavily damped through control of the backplate hole density and air gap spacing. When the more heavily damped diaphragm is subsequently placed in a sound field, the increase in sound pressure at the diaphragm due to the microphone body will be offset by the damped diaphragm mechanical response, resulting in a flatter overall microphone frequency response (Figure 5-26). Naturally, the increase in diaphragm damping must be carefully controlled so that the noise floor of the microphone is not dramatically increased.

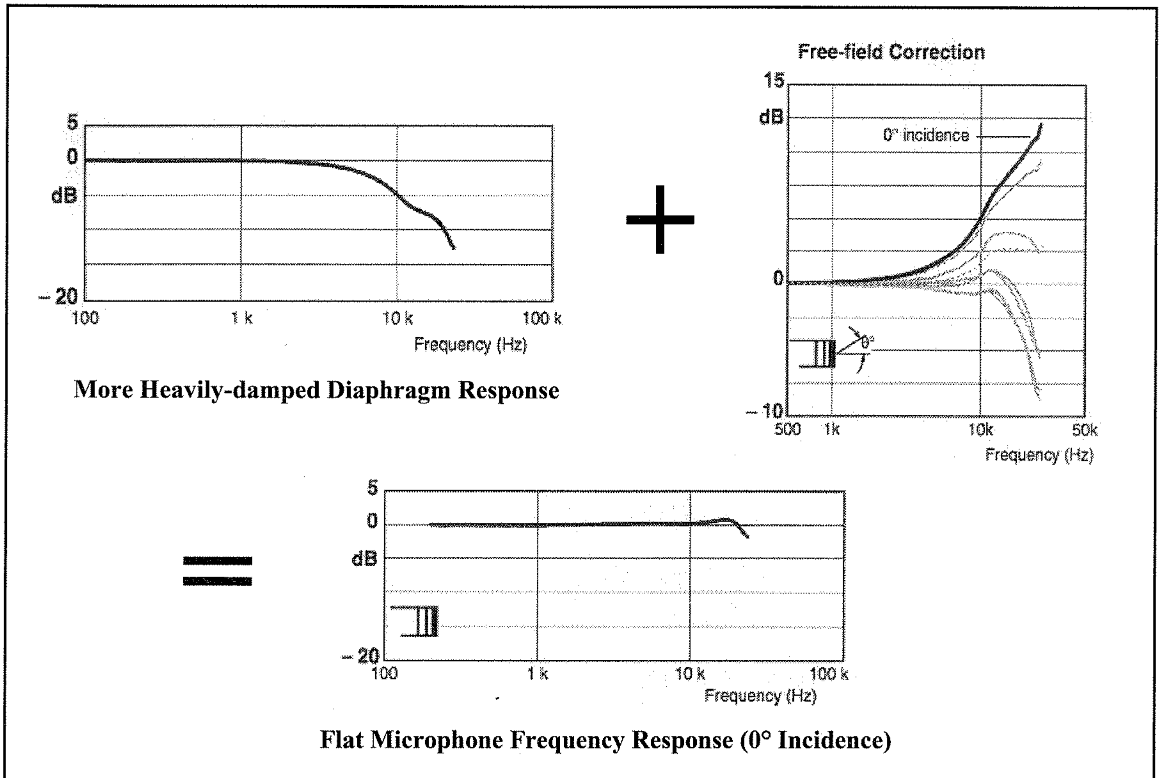

Figure 5-26. Compensation for the upward sloping microphone frequency response [6].

In terms of fabricating the diaphragm and backplate chips, there were no major problems. The most difficult challenge arose during the assembly and packaging steps. Often the fragile microphone diaphragm would unexpectedly rupture if the brass housing lid was screwed on too tightly, or if a sharp particle became trapped in the air gap between the microphone diaphragm and backplate. It was also difficult to overlay the two chips such that the small electrode bonding pads could be openly accessible for bonding to gold wires (Figure 5-20). Furthermore, attaching a 25 μm diameter gold wire to the backplate electrode bonding pads also proved to be very tricky. Because the Cr/Au electrode was deposited on top of a compressible 2.5 μm Parylene C film, a wedge-bonder could not be used to bond the gold wire. The only feasible solution was to glue the gold wire to the 200 × 200 μm^2 bonding pads with conductive silver paste. This had to be done without spreading the silver paste all over the backplate chip and before the tiny amount of silver paste dried up (usually within 30 seconds). Care also had to be taken to avoid severing the 1100 Å thick Cr/ Au electrode with an accidental swipe from

the sharp tweezer tip (Figure 5-27). The percentage of microphones that passed the grueling assembly process and worked was less than 10%!

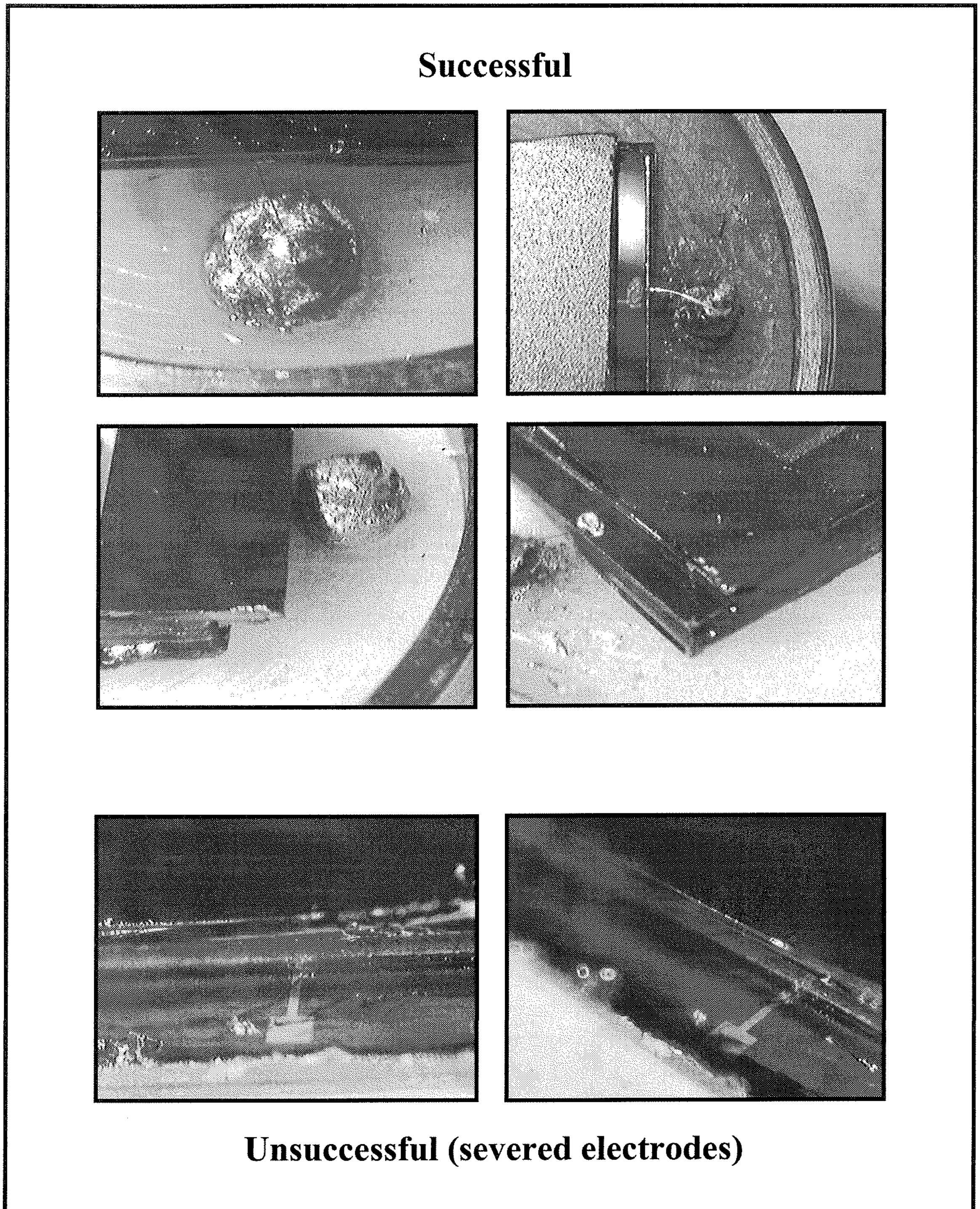

Figure 5-27. Pictures of wires used to connect the MEMS microphone to its housing.

5.7 Summary

This chapter has described the first successful application of thin film Teflon AF electrets to MEMS electret microphones. The BLT was also proven as an effect tool for electron implantation into Teflon AF 1601S. Using this new thin film Teflon AF electret technology, the fabrication, packaging, testing and analysis of three different MEMS electret microphone designs was reported. All of them utilize silicon nitride/Teflon AF composite diaphragms. Each version uses a backplate that is a refinement on the previous one. The design and processing parameters that affect mechanical and electrical sensitivity have also been reviewed. Wherever appropriate, microphone theory from Chapter 2 has been used to formulate design criteria and/or to evaluate microphone performance. Preliminary calculations suggest higher sensitivities, wider dynamic range and flatter frequency response can be achieved through refinement of the microphone structure, materials, electret properties and packaging. The high degree of design freedom confirms that MEMS thin film Teflon electret microphones can be built for a wide range of acoustic-sensing applications.

5.8 References

[1] O. Tabata, R. Asahi, H. Funabashi, K. Shimaoka, and S. Sugiyama, "Anisotropic Etching of Silicon in TMAH Solutions," Sensors and Actuators (A: Physical), Vol. 34, pp. 51-57, 1992

[2] R.A. Stewart, J. Kim, E.S. Kim, R.M. White and R.S. Muller, "Young's Modulus and Residual Stress of LPCVD Silicon-Rich Silicon Nitride Determined from Membrane Deflection," Sensors and Materials, 2, 5, pp. 285-298, 1991

[3] P. Scheeper, "A Silicon Condenser Microphone: Materials and Technology," Ph.D. Thesis, University of Twente, 1993

[4] R.D. Blevins, "Formulas for Natural Frequency and Mode Shapes," Van Nostrand Reinhold Company, New York, 1979

[5] J.A. Voorthuyzen, A.J. Sprenkels, A.G.H. Van der Donk, P.R. Scheeper and P. Bergveld, "Optimization of Capacitive Microphone and Pressure Sensor Performance by Capacitor-Electrode Shaping," Sensors and Actuators A, 25-27, pp. 331, 1991

[6] "Bruel & Kjaer Microphone Handbook," Vol. 1, July 1996

Chapter 6
MEMS Electret Microphones with Parylene Diaphragms

6.1 Preface

While a two-chip MEMS electret microphone lends itself best to proof-of-concept and prototype optimization in the research lab (both the diaphragm and backplate can be characterized and modified separately), a single-chip MEMS electret microphone is more commercially viable from the fabrication, assembly, performance and reliability standpoint. However, before the thin film Teflon AF electret technology and MEMS electret microphone design know-how can be directly applied to a single-chip device, certain high temperature structural materials must first be replaced by low temperature ones. The most obvious choice for replacement is LPCVD silicon nitride.

The MEMS electret microphone diaphragms described in Chapter 5 are all made from silicon nitride, an intrinsically stressed and high temperature material that is not optimal from the standpoint of low temperature post-IC processing or integration with microelectronics. This is because LPCVD silicon nitride is deposited at 835°C, while the upper temperature limit for CMOS electronics is only 400°C. There are a number of alternative materials whose lower deposition temperature and mechanical properties may be suitable for use in MEMS electret microphone diaphragms. A good candidate is Parylene, a family of thermoplastic polymers that can be deposited in thin film form at room temperature.

6.2 Parylene Diaphragms

Parylene was developed in the 1950s by William F. Gorham and was commercialized in 1965 by the Union Carbide Corporation [1]. It is typically used as a passivation layer in a wide range of commercial applications. Parylene (poly-para-

xylylene) is a polymer produced from the starting dimer para-xylylene (di-para-xylylene). It is deposited from vapor phase at room temperature under medium vacuum.

There are three commercially available types of Parylene (Figure 6-1). Parylene N is a completely linear and highly crystalline polymer that exhibits very low dissipation and high dielectric strength. Parylene C has a chlorine atom substituted for an aromatic hydrogen. It has very low permeability to moisture and other corrosive gasses. Parylene D has two aromatic hydrogens replaced by chlorine atoms. It is similar to Parylene C, but has better thermal stability at high temperatures. Table 6-1 lists some properties of Parylene N, C and D.

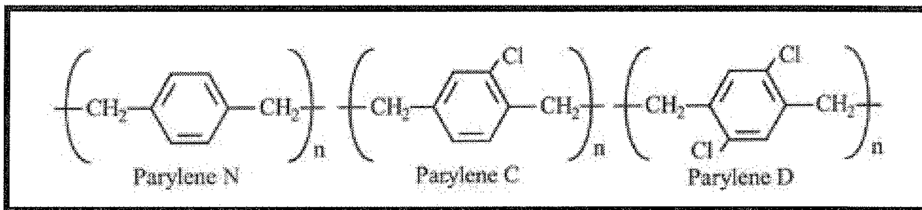

Figure 6-1. Chemical structures of Parylene N, C and D [1].

Table 6-1. Properties of Parylene N, C and D [1].

	Parylene N	**Parylene C**	**Parylene D**
Dielectric Strength [V/μm]	275	220	220
Dielectric Constant	2.6	3.1	2.8
Young's Modulus [GPa]	2.5	2.8	2.7
Yield Strength [MPa]	42	55	62
Elongation to Break [%]	20-250	200	10
Density [g/cm^3]	1.10-1.12	1.29	1.42
Index of Refraction	1.66	1.64	1.67
Melting Point [°C]	420	290	380
Glass Transition [°C]	>300	240	240
Linear Coef. of Expansion [/°C]	6.9×10^{5}	3.5×10^{5}	$3\text{-}8\times10^{5}$
Water Absorption [% after 24 hrs]	< 0.1	< 0.1	< 0.1
Thermal Cond. @ 20°C [cal/cm°C]	3×10^{-4}	2×10^{-4}	-

The Parylene deposition process is favorable for use in the fabrication of MEMS electret microphones because it is carried out at room temperature under medium vacuum. No catalysts or solvents are involved, resulting in very conformal and pinhole free films that can range in thickness from a few hundred nanometers to a few tens of microns. Figure 6-2 shows a schematic of the Parylene deposition system. The deposition process consists of three main steps. The first step involves vaporizing Parylene from its solid dimer form at temperatures between 140-170°C under vacuum. The second step is pyrolysis at temperatures above 650°C, where gaseous Parylene dimer is split into monomers. The last step is the room temperature polymerization of gaseous monomer into thin film Parylene.

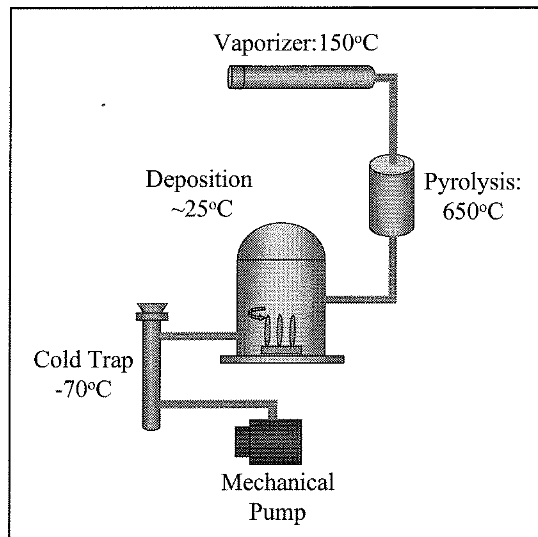

Figure 6-2. A schematic of the Parylene deposition system [2].

Parylene can be rapidly etched by oxygen plasma. By using photoresist as a protective mask, it can be patterned using standard lithographic processes. Parylene is inert, non-toxic and non-hazardous. It is highly resistant to chemical attacks at room temperature and is insoluble in all organic solvents up to 175°C. For the MEMS electret microphone presented in this chapter, Parylene C will be used as the diaphragm material. It was chosen over the other two types of Parylene because of its high deposition rate and high elongation to break. All Parylene C depositions were carried out in a PDS 2010 LABCOTER 1 from Specialty Coating Systems Inc.

6.3 Parylene C/Teflon AF Composite Diaphragm Characteristics

The MEMS electret microphone diaphragms described in this chapter are all Parylene C, Cr, Au and Teflon AF composite structures. The Parylene C is typically 0.75 to 2.5 μm thick and acts as the main stress-determining material. The evaporated 100 Å Cr and 1300-2000 Å Au layers form the diaphragm electrode. The Teflon AF film serves as the electret layer and is about 1.3 μm thick.

By measuring the resonant frequency, f_0, of these composite diaphragms with a Laser Doppler Vibrometer (LDV) and by applying the membrane model, the residual tensile stress can be approximated by equation (2-13):

$$f_0 = \sqrt{\frac{\sigma}{2a^2\rho}} \qquad \text{[Hz]}$$

where:

σ: residual tensile stress of the composite diaphragm [N/m^2]

ρ: density of the main stress-contributing diaphragm material [kg/m^3]

a: length of one side of square diaphragm [m]

Experiments were performed on several composite and pure Parylene C diaphragms to study their mechanical stability under different environmental conditions. Table 6-2 shows the results. All resonant frequency data was obtained at room temperature by the LDV. The following observations can be summarized from the data:

- The residual stress of Parylene C diaphragms is tensile. This tensile stress seems to increase with the thickness of Parylene C (24 MPa-tensile for a 0.75 μm thick diaphragm to 44 MPa-tensile for a 2.5 μm thick diaphragm).
- Teflon AF (annealed at 170°C for 15 minutes) adds more tensile stress (several MPa) to the pure Parylene C diaphragm on which it is deposited. However, Parylene C is still the main stress-contributing material.
- Similarly-sized Parylene C/Teflon AF composite diaphragms that have undergone the same processing histories have the same resonant frequencies; and therefore, the same tensile stress. This is true within a given batch of wafers and across different batches.

- Humidity levels of 99% RH, combined with a temperature of 85°C, have no significant effect on the residual tensile stress of Parylene C/Teflon AF composite diaphragms.
- The adhesion of Teflon AF to Au and Parylene C is good under 99% RH and 85°C conditions. No bubble formation or delaminating of Teflon AF film was observed.

Although the volume of data is not huge, these preliminary results strongly suggest that Parylene C **can** be used as a substitute diaphragm material for LPVCD silicon nitride. The residual tensile stress of Parylene C is large enough such that the fundamental resonant frequencies of its diaphragms are above the 100 Hz to 11 kHz audio frequency range. The good mechanical stability of Parylene C diaphragms under different environmental conditions is also promising because this will ultimately translate into more stable MEMS electret microphones.

Table 6-2. Environmental influences on Parylene C/Teflon AF diaphragms.

Membrane Thickness Size	**Paryl. C 0.75 um (8 mm)^2**	**Paryl. C 0.75 um (8 mm)^2**	**Paryl. C 2.5 um (8 mm)^2**	**Paryl. C 2.5 um (8 mm)^2 Batch B**	**Paryl. C 2.5 um (8 mm)^2 Batch A**	**Paryl. C 1.75 um (8 mm)^2**	**Paryl. C 1 um (3 mm)^2**	**Paryl. C 1 um (2 mm)^2**
Teflon AF 1601S	1.3 um 170C anneal (15 min)	← *None* 170C anneal (15 min)	*None* 170C anneal (15 min)	*None* → *None*	1.3 um 170C anneal (15 min)	1.3 um 170C anneal (15 min)	1.3 um 170C anneal (15 min)	1.3 um 170C anneal (15 min)
Cr	*None*	*None*	*None*	100 A	100 A	100 A	100 A	100 A
Au	*None*	*None*	*None*	2000 A	2000 A	2000 A	2000 A	2000 A
1st Mode Resonant Frequency	*12.90* 13.05 kHz	← 11.90 ← 12.00 kHz	16.30 kHz	11.10 → 11.00 → kHz	14.05 13.75 *13.93* 14.35 14.10 kHz	12.70 kHz	21.06 21.52 kHz	26.00 26.7 kHz
Parylene C Stress		~ 24 MPa Tensile	~44 MPa Tensile					
After 23°C, 99% RH 24 Hrs	*12.70* kHz				*13.73* kHz	12.50 kHz		
After 85°C Room RH 24 Hrs	*12.90* kHz				*14.20* kHz	12.90 kHz		
After 85°C Room RH 72 Hrs	*12.90* kHz				*14.15* kHz	12.85 kHz		
After 85°C 99% RH 7 days	*12.65* kHz				*13.90* kHz	12.50 kHz		

Meaning of the arrow in the table above: before condition → after condition

6.4 Parylene C/Silicon Nitride Composite Backplate Microphone

Tests on Parylene C diaphragms suggest that their mechanical properties are similar to the silicon nitride diaphragms described in Chapter 5. Low temperature Parylene C should therefore be a good substitute material for high temperature LPCVD silicon nitride. To put this hypothesis to the test, a fourth type of MEMS electret microphone was fabricated. This new design combines a Parylene C/Teflon AF composite diaphragm with the perforated Parylene C/Silicon Nitride composite backplate of section 5.6. The use of the same backplate chip allows the performance of Parylene C composite diaphragms to be directly compared to identically-sized silicon nitride composite diaphragms.

6.4.1 Fabrication and Packaging

The fourth MEMS electret microphone uses the **same** perforated Parylene C/silicon nitride backplate chip as the microphone in section 5.6, but uses a Parylene C composite diaphragm instead of a silicon nitride one. The process flow of the backplate is provided again as a reference (Figure 6-3).

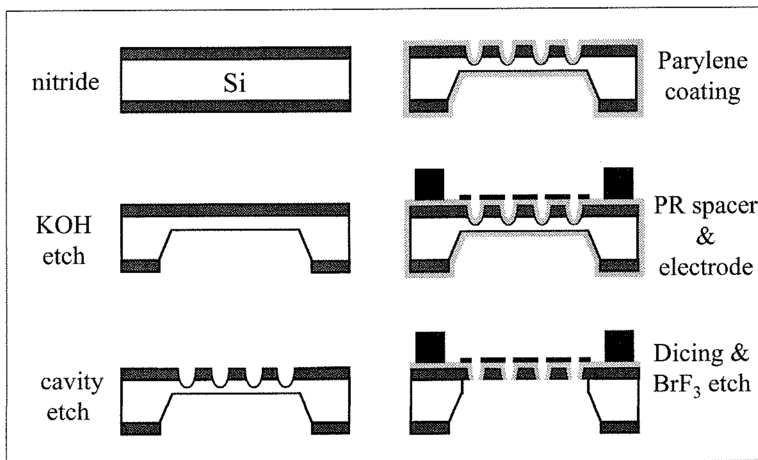

Figure 6-3. Process flow of 8 × 8 mm^2 perforated Parylene C/silicon nitride backplate.

The fabrication steps of the Parylene C/Teflon AF diaphragm are shown in Figure 6-4. Diaphragm formation begins with a <100> silicon substrate coated with 2 μm thermal silicon dioxide (serves as electrical insulation and as an etch stop for KOH and BrF_3).

The oxide on the backside of the wafer is then masked with photoresist, patterned and etched with BHF to form a back-etch window. A timed KOH anisotropic back-etch follows, leaving a 20 μm thick silicon membrane. A 0.75 μm thick film of Parylene C is then deposited onto the front side of the wafer. This acts as electrical insulation for the diaphragm electrode. A 1400 Å thick layer of Cr/Au is evaporated onto the Parylene C and after patterning with photoresist, this forms the diaphragm electrode. BrF_3 is used to etch away the remaining 20 μm silicon beneath the 0.75 μm Parylene C membrane. The remaining silicon dioxide is etched away in a one-sided BHF etch.

Teflon AF 1601S-6 solution is then spin-cast over the front surface of the membrane and is baked at 115°C for 45 minutes and then at 170°C for 15 minutes to drive off the FC-75 solvent. The resulting film thickness is 1.3 μm. Further annealing at 330°C is not carried out because the melting point of Parylene C is only 290°C. Electrons with 7 keV of energy are then implanted into the Teflon using the BLT. The electret is aged by baking at 100°C in air for 3 hours. For this MEMS electret microphone, a stable charge density on the order of 10^{-5} C/m^2 was obtained as measured by the Monroe Isoprobe Electrostatic Voltmeter.

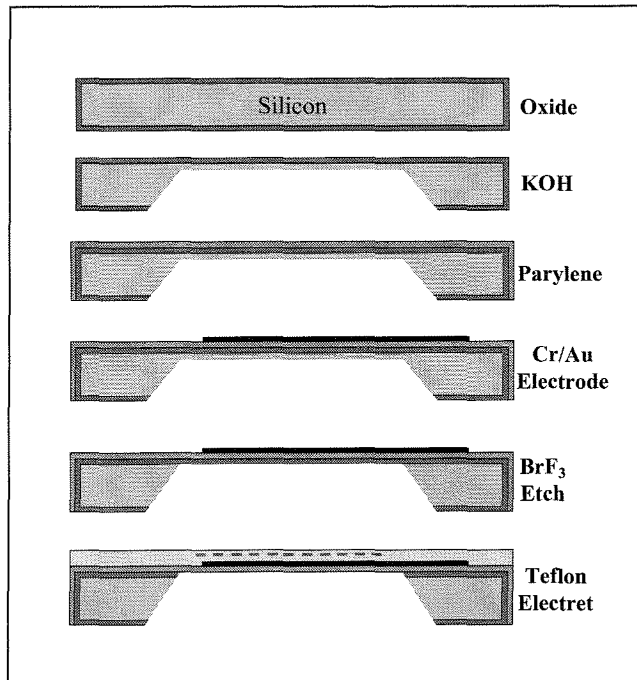

Figure 6-4. Process flow of 8 × 8 mm^2 Parylene C/Teflon AF diaphragm.

The schematic cross-section of the assembled microphone (Figure 6-5) is similar to that of the nitride diaphragm MEMS electret microphone in section 5.6. The diaphragm and backplate chips are mechanically clamped together and are enclosed in a brass housing that provides electromagnetic shielding (Figure 6-6). The rear of the housing is threaded so that it will seamlessly screw onto a B&K Type 2669 preamplifier. The backplate chip is double-side taped to an electrically insulating surface inside the housing and its electrode is connected to a non-grounded terminal that will be coupled to preamplifier input. The diaphragm chip is then placed on top of the backplate chip and is held in place by pressure from the top half of the brass housing. The diaphragm electrode is connected to ground.

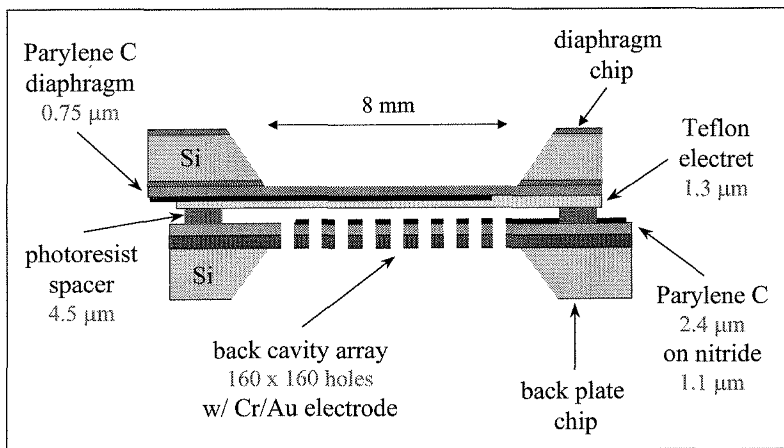

Figure 6-5. Cross-section of MEMS electret microphone with Parylene C diaphragm.

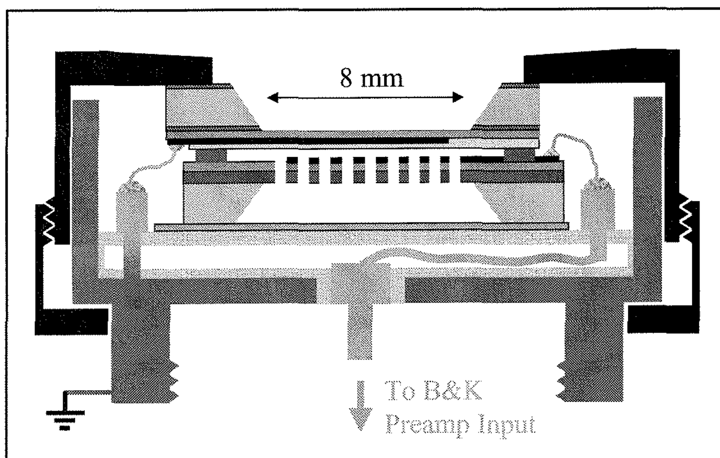

Figure 6-6. Cross-section of MEMS electret microphone housing.

6.4.2 Testing and Performance

Using a LDV the resonant frequency of the 0.75 μm Parylene C diaphragm with 1400 Å Cr/Au and 1.3 μm Teflon electret was determined to be 12.40 kHz (Figure 6-7). From the fundamental resonant frequency equation (2-13), $f_0 = (\sigma/2a^2\rho)^{0.5}$, for a square Parylene C diaphragm with tensile stress, where: f_0 = 12.40 kHz, Parylene C density, ρ = 1290 kg/m^3 and length of one side of the square diaphragm, a = 8 mm, the residual tensile stress of the composite diaphragm, σ, is about 25 MPa. The same measurement was performed for the highly perforated Parylene C/silicon nitride backplate. Its fundamental resonant frequency was measured at 12.88 kHz (Figure 6-7).

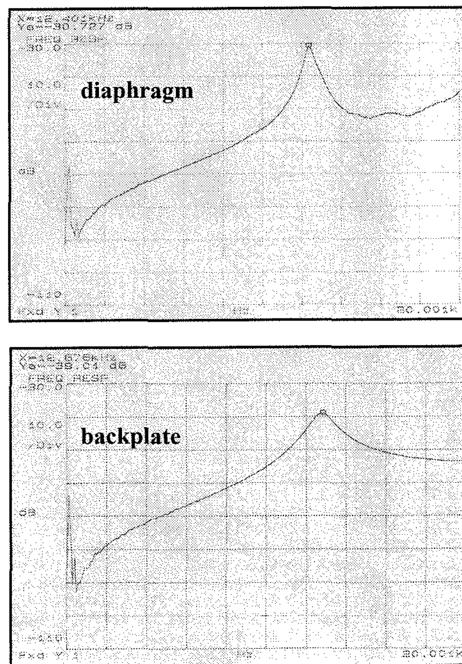

Figure 6-7. Resonance of Parylene/Teflon diaphragm and Parylene/nitride backplate.

For a 4.5 μm air gap, a 1.3 μm thick Teflon electret, a backplate with a hole opening ratio of 0.3 and an electrode area of 25 mm^2, the theoretical capacitance of the microphone is about 30 pF. The measured microphone (minus stray) capacitance was 21 pF. The discrepancy between the theoretical and experimental values can probably be attributed to a larger air gap than designed. This could happen if a small foreign object

became trapped between the two chips when one was placed on top of the other. The corresponding air gap that would result in a 21 pF microphone capacitance is 6.5 μm.

The electret microphone was tested in a B&K Type 4232 anechoic test chamber (Figure 5-10). An integrated speaker in the test chamber served as the acoustic source. A B&K Type 4189 1/2-inch reference microphone was used to measure the sound pressure level at the test position. The reference microphone was connected to a B&K Type 2669 preamplifier and a B&K Type 5935 dual channel amplifier/power supply. The electret microphone under test was also connected to a B&K Type 2669 preamplifier, and it shared the same B&K dual channel amplifier/power supply with the reference microphone. This ensured that the only variable in the entire test system was the MEMS electret microphone and that the other components were kept constant.

The schematic representation of the electret microphone-preamplifier circuit is shown in Figure 5-11. The electrical response of the circuit is given by equation (2-9):

$$H_e(\omega) = \frac{v_{out}}{v_{oc}} = \frac{j\omega R_i C_m}{1 + j\omega R_i (C_s + C_m + C_i)}$$

where ω is the frequency in rad/s. For an electret microphone capacitance, C_m = 21 pF, package stray capacitance, C_s = 2 pF, preamplifier input capacitance, C_i = 0.45 pF, preamplifier input resistance, R_i = 15 GΩ, and preamplifier output resistance, R_o = 25 Ω, $H_e(\omega)$ is a constant and equal to 0.90 over the frequency range of interest (100 Hz - 13 kHz). The electrical low-frequency roll-off is less than 1 Hz, and the preamplifier high frequency cut-off is much greater than 20 kHz. Thus, the electrical response is well suited for acoustic signals in the audible range.

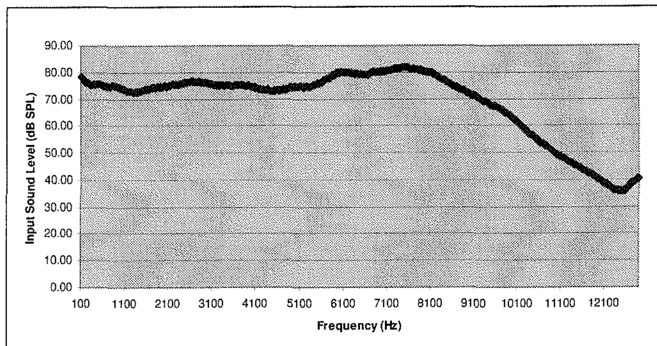

Figure 6-8. Input sound pressure level for frequency response measurement.

Using a Stanford Research Systems Model SR785 Dynamic Signal Analyzer to apply an input sinusoidal signal of known sound pressure level from 100 Hz to 12.896 kHz, the frequency response of the MEMS electret microphone was obtained. Sound pressure levels with higher frequencies were not used because above 13 kHz the output of the built-in speaker in the anechoic sound chamber is severely attenuated (Figure 6-8). The microphone frequency response data shows that the measured open circuit sensitivity of the microphone varies from 3.5 to 12.5 mV/Pa from 1 kHz to 11 kHz (Figure 6-9). A peak sensitivity of 44 mV/Pa was measured at 13 kHz and a trough of 0.9 mV/Pa was measured at 12.1 kHz.

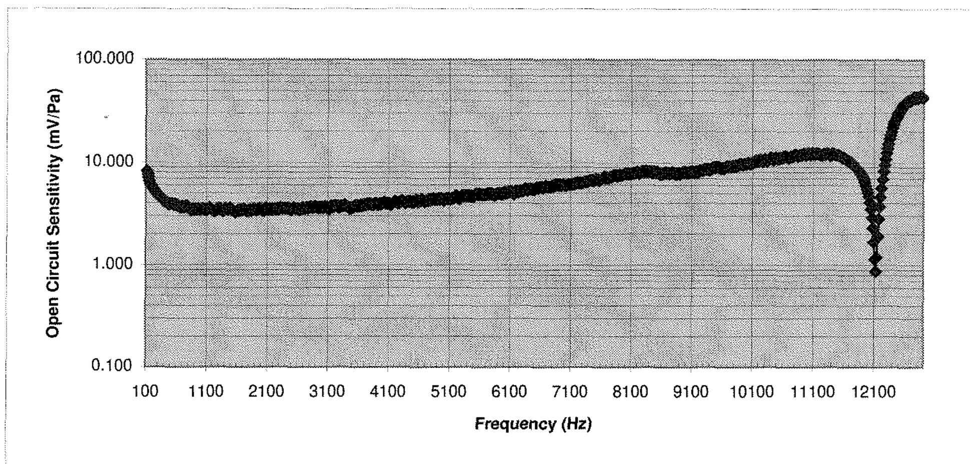

Figure 6-9. Frequency response of MEMS electret microphone w/ Parylene diaphragm.

Similar to the frequency response curve of the MEMS electret microphone with silicon nitride diaphragm in section 5.6 (Figure 5-23), there is again an unusual anti-resonance. This time, however, it is at 12.1 kHz and the drop in open-circuit sensitivity is much steeper than before. An explanation is that the fundamental resonant frequency of the perforated Parylene C/silicon nitride backplate (12.88 kHz) is practically identical to that of the Parylene C/Teflon AF diaphragm (12.40 kHz). Consequently, as the diaphragm and backplate are driven toward their resonant frequencies, their phase and amplitude of vibration will become nearly identical and the relative displacement between the two microphone electrodes will diminish rapidly. This results in an accelerated loss in open-circuit sensitivity characterized by the sharp notch in the frequency response at 12.1 kHz.

Like the MEMS electret microphone with silicon nitride diaphragm in section 5.6, there is a rise in open-circuit sensitivity for frequencies below 1 kHz and at high frequencies. Since this microphone uses the same backplate chip and brass housing as the microphone in section 5.6, the explanation for the frequency response increase should be the same, i.e. the low frequency behavior is a result of the pressure equalization hole not being exposed to the sound field (section 2.4.1), and the high frequency behavior is due to the presence of the microphone body in the sound field which causes an increase in the measured sound pressure at the diaphragm (section 5.6.2).

For diaphragm deflections smaller than the air gap thickness and assuming a square nitride membrane with large initial stress, a first-order calculation of the theoretical microphone open-circuit sensitivity, S_{oc}, is given by a slightly modified form of equation (2-7):

$$S_{oc} = \left(\frac{a^2}{3.04t\sigma 2}\right)\left(\frac{\frac{\sigma_e s_e}{\varepsilon_0 \varepsilon_e}}{\frac{s_e}{\varepsilon_e} + s_a}\right)(R) \approx 23 \text{ mV/Pa}$$

where: electret thickness, s_e = 1.3 μm, electret surface charge density, $\sigma_e = 6\times10^{-5}$ C/m^2, air gap thickness, s_a = 6.5 μm, permittivity of free space, $\varepsilon_0 = 8.85\times10^{-12}$ F/m, relative permittivity of the Teflon electret, ε_e = 1.9, length of one side of the square diaphragm, a = 8 mm, nitride membrane thickness, t = 3.3 μm (effective thickness of a pure Parylene diaphragm that would result in the same mass as the composite diaphragm), and stress in the nitride membrane, σ = 25 MPa and ratio of Cr/Au electrode area to the total membrane area, R = 0.273. Because this equation does not take into account the compliance of the thin perforated nitride/Parylene C backplate, which may cause it to lose relative displacement with respect to the diaphragm or have a DC displacement towards the diaphragm, it is expected that the theoretical open-circuit sensitivity will be an over-estimate of the measured open-circuit sensitivity.

According to equation (2-18) and (2-19), the flexible diaphragm will collapse to the flexible backplate for an electret surface charge density of around 1.25×10^{-4} C/m^2. This assumes the entire diaphragm and backplate areas are covered by metal electrodes. Since the electret surface charge density for this microphone is only 6×10^{-5} C/m^2 and the

electrodes only occupy 27.3% of the total 8 mm × 8mm diaphragm area, there is little risk of diaphragm collapse due to electrostatic attraction.

The measured noise level of the MEMS electret microphone with B&K Type 2669 preamplifier is less than 30dB SPL at 25°C. In comparison, a B&K Type 4189 1/2-inch electret microphone with the same preamplifier and at the same temperature has a noise level of 17 dB SPL. Using equation (2-14), the theoretical mechanical air-streaming resistance, R_a, of this microphone is a low 0.008 Ns/m. If we plug this value into equation (2-17) and assume a bandwidth of 14 kHz, the theoretical linear noise pressure of the microphone itself is only 0.5 dB SPL. The low empirical and theoretical noise levels should not be surprising because the backplate has a high acoustic hole density and hole opening ratio.

The 3% distortion limit was found to be above 110 dB SPL (the maximum output of the anechoic sound chamber speaker). At 110 dB SPL and 1 kHz the measured Total Harmonic Distortion of the MEMS electret microphone was 1.5 %. Since the lowest detectable sound pressure level is below 30 dB SPL, this translates into a microphone dynamic range that is greater than 80 dB SPL.

Table 6-3. Characteristics of MEMS electret microphone w/ Parylene C diaphragm.

	Diaphragm Chip	**Backplate Chip**
Dimensions & Material	8mm × 8mm × 0.75 μm Parylene C	8mm × 8mm × 1.1 μm Silicon Nitride
Electrode Dimensions	100Å Cr / 1300 Å Au 5mm × 5mm	100Å Cr / 1000 Å Au 5mm × 5mm
Polymer Coating	1.3 μm Teflon AF 1601S	2.4 μm Parylene C
Acoustic Holes	None	160 × 160 array 30 μm diameter 50 μm center-to-center (0.3 opening ratio)
1st Resonant Frequency	12.40 kHz	12.88 kHz
Electret Surface Charge Density	6×10^{-5} C/m^2	None
Capacitance	21 pF	
Open-circuit Sensitivity	3.5-12.5 mV/Pa	
Useful Frequency Range	100 Hz - 11.5 kHz	
Dynamic Range	Less than 30 dB - 110+ dB SPL	
Total Harmonic Distortion	1.5% @ 110 dB SPL, 1 kHz	

6.4.3 Analysis

The microphone performance results (Table 6-3) show that Parylene C **can** be used as an effective diaphragm material in MEMS electret microphones. The open-circuit sensitivity is high enough to allow good sound measurements in the 100 Hz to 11.5 kHz audio frequency range with minimal or no signal amplification. In fact, the performance characteristics of the silicon nitride diaphragm microphone and Parylene C diaphragm microphone are practically identical (Table 6-4). Both show the same antiresonance at around 12 kHz and an increase in open-circuit sensitivity at low and high frequencies.

The main difference between the two materials is that Parylene C diaphragms have much lower residual tensile stress (25 MPa) than silicon nitride diaphragms of equivalently thickness (70 MPa). This imparts Parylene C diaphragm microphones with a larger mechanical sensitivity, so lower electret charge densities can be used to achieve the same open-circuit sensitivity as similarly-sized silicon nitride diaphragm microphones. The lower residual stress also allows for the design of smaller microphones with high mechanical sensitivity. The only disadvantage of the more compliant Parylene C diaphragms is that their microphones have slightly higher Total Harmonic Distortion for large sound pressure levels.

Table 6-4. Nitride diaphragm vs. Parylene diaphragm in MEMS electret microphones.

	Nitride Diaphragm	**Parylene C Diaphragm**
Dimensions	8mm × 8mm × 0.5 μm	8mm × 8mm × 0.75 μm
Electrode Dimensions	100Å Cr / 1000 Å Au 5mm × 5mm	100Å Cr / 1300 Å Au 5mm × 5mm
Teflon AF 1601S	0.9 μm	1.3 μm
Electret Surface Charge Density	1.5×10^{-4} C/m^2	6×10^{-5} C/m^2
1st Resonant Frequency	13.25 kHz	12.40 kHz
Residual Tensile Stress	70 MPa	25 MPa
When combined w/ a 8 mm × 8 mm Perforated Parylene C/Silicon Nitride Backplate		
Capacitance	15 pF	21 pF
Open-Circuit Sensitivity	3.5-16.5 mV/Pa	3.5-12.5 mV/Pa
Useful Frequency Range	100 Hz - 11.5 kHz	100 Hz - 11.5 kHz
Dynamic Range	Less than 30 dB - 110+ dB SPL	Less than 30 dB - 110+ dB SPL
Total Harmonic Distortion	<1% @ 110 dB SPL 1 kHz	1.5% @ 110 dB SPL 1 kHz

In terms of assembling and packaging the Parylene C/Teflon AF diaphragm chip with the perforated Parylene C/Silicon Nitride backplate chip, the same difficulties were encountered as described in section 5.6.3. There were, however, additional problems related to the fabrication of the Parylene C diaphragm itself. The most significant one was the presence of cracks in the Parylene C diaphragm after its release from the silicon substrate (Figure 6-10). These cracks often ruptured membranes or severed Cr/Au electrodes. These cracks are most likely the result of stress buildup in the Parylene C material rather than the result of chemical attack. This is because Parylene C is resistant to chemical attack by HF (used to etch silicon dioxide) and BrF_3 (used to etch silicon) [2]. However, the random appearance and distribution of these cracks makes the source elusive. It is unlikely that these cracks are due to exposure of the Parylene C to temperatures above its physical limits, since the maximum process temperature is only 170°C (annealing of Teflon AF 1601S), whereas the melting point and glass transition temperature of Parylene C is 290°C and 240°C, respectively. Further research must be done to more closely examine this phenomenon. The use of Parylene N and D as diaphragm materials should also be performed to see if the same cracking is observed.

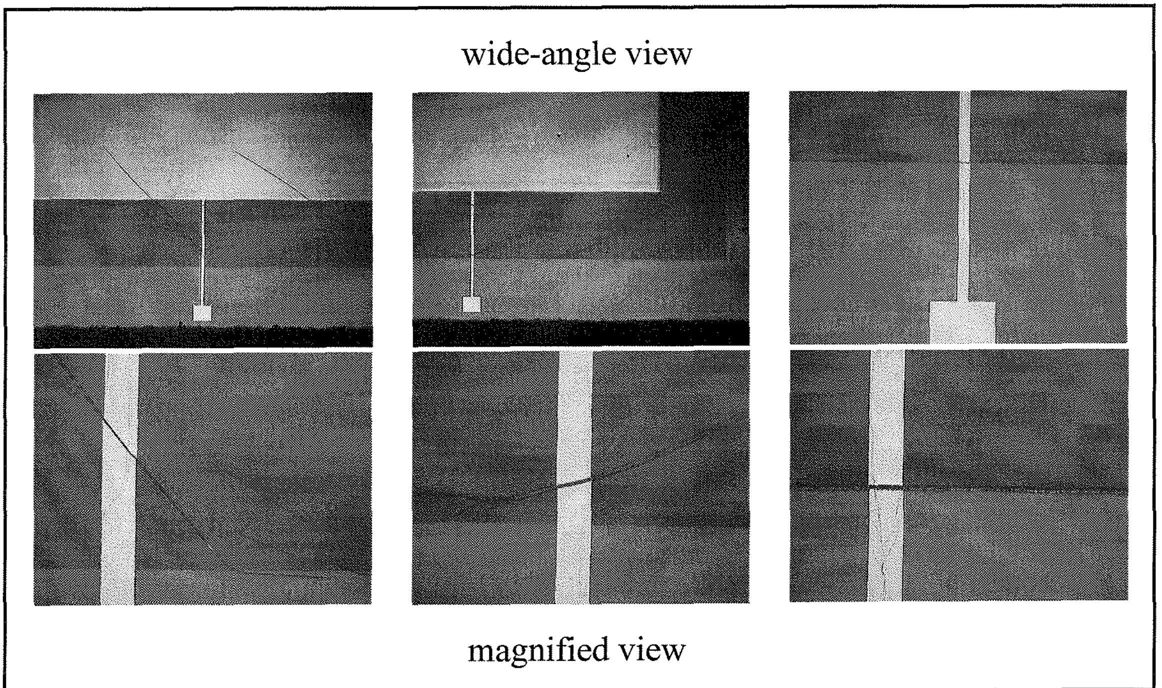

Figure 6-10. Parylene C diaphragm cracking problems.

6.5 Summary

This chapter has described the first successful use of Parylene C diaphragms in MEMS electret microphones. Parylene C was found to be compatible with thin film Teflon AF electret technology. When combined, Teflon AF 1601S and Parylene C form a mechanically, chemically and electrically stable composite diaphragm structure. The fabrication, packaging, testing and analysis of an electret microphone that uses a Parylene C/Teflon AF composite diaphragm was also reported. Preliminary microphone performance characteristics show that Parylene C diaphragms are just as, if not more, effective than silicon nitride diaphragms for use in MEMS acoustic sensors.

The promising results presented here opens up the new possibility of using Parylene as a diaphragm and structural material for surface micromachined single-chip electret microphones that can be integrated with microelectronics. The room temperature deposition of Parylene would allow such a device to be fabricated in a post-IC process. If successfully developed, this miniature, self-biasing, low-cost, microelectronics-compatible condenser microphone would revolutionize the entire acoustic sensor industry.

6.6 References

[1] "Parylene Conformal Coatings Specifications and Properties," Specialty Coating Systems Inc., Indianapolis, Indiana, 1997

[2] X.Q. Wang, "Integrated Parylene Micro Electro Mechanical Systems (MEMS)," Ph.D. Thesis, Caltech, 2000

Chapter 7
Conclusion

This thesis describes the development of miniature thin film Teflon electret condenser microphones that are fabricated from silicon substrates using Micro Electro Mechanical Systems (MEMS) technology. Device issues such as material selection, design, modeling, fabrication, packaging, testing and performance were studied.

First, a suitable electret material had to be selected. Teflon AF 1601S, a brand of Du Pont fluoropolymer, was chosen for its excellent charge storage characteristics, chemical inertness, good adhesion and high temperature stability. Its ability to be spin-cast at room temperature to form micron-thick films and its ability to be patterned using standard lithographic techniques makes it compatible with MEMS fabrication processes. Thin film Teflon AF was found to adhere well to silicon nitride and Parylene diaphragms even under extreme humidity and temperature conditions.

Next, a Back-Lighted Thyratron electron implantation system was developed to transform thin film Teflon AF into an electret. Benefits such as room temperature operation, variable electron beam energy, large beam size, high electron dose, high throughput, robustness, wafer-level compatibility and low cost made the BLT a better choice over other electron beam sources, such as a SEM. By combining Teflon AF with the BLT, an effective MEMS-compatible thin film Teflon electret technology was developed. Thermal annealing was used to stabilize the implanted charge and two instruments based on the electric field compensation method were used to measure electret surface charge density. Stable values on the order of 10^{-5} to 10^{-4} C/m^2 were obtained.

Using this new thin film Teflon electret technology, the fabrication, packaging and testing of four different MEMS electret microphone designs were investigated. All four microphones were fabricated using bulk-micromachining techniques. Each microphone was manufactured as a two piece structure, comprising a microphone diaphragm chip and a perforated backplate chip. When one is placed on top of the other, the two chips form a

silicon microphone that can produce a signal without the need for external biasing. The first three designs used silicon nitride diaphragms with silicon, glass and silicon nitride backplates. These microphones were instrumental at emphasizing the importance of minimizing stray capacitance, increasing backplate acoustic hole density, increasing diaphragm area, decreasing diaphragm thickness, increasing backplate stiffness and increasing electret charge density. These refinements were gradually implemented over the evolution of the first three microphones. It also became apparent that the design of the microphone package is just as important as the design of the microphone itself.

Lastly, a fourth generation MEMS electret microphone was developed to show that Parylene C could be used as a microphone diaphragm material. This is important for the future development of single-chip Parylene-based electret microphones that can be integrated with microelectronics. The room temperature deposition of Parylene would allow such a device to be fabricated in an all-surface-micromachined post-IC process. Experiments showed that Parylene C diaphragms are just as good, if not better than silicon nitride diaphragms for use in MEMS electret microphones. When combined with Teflon AF 1601S, Parylene C formed mechanically, chemically and electrically stable composite diaphragm structures.

Overall, the third and fourth generation MEMS electret microphones displayed very low stray capacitance, structural simplicity and good stability over time in the ordinary environment. The dynamic range of these two microphones was from less than 30 dB to above 110 dB SPL and the open-circuit sensitivities obtained range from 3.5 - 44 mV/Pa over the frequency range 100 Hz - 13 kHz. The total harmonic distortion of both devices was less than 2% at 110 dB SPL, 1 kHz. A more rigid backplate, a more damped diaphragm and a microphone housing that is vented to the sound field would immediately improve the low and high frequency response of both devices.

If the growth of portable electronics, wireless communication devices and voice-driven applications continues at its current torrid pace, smaller, better performing, and more highly integrated acoustic systems will eventually be needed. These are likely to take the form of miniature acoustic chips that integrate the microphone element with microelectronic circuitry. These chips will not only be able to convert acoustic signals into electrical ones, but will have the processing power to provide additional functionality

such as directivity, noise cancellation, voice recognition and/or sound forming. The work presented in this thesis was meant to serve as a foundation for the development of these types of integrated acoustic sensing solutions.